The Role of Hippo Pathway as a Non-genetic Mechanism of Acquired Resistance to Targeted Therapies

University of Turku
Institute of Biomedicine
MDP in Biomedical Sciences
Drug Discovery and Development
Master's thesis

Author:
Ira Kouru

Supervisors:
Maria Georgiadou, PhD
Reetta Riikonen, MSc
Prof. Ullamari Pesonen, PhD

30.4.2023
Turku

Master's thesis

Subject: Institute of Biomedicine, MDP in Biomedical Sciences, Drug Discovery and Development
Author: Ira Kouru
Title: The Role of Hippo Pathway as a Non-genetic Mechanism of Acquired Resistance to Targeted Therapies
Supervisors: PhD Maria Georgiadou, MSc Reetta Riikonen, PhD Ullamari Pesonen,
Number of pages: 96 pages
Date: 30.4.2023

Almost half of melanomas are driven by mutations in the gene encoding a MAPK pathway kinase BRAF. The current standard of care in these tumors relies on the inhibition of BRAF in combination with the downstream kinase MEK. However, resistance to these inhibitors develops rapidly and inevitably. An urgent need for new therapeutics has led researchers to study the underlying mechanisms of treatment resistance. One proposed escape mechanism has been the activation and nuclear localization of YAP, the co-activator of the TEAD transcription factors. YAP-TEAD transcriptional activation regulates cell proliferation and inhibition of apoptosis.

Here, BRAF-driven A375 melanoma cells were treated with the BRAF inhibitor dabrafenib and MEK inhibitor trametinib. Already after 3 days, dabrafenib alone or in combination with trametinib (DT) diminished cell number and decreased proliferation. The effect was more pronounced after 7 days of treatment. ERK phosphorylation, which was used as the readout of MAPK pathway activity, was inhibited by dabrafenib and even more by DT, as expected, and the effect was highest on day 3. In addition, clear morphological changes were seen, and the cells changed toward an EMT-like phenotype. Furthermore, a 3-day treatment with dabrafenib or DT increased TEAD-target gene expression, suggesting activation of YAP-TEAD.

After continuous DT treatment for over 2 months, the cells, hereby referred to as A375-DT, became partly resistant to the treatment and resumed proliferation. In these A375-DT cells, ERK phosphorylation was lower than in parental cells, while YAP nuclear localization and TEAD target gene expression were modestly, but significantly, enhanced. Hence, the activation of YAP-TEAD may be one of the mechanisms leading to DT treatment resistance.

As a next step, compounds that have been shown to bind TEAD and inhibit its transcriptional activity, here referred to as TEAD inhibitors (TEADi), were used. When TEADi were combined with DT in parental cells, TEAD inhibition only modestly inhibited cell growth in comparison to the DT treatment alone. However, when TEADi were combined with DT in the A375-DT cells, a significantly higher, yet partial, inhibition of cell growth was observed. Importantly, TEADi decreased the YAP-TEAD target gene expression in A375-DT cells. Together these results suggest that although YAP-TEAD is activated, the A375 cells use also other resistance mechanisms. Thus, further studies in other BRAF mutant melanoma cell models are needed to determine the relevance of TEADi in combination with standard of care (BRAF and MEK inhibitors) in the treatment of melanoma patients.

Keywords: Melanoma, YAP, TEAD, BRAF, MEK, Hippo pathway.

1 INTRODUCTION

1.1 Drug resistance

1.1.1 Intrinsic and acquired resistance

Despite the latest advances in cancer treatment, the emergence of treatment resistance remains a major challenge (Marine *et al*., 2020; Holohan *et al*., 2013). Drug resistance, in specific, implies a phenomenon in which the tumor does not respond to the pharmacological treatment, or the treatment loses its ability to prevent the growth and spreading of cancer cells. In other words, the tumor cells become tolerant to the drug, but in contrast to the drug-tolerant cells, the drug-resistant cells can proliferate under the treatment. (Marine *et al*., 2020)

Drug resistance can be roughly divided into intrinsic (primary) and acquired (secondary) resistance (Holohan *et al*., 2013; Marine *et al*., 2020). The categorization into these two groups is not straightforward and can vary depending on the mode of response assessment (Marine *et al*., 2020). However, in this master's thesis, intrinsic resistance refers to resistance where the treatment does not lead to an objective clinical response at any point of treatment, and acquired resistance refers to resistance that develops after a clinical response is initially achieved with treatment (de Conti *et al*., 2021; Marine *et al*., 2020).

1.1.2 Genetic and non-genetic resistance

The genetic evolution of cancer cells is often considered a primary means to elicit treatment resistance. In genetic evolution, some cancer cells carry a pre-existing genetic change or obtain new genetic changes that give the cells a survival advantage against the treatment (Figure 1. A). These genetic changes include mutations, gene amplifications, gene deletions, and chromosomal translocations. (Marine *et al*., 2020) Mutations can cause resistance for example by altering the drug binding (Chong and Jänne, 2013), modifying the targeted signaling pathway to be constitutively active (Diaz *et al*., 2012; Siravegna *et al*., 2015), changing into another survival pathway (Miller *et al*., 2011), or making somatic gene reversion mutations (Christie *et al*., 2017). However, all the treatment-resistant cancers do not bear any specific mutations which could explain the emergence of the treatment resistance (Figure 1. B). This observation has led the researchers to suspect that there must be other, non-genetic, mechanisms that induce the cells to become resistant to the therapy. (Marine *et al*., 2020)

Non-genetic resistance mechanisms often include transcriptional reprogramming, which is achieved by the simultaneous activation of epigenetic regulators and transcription factors. Cancer cells can also utilize regulatory elements that are silenced in healthy cells. (Marine *et al*., 2020; Bell *et al*., 2019; Knoechel *et al*., 2014) The cells can for example use developmental programs (Bell *et al*., 2019; Marine *et al*., 2020) and switch their whole phenotype towards an undifferentiated/invasive phenotype (Kemper *et al*., 2014; Shaffer *et al*., 2017; Marine *et al*., 2020), which leads to increased treatment resistance (Konieczkowski *et al*., 2014). Studies have shown that some cells that are already present in the treatment-naïve tumor can survive under primary drug treatment and move on into a transcriptional state that makes the cells tolerant to the treatment and eventually enables the cells to proliferate under the treatment conditions. These cells are called drug-tolerant persister (DTP) cells. (Bell *et al*., 2019; Marine *et al*., 2020; Sharma *et al*., 2010) These DTP cells form minimal residual disease (MRD), which drives relapse in cancer patients (Rambow *et al*., 2018).

The cells surviving in the presence of therapeutic pressure share multiple characteristics. Usually, these cells have a restricted cell cycle, and they resemble quiescent cells that have temporarily arrested their cell cycle into the G0 state. In a physiological context, quiescence is common in adult stem cells that are present in tissues with a low need for regeneration. Importantly, quiescence is also a common feature observed in cancer stem cells. (de Conti *et al*., 2021) The surviving cancer cells can also become senescent. In contrast to quiescence, in senescence, the cells exhibit generally irreversible cell-cycle arrest that in a physiological context is induced by, for example, DNA damage, telomere shortening, oncogene activation, or increased stress signaling. In cancer cells, senescence can be induced by cancer treatment such as chemo- or radiotherapy. In contrast to healthy cells, senescent cancer cells can return to the cell cycle as a result of changes in the microenvironment or epigenetic alterations. (Gorgoulis *et al*., 2019; Patel *et al*., 2016; Saleh *et al*., 2019; de Conti *et al*., 2021)

Another characteristic frequently seen in treatment-resistant cell populations is altered cellular metabolism. Resistant cells often have slowed down metabolism, and the cells rely on oxidative phosphorylation in their energy production while they downregulate glycolysis. This predisposes the resistant cells to increased oxidative stress. (de Conti *et al*., 2021; Viale *et al*., 2014) In addition, resistant cells can use substitutive sources of energy, including fatty acid oxidation and autophagy, which maintain sufficient ATP production in the resistant cells (Ma *et al*., 2014; Li *et al*., 2019; Viale *et al*., 2014; de Conti *et al*., 2021).

Treatment-resistant cells are often anti-apoptotic. Resistance to apoptosis has been found necessary for drug resistance, however, it remains unknown if the deficient apoptotic process is the most important factor enabling the survival of a small population of resistant cells. In addition, the resistant cells have been noticed to use immune evasion and they have increased cellular plasticity. (de Conti *et al*., 2021) Cellular plasticity paves the way for other non-genetic resistance mechanisms to emerge. It is a result of changes in the cell's transcriptional programs, epigenome, signaling pathways, and transcription factors. (de Conti *et al*., 2021; Sharma *et al*., 2010) Additionally, to maintain cellular homeostasis, the cancer cells activate different stress response pathways to tackle abnormal oncogenic signaling, which allows the cancer cells to survive under the stressful environment induced by the drug (de Conti *et al*., 2021). Cancer cells can simultaneously use multiple of these above-mentioned processes for therapeutic evasion (Marine *et al*., 2020).

Genetic and non-genetic resistance do not occur in isolation from one another. Instead, genomic changes and the treatment-induced epigenetic and transcriptional changes together contribute to the emergence of treatment resistance. For example, studies have shown that some genetic alterations in cancer cells can predispose the cells to certain non-genetic resistance mechanisms. (Marine *et al*., 2020) It has also been suggested that non-genetic resistance mechanisms provide a small population of cells with rapid means to survive under the treatment. These cells can later develop genetic changes that reinforce the resistance and lead to the disease progression (Figure 1. C). (de Conti *et al*., 2021; Hata *et al*., 2016)

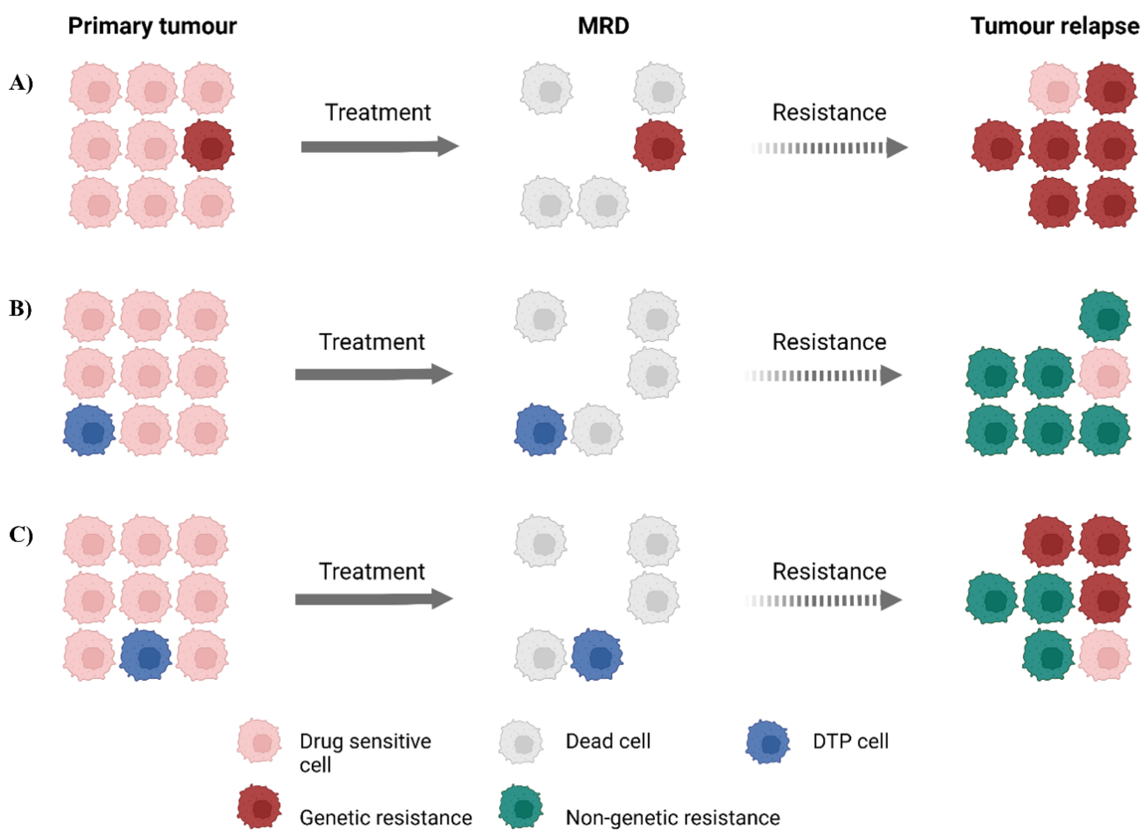

Figure 1. The development of genetic and non-genetic resistance. A cancer cell with certain genetic alterations can survive under the drug treatment and form minimal residual disease (MRD). Later these cells can develop resistance and start to expand causing relapse (A). Cancer cells without pre-existing genetic alterations that could enable cell survival, can undergo transcriptional and epigenetic changes that allow the cell survival upon treatment. These cells are called drug-tolerant persister (DTP) cells. The DTP cells can later develop non-genetic resistance and begin to expand, which causes cancer to relapse (B). In addition to non-genetic resistance mechanisms, the DTP cells can develop genetic resistance that provides the cells with a survival advantage under the treatment (C). The figure is modified from de Conti *et al.*, 2021 and created with BioRender.com.

1.2 The Hippo pathway

1.2.1 The biology of the Hippo Pathway

The first discovered component of the Hippo pathway, Warts kinase, was found in *Drosophila melanogaster* in 1995. The discovery of Warts was soon after accompanied by the discovery of other kinases in this pathway. Later in mammals, the counterpart kinases were discovered one by one, which eventually led to the discovery of this conserved pathway also in mammals. The name, Hippo pathway, originates from studies in *Drosophila* larvae, in which it was noticed that dysregulation of the pathway led to the reduction of apoptosis and hyperproliferation of cells, which resulted in a hippopotamus-like overgrowth of organs and development of tumors. (Piccolo *et al.*, 2014)

The Hippo pathway in mammals consists of two kinases: mammalian sterile 20-like kinase 1/2 (MST1/2) and large tumor suppressor kinase 1/2 (LATS1/2). Both kinases need a regulatory subunit, SAV1 for MST1/2 and MOB1 for LATS1/2, for their function. First, MST1/2 binds with SAV1 which causes the phosphorylation and activation of the LATS1/2-MOB1 complex. (Chan *et al*., 2005; Piccolo *et al*., 2014; Yamaguchi and Taouk, 2020) Secondly, LATS1/2 phosphorylates Yes-associated protein (YAP) and transcriptional co-activator with a PDZ-binding motif (TAZ) (Yamaguchi and Taouk, 2020; Piccolo *et al*., 2014). Finally, the phosphorylated YAP/TAZ interact with 14-3-3 which leads to the cytoplasmic retention of YAP/TAZ (Zhao *et al*., 2007; Yamaguchi and Taouk, 2020). Phosphorylated YAP/TAZ can also be ubiquitinated by E3 ligase Beta-transducin repeat-containing protein (β-TrCP) which results in the proteosome-dependent degradation of YAP/TAZ (Yamaguchi and Taouk, 2020; Zhao *et al*., 2010). Thus, the activation of the Hippo pathway inhibits the activation of YAP and TAZ. When YAP/TAZ are dephosphorylated, they move into the cell’s nucleus. YAP/TAZ lack a DNA-binding domain, and therefore, they must bind with different DNA-binding transcription factors, such as TEA domain family transcription factors (TEAD) 1–4, to begin the expression of the target genes (Piccolo *et al*., 2014; Nguyen and Yi, 2019). In the nucleus, YAP/TAZ regulate genes that are associated with cell proliferation, growth, and migration. These genes include for example *CTGF*, *MYC (*MYC proto-oncogene), *AXL* (AXL receptor tyrosine kinase), *CYR61* (Cysteine-rich angiogenic inducer 61), and *CCND1* (Cyclin D1). (Yamaguchi and Taouk, 2020) A simplified schematic of the Hippo pathway is illustrated in Figure 2.

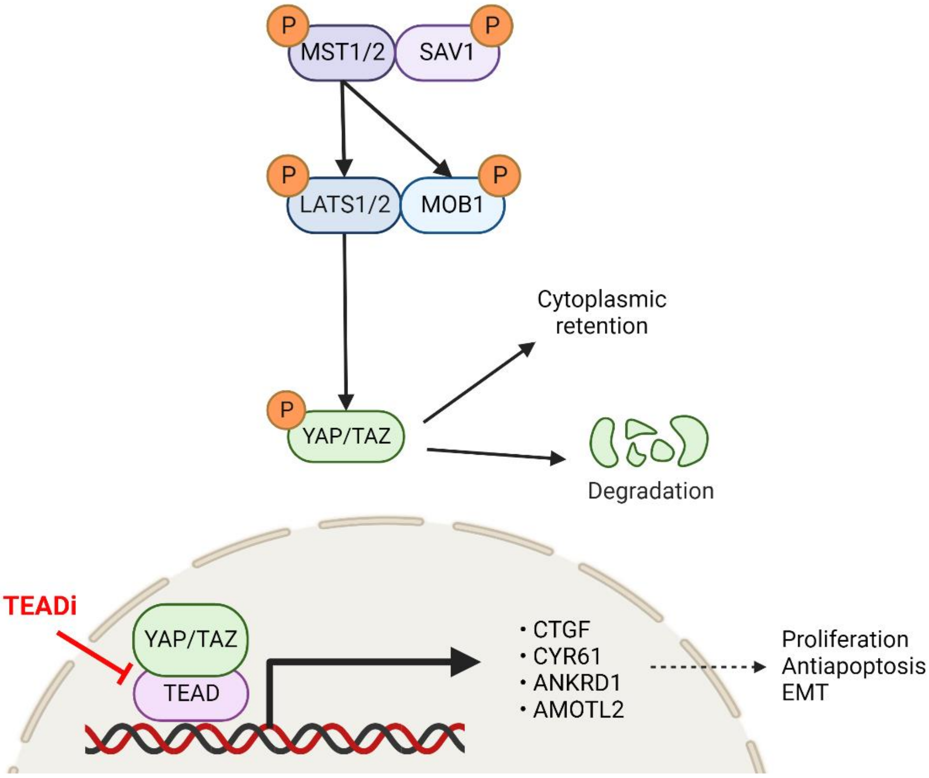

Figure 2. The mammalian Hippo pathway. Mammalian sterile 20-like kinase 1/2 (MST1/2) binds with its regulatory subunit SAV1 and phosphorylates the complex of large tumor suppressor kinase 1/2 (LATS1/2) and its regulatory subunit MOB1. LATS1/2-MOB1 phosphorylates Yes-associated protein (YAP) and transcriptional co-activator with a PDZ-binding motif (TAZ). The phosphorylated YAP/TAZ interact with 14-3-3 which leads to the cytoplasmic retention of YAP/TAZ. The phosphorylated YAP/TAZ can also be ubiquitinylated by E3 ligase β-TrCP, which results in the proteosome-dependent degradation of YAP/TAZ. Inactivation of the Hippo pathway leads to the dephosphorylation of YAP/TAZ. Dephosphorylated YAP/TAZ move into the cell's nucleus and form a transcription complex with TEA domain family transcription factors (TEAD) 1–4 and begin the expression of target genes. YAP/TAZ regulate genes that are associated with cell proliferation, growth, and migration, such as *CTGF*, *CYR61*, *ANKRD1*, and *AMOTL2*. Modified from Piccolo *et al.*, 2014. The figure is created with BioRender.com.

The identified regulators of the Hippo pathway, and therefore regulators of YAP/TAZ, are for example Thousand and one (Tao) kinase, multiple mitogen-activated protein kinase kinase kinase kinase family members, Serine/Threonine Kinase 25, Scribble, the Crumbs complex, and Neurofibromin-2 (NF2) (Plouffe *et al.*, 2016; Meng *et al.*, 2015; Zheng *et al.*, 2015; Cordenonsi *et al.*, 2011; Varelas *et al.*, 2010; Lim *et al.*, 2019; Yin *et al.*, 2013). It is known that the Hippo pathway is one of the most important regulators of YAP/TAZ activity, but other regulators have been identified as well. Another well-established controller of YAP/TAZ activity are the mechanical signals that are created by the cell's extracellular microenvironment. It has been observed that stretching of the cell causes the activation of YAP/TAZ and their nuclear accumulation. (Dupont *et al.*, 2011) In contrast, when the cell morphology is controlled to be round, YAP/TAZ become inactivated and locate in the cytoplasm (Piccolo *et al*., 2014). It has also been noticed that a more rigid extracellular matrix promotes the nuclear localization and activation of YAP/TAZ whereas softer extracellular matrix results in YAP/TAZ inactivation (Dupont *et al*., 2011). In addition to mechanical signals and the Hippo pathway, YAP/TAZ are also regulated by Rho-GTPases and G protein-coupled receptors (Dupont *et al*., 2011; Piccolo *et al*., 2014; Yu *et al*., 2012).

YAP/TAZ expression is redundant in normal and healthy cells, but they are crucial in promoting tissue repair upon injury (Bai *et al*., 2012; Cai *et al*., 2010; Chen *et al*., 2014; Lee *et al*., 2014; Su *et al*., 2015) and during embryonic development (Halder *et al*., 2012). YAP/TAZ also play a role in mediating the cell's structural characteristics like polarity, cytoskeletal organization, and shape (Halder *et al*., 2012). Interestingly, researchers have found that YAP/TAZ function as oncogenic co-transcription factors in most solid tumors. It has been suggested that YAP/TAZ are necessary for the formation and growth of these cancers. (Zanconato *et al*., 2016b) More specifically, YAP/TAZ activation has been shown to induce aberrant cell proliferation (Camargo *et al*., 2007; Dong *et al*., 2007; Zhao *et al*., 2007), avoidance of apoptosis (Dong *et al*., 2007; Kurppa *et al*., 2020), cancer stem cell features (Cordenonsi *et al*., 2011), chemoresistance, and metastasis (Zanconato *et al*., 2016b; Chan *et al*., 2008). In addition, high expressions of YAP/TAZ and/or their nuclear localization have been found to correlate with poor clinical outcomes and disease progression in a variety of cancers (Zanconato *et al*., 2016b; Piccolo *et al*., 2014; Sun *et al*., 2015; Muramatsu *et al*., 2011; Wang *et al*., 2010; Zhang *et al*., 2011; Hall *et al*., 2010; Xu *et al*., 2009; Kang *et al*., 2011).

It has been discovered that the Hippo pathway is one of the most frequently altered pathways in cancer (Sanchez-Vega *et al*., 2018), and mutations and/or epigenetic silencing have been found in several Hippo pathway proteins, such as MST1/2, LATS1/2, Salvador Family WW Domain Containing Protein 1 (WW45), MOB, NF2, and Kidney and Brain Expressed Protein (KIBRA) in human cancers (Pan, 2010; Bao *et al*., 2011; Hill *et al*., 2011). However, these mutations alone cannot explain the magnitude of YAP/TAZ dysregulation found in cancers, and therefore the researchers suspect that there might be a still missing link in the pathway that could explain this dysregulation. One possible explanation is the non-genetic alterations taking place in the cell, such as an epigenetic inactivation of the Hippo pathway. (Piccolo *et al*., 2014)

1.2.2 YAP upregulation as a resistance mechanism to targeted therapies

Most cancer patients eventually develop resistance to targeted therapies, which creates one of the biggest challenges in current cancer treatment. Interestingly, YAP/TAZ signaling has been identified as an important mediator of treatment resistance, especially to compounds targeting the epidermal growth factor receptor (EGFR) and mitogen-activated protein kinase (MAPK) pathway. (Nguyen and Yi, 2019)

Studies in BRAF^{V600E}-mutant melanoma have shown that BRAF inhibitor treatment considerably increases the expression of NF2 single guide RNAs (Shalem *et al*., 2013). *NF2* gene encodes Merlin which belongs to the ezrin-radixin-moesin protein family. Merlin is a scaffold protein that mediates cytoskeletal messages inside the cell by activating LATS1/2 and MST1/2, which in turn leads to the inactivation of YAP/TAZ (Yin *et al*., 2013; Zhang *et al*., 2010). In addition, studies have identified that a long noncoding RNA EMICERI mediates BRAF inhibitor resistance (Joung *et al*., 2017). EMICERI promotes resistance by increasing the expression of *MOB3B*, a member of the striatin-interacting phosphatase and kinase (STRIPAK) complex that prevents the activation of the Hippo pathway components LATS1/2 and MST1/2. Thus, expression of EMICERI results in increased YAP/TAZ activation and BRAF inhibitor resistance. (Joung *et al*., 2017; Bae *et al*., 2017; Hwang and Pallas, 2014; Nguyen and Yi, 2019) Moreover, in BRAF-mutant melanoma cells, BRAF inhibitor treatment promoted actin cytoskeleton remodeling, which has been suggested to lead to Rho-mediated LATS1/2 inhibition and subsequent activation of YAP (Kim *et al*., 2016; Yu *et al*., 2012). In BRAF or Kirsten rat sarcoma viral oncogene homolog (KRAS) mutant tumor cells, YAP inhibited apoptosis upon treatment with the MAPK pathway inhibitors by binding with TEAD and increasing the transcription of *BCL2L1*, a gene encoding an antiapoptotic protein Bcl-xL (B-cell lymphoma-extra large) (Nguyen and Yi, 2019; Lin *et al*., 2015). YAP1 has also been shown to mediate resistance to trametinib in head and neck squamous cell carcinoma (Mudianto *et al*., 2021).

EGFR, a receptor tyrosine kinase upstream of the MAPK pathway, is frequently mutated or amplified in several human cancers. Mutations in EGFR drive tumorigenesis and drug resistance, and therefore, tyrosine kinase inhibitors are developed to inhibit the aberrant EGFR signaling. Increased YAP activation has been found to function as a resistance mechanism to EGFR inhibitors, which is not surprising because receptor tyrosine kinases function upstream of the MAPK pathway. Thus, resistance to EGFR inhibitors and MAPK pathway inhibitors are arguably mediated by a similar collection of YAP/TAZ target genes. (Nguyen and Yi, 2019) For example, *AXL*, a target gene of YAP/TAZ, has been found to mediate resistance to BRAF and EGFR inhibitors in non-small cell lung cancer (NSCLC) (Ghiso *et al*., 2017; Lee *et al*., 2016; Xu *et al*., 2015; Zuo *et al*., 2018). It has also been shown that combined inhibition of EGFR and Mitogen-activated protein kinase kinase (MEK) in EGFR mutant NSCLC uncovers a population of dormant cells that show high activation of YAP. In these dormant cells, YAP-TEAD in complex with an epithelial to mesenchymal transition (EMT) transcription factor Snail Family Transcriptional Repressor 2 (SLUG) inhibited the expression of pro-apoptotic Bcl2 Modifying Factor (BMF) and restricted the apoptosis induced by EGFR/MEK blockade. In addition, the deletion of *YAP1* or combined pharmacological inhibition of TEAD and YAP both enhanced the EGFR/MEK inhibitor treatment-induced apoptosis resulting in the depletion of the dormant cell population. (Kurppa *et al*., 2020)

YAP1 has also been observed to bypass oncogene addiction after the ablation of KRAS, a GTPase belonging to the MAPK pathway (Zanconato *et al*., 2016a). Genome-scale DNA screens of human KRAS mutant colon cancer cell lines revealed that YAP1 promoted survival upon *KRAS* knockdown. YAP1 rescued the loss of *KRAS* by binding with Activator protein 1 (AP-1) transcription factor and Fos Proto-Oncogene, AP-1 Transcription Factor Subunit (FOS) to promote EMT. (Shao *et al*., 2014) Another study found that after the extinction of oncogenic KRAS, the *YAP1* gene locus was amplified and overexpressed in an advanced pancreatic ductal adenocarcinoma mouse model that was genetically engineered. In this model, YAP1 in complex with TEAD2 was shown to promote DNA replication and cell cycle progression co-operatively with the E2F transcription factor. (Kapoor *et al*., 2014; Nguyen and Yi, 2019) Moreover, *YAP* knockdown has been shown to block the activation of a compensatory Phosphoinositide 3-kinase-AKT serine/threonine kinase (PI3K-AKT) signaling in KRAS mutant pancreatic ductal adenocarcinoma cells, which sensitized these cells to pan-RAF inhibitor treatment (Zhao *et al*., 2017; Nguyen and Yi, 2019).

Taken together, YAP/TAZ use multiple different downstream effectors to convey the emergence of treatment resistance. Therefore, it is important to study how and to what extent different YAP effector pathways promote the development of treatment resistance in different circumstances. It is also important to study how different mutations, epigenetic changes, and the tumor microenvironment affect the cell subpopulations within the tumor to choose their resistance mechanism against the same treatment. (Nguyen and Yi, 2019)

1.2.3 TEAD

TEAD activation has been shown to contribute to the resistance against MAPK pathway inhibition in melanoma cells (Huh *et al*., 2019; Verfaillie *et al*., 2015). Mammals have four evolutionary conserved homologs of TEAD (TEAD1–4), which are S-palmitoylated (Noland *et al*., 2016; Huh *et al*., 2019). Protein palmitoylation in general is important for the protein's localization in membrane and protein trafficking (Huh *et al*., 2019). However, it is known that the S-palmitoylation of TEAD is not necessary for its nuclear localization (Tang *et al*., 2021). It is still controversial if the S-palmitoylation is needed to ensure the TEADs' stability (Noland *et al*., 2016; Tang *et al*., 2021), but it is known as essential for the YAP/TAZ-TEAD-interaction and therefore for TEADs' transcriptional activity (Noland *et al*., 2016; Tang *et al*., 2021).

The TEAD-interaction domain of YAP has been found essential for YAP-mediated tumor growth, EMT, and oncogenic transformation (Lamar *et al*., 2012; Zhao *et al*., 2008). In a previous study, the YAP-TEAD-interaction was shown to be necessary for A375 melanoma cells in mediating cell proliferation and survival under vemurafenib treatment (Fisher *et al*., 2017). In addition, it has been observed that YAP's ability to provoke the invasion of melanoma cells is reliant on TEAD1–4 (Fisher *et al*., 2017; Zhang *et al*., 2020). The cell invasion was regulated by the expression of YAP-TEAD target genes *AXL*, *THBS1*, and possibly *CYR61*, and *CRIM1* (Zhang *et al*., 2020).

YAP-TEAD has become an interesting target for drug discovery and development. Small molecule inhibitors that disrupt the YAP-TEAD-interaction have been developed of which photosensitizer verteporfin was first identified in 2012 (Liu-Chittenden *et al*., 2012; Zhou *et al*., 2014; Santucci *et al*., 2015). Later, inhibitors of TEAD transcriptional activity and peptidomimetic compounds that disrupt the YAP-TEAD-interaction have been developed (Santucci *et al*., 2015; Fan *et al*., 2022; Nouri *et al*., 2019; Liu-Chittenden *et al*., 2012; Jiao *et al*., 2014). However, peptide-based inhibitors have often poor pharmacokinetic properties and cell permeability, which limit their therapeutic potential. Moreover, due to its shallowness and large surface area, the YAP-TEAD interaction site is an arduous target to develop new small molecule inhibitors with eligible potency. (Hu *et al*., 2022)

Given the importance of TEAD auto-palmitoylation for the YAP-TEAD interaction and transcriptional activity, the auto-palmitoylation site has become an interesting drug target. Indeed, the conserved and deep hydrophobic binding pocket that lays away from the YAP-TEAD interaction site has made the TEAD auto-palmitoylation site a promising target. (Hu *et al*., 2022; Chan *et al*., 2016) To this day, several compounds that covalently or non-covalently inhibit TEAD auto-palmitoylation have been developed (Bum-Erdene *et al*., 2019; Kaneda *et al*., 2020; Li *et al*., 2020; Tang *et al*., 2021; Holden *et al*., 2020; Hu *et al*., 2022).

In this master's thesis, two novel TEAD inhibitors (TEADi), Compound A and VT-103 are used. Compound A is a TEAD inhibitor developed by Orion Pharma that inhibits the auto-palmitoylation of TEAD1–4. VT-103 is a selective non-covalent inhibitor of TEAD1 auto-palmitoylation that blocks the palmitoyl-CoA binding site. VT-103 disrupts YAP/TAZ-TEAD1 protein-protein interaction, and in mice, it had an excellent oral bioavailability (≥75%) and long half-life (>12h). In human NF2-deficient mesothelioma (NCI-H226 cells) xenograft model VT-103 significantly downregulated the expression of YAP-TEAD target genes *CTGF* and *CYR61*. More importantly, VT-103 dose-dependently led to the regression of NCI-H226 tumors in mice without showing adverse effects on body weight. In another mouse xenograft model with NCI-H2373 mesothelioma cells, VT-103 downregulated *CTGF* expression. In a mouse xenograft model with NCI-H2373 cell line-derived NCI-H2373-Tu-P2 tumors, VT-103 induced tumor regression without showing an adverse effect on body weight. (Tang *et al*., 2021)

1.3 Melanoma

1.3.1 The development and treatment of melanoma

Melanoma is a cancer of melanocytes which are located in the deep layer of the epidermis and produce the pigment of the skin (Patel *et al*., 2020; Isola *et al*., 2016). It is the third most common type of skin cancer after basal cell carcinoma and squamous epithelial cell carcinoma, but it has the highest mortality rate. Over the past 30 years, the incidence of skin melanoma has promptly increased resulting in a higher number of patients with invasive melanoma, however, in younger age groups the incidence of melanoma seems to be decreasing. (American Cancer Society, 2022; Batus *et al*., 2013; Siegel *et al*., 2022)

One of the most important risk factors for melanoma is exposure to ultraviolet (UV) radiation (American Cancer Society, 2022; Patel *et al*., 2020). Chronic and direct UV radiation causes damage to melanocyte DNA which may lead to cancer-initiating genetic changes (Patel *et al*., 2020; Hodis *et al*., 2012). In addition to UV radiation, also genetics plays a role in the development of melanoma (Palmer *et al*., 2000; Patel *et al*., 2020). Mutations in Cyclin-dependent kinase inhibitor 2A (CDKN2A) and cyclin-dependent kinase 4 (CDK4) are the most frequently found heritable genetic alterations in melanoma patients (Patel *et al*., 2020; Isola *et al*., 2016). Moreover, increased melanocortin-1 receptor polymorphism may also increase the risk for the development of melanoma (Patel *et al*., 2020; Liu and Sheikh, 2014). Melanocortin-1 receptor controls skin pigmentation in response to UV radiation (Wolf Horrell *et al*., 2016). Other risk factors for melanoma include male sex, fair skin, age, and a high number of (atypical) nevi (Siegel *et al*., 2022; American Cancer Society, 2022; Liu and Sheikh, 2014; Lasithiotakis *et al*., 2008).

The first change in melanoma is the formation of a benign nevus, which is a result of melanocyte proliferation. However, the formation of a nevus is a common, harmless, and non-cancerous event. Next, melanocytes form a dysplastic nevus with large and atypical melanocytes. This is followed by a radial growth phase and in situ melanoma, which is usually confined to the epidermis. The radial growth phase is followed by the vertical growth phase and the tumor starts to spread into the dermis and subcutis forming a malignant melanoma. Finally, the tumor starts to metastasize into distant tissues, primarily to lymph nodes, and skin, but also to the lungs, bone, liver, brain, and small intestine. (Chin *et al*., 1998; Patel *et al*., 2020)

Melanoma is treated with surgery, radiotherapy, chemotherapy, photodynamic therapy, immunotherapy, and targeted therapy. If melanoma is detected early, in stages I or II, it is usually curable with surgery. (Domingues *et al*., 2018; Patel *et al*., 2020) In association with the surgery, a biopsy can be taken from the sentinel lymph node to exclude the possibility of metastasis (Patel *et al*., 2020). However, in stages III and IV, when the tumor has spread, melanoma is a very aggressive cancer with limited treatment options (Batus *et al*., 2013; Patel *et al*., 2020). In these later stages, more systemic treatments are needed, such as chemotherapy, targeted therapy, and immunotherapy (Domingues *et al*., 2018; Batus *et al*., 2013; Patel *et al*., 2020). Before immunotherapies, the five-year survival rate for metastatic melanoma was only 15–20 %. Luckily, immunotherapies have increased the long-term survival rate by up to 50 %, but the variation between patients remains high. (Dickson & Gershenwald, 2011; Dobry *et al*., 2018; Larkin *et al*., 2019; Patel *et al*., 2020; Robert *et al*., 2019; Silva & Long, 2017)

1.3.2 The MAPK pathway in melanoma

The development of a malignant tumor starts after melanocytes develop molecular changes in growth regulatory pathways. These molecular changes can occur, for example, in the MAPK signaling pathway. The MAPK pathway is a conserved signaling pathway that transmits forward extracellular signals that guide and control cell proliferation, growth, differentiation, migration, and apoptosis. Thus, mutations in this pathway have multiple effects on cell function that can drive the development and progression of cancer. (Savoia *et al*., 2019; Patel *et al*., 2020; Dhillon *et al*., 2007; Burotto *et al*., 2014)

Physiologically the MAPK pathway activation is initiated when a hormone, growth factor, or cytokine binds into a transmembrane protein, a receptor tyrosine kinase (RTK). The RTKs dimerize, undergo autophosphorylation, and are bound by adaptor proteins (mainly Growth factor receptor-bound protein 2 (GRB2)), which link guanine nucleotide exchange factors, such as Son of Sevenless homolog (SOS), to RTKs. This leads to the replacement of GDP to GTP in Ras-GTPases (KRAS, Neuroblastoma RAS viral oncogene homolog (NRAS), and HRas proto-oncogene (HRAS)). The Ras-GTPase subsequently phosphorylates one of the three isoforms of RAF serine-threonine protein kinases: ARAF, BRAF, or CRAF. The RAFs phosphorylate and activate MEK1 and MEK2 kinases, which eventually phosphorylate ERK1 and ERK2, the only known target molecules of MEKs. Finally, the ERKs can directly or indirectly affect the cell's function by phosphorylating several different proteins in the cytoplasm and nucleus. This eventually leads to changes in cell proliferation, survival, and apoptosis. (Savoia *et al*., 2019; Kun *et al*., 2021) A schematic of the MAPK pathway is illustrated in Figure 3.

NRAS is the most frequently mutated RAS in melanoma (found mutated in 15–20 % of melanomas) whereas mutations in *HRAS* and *KRAS* are rare (McCain, 2013). However, the most common mutations resulting in the increased activation of the MAPK pathway are found in the *BRAF* gene (Burotto *et al*., 2014; Dhillon *et al*., 2007; Long *et al*., 2011; Cheng *et al*., 2017). Indeed, mutations in the *BRAF* are present in over 50 % of the melanomas that have metastasized (Davies *et al*., 2002; Burotto *et al*., 2014; Cheng *et al*., 2017; Patel *et al*., 2020; Pollock *et al*., 2002; Omholt *et al*., 2003; Dhillon *et al*., 2007).

The most common BRAF mutation is the $BRAF^{V600E}$ which accounts for 80–90 % of mutations found in this kinase. In this mutation, the 600th amino acid valine (V) is substituted with glutamic acid (E). (Davies *et al*., 2002; Savoia *et al*., 2019; Omholt *et al*., 2003; McCain, 2013) The mutated $BRAF^{V600E}$ breaks out from the RAS-GTP-mediated regulation, begins to activate independently, and avoids the inhibition from repressor molecules, such as Sprouty RTK Signaling Antagonist 2 (SPRY2), which leads to the MAPK pathway overactivation (Dhillon *et al*., 2007; Kun *et al*., 2021). Patients with BRAF-mutant melanoma are usually younger than patients with wild-type BRAF (Patel *et al*., 2020; Hodis *et al*., 2012; Long *et al*., 2011), and the tumor can locate in regions that have not been chronically exposed to the sun (Long *et al*., 2011; Cheng *et al*., 2017; Burotto *et al*., 2014; Dhillon *et al*., 2007; Hodis *et al*., 2012). BRAF-mutant melanoma patients have also a shorter survival time than patients with non-BRAF-mutant melanoma (Patel *et al*., 2020; Long *et al*., 2011; Cheng *et al*., 2017; Burotto *et al*., 2014; Dhillon *et al*., 2007).

The current standard of care for BRAF-mutant metastatic melanoma includes metastasectomy if the patient is eligible for the procedure, and a treatment regimen with molecularly targeted therapies or immune checkpoint inhibitors is designed for the patient (Cheng *et al*., 2017; Patel *et al*., 2020). Currently, the molecularly targeted therapies consist of a combination treatment with BRAF and MEK inhibitors. However, treatment with BRAF and MEK inhibitors eventually leads to the emergence of resistance against these inhibitors, which has been a trigger for the development of immune therapies and small molecule inhibitors with new targets. (Patel *et al*., 2020) Currently available immunotherapies against metastatic melanoma target cytotoxic T-lymphocyte antigen 4 (CTLA-4) and programmed cell death protein 1 (PD1) (Millet *et al*., 2017; Patel *et al*., 2020). New small molecule inhibitors target for example C-ros oncogene (ROS) and AXL, which have been associated with the emergence of drug resistance (Patel *et al*., 2020).

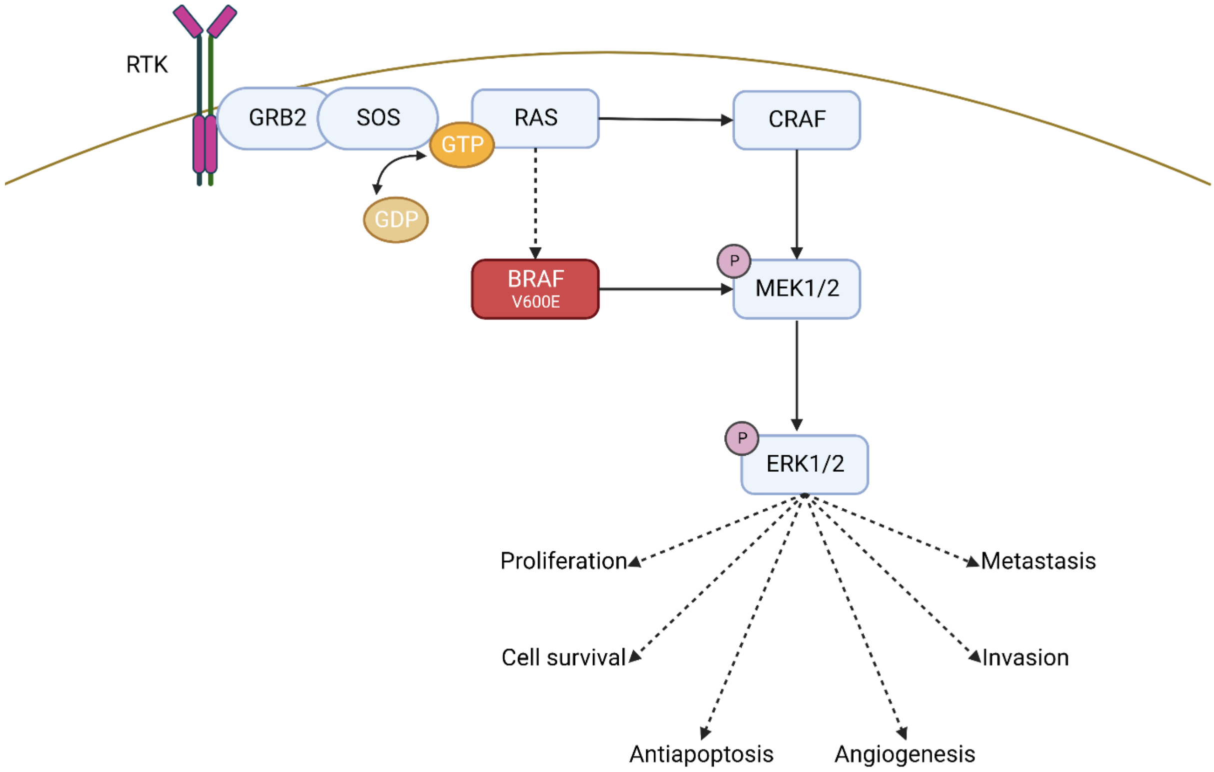

Figure 3. The MAPK pathway. In physiological conditions, the MAPK pathway is activated by the binding of a hormone, growth factor, or cytokine into the receptor tyrosine kinase (RTK). The RTKs dimerize, undergo autophosphorylation, and bind to guanine nucleotide exchange factors (GRB2, SOS). The guanine nucleotide exchange factors catalyze the replacement of GDP to GTP in Ras-GTPases (RAS). Subsequently, the Ras-GTPase phosphorylates RAF serine-threonine protein kinases (CRAF, BRAF), which further phosphorylate MEK1/2. The signaling cascade finally leads to the phosphorylation of ERK1/2. The ERK1/2 can phosphorylate several proteins in the cell's cytoplasm and nucleus, which leads to the changes in cell's function. These changes include decreased apoptosis and increased cell proliferation, survival, angiogenesis, metastasis, and invasion. In BRAF mutant melanoma the BRAF is constitutively active due to genetic mutations BRAF, such as V600E. This leads to the overactivation of the MAPK pathway and aberrant cell growth that contributes to the development and progression of the melanoma tumor. Modified from Kun *et al.*, 2021. The figure is created with BioRender.com.

1.3.3 BRAF and MEK inhibitors in the treatment of BRAF-mutant melanoma

Before targeted therapies, the patients with BRAF-mutant metastatic melanoma had a worse prognosis than patients with wildtype BRAF (Long *et al*., 2011; Sullivan & Flaherty, 2013). The development of compounds targeting the MAPK pathway has improved the prognosis of melanoma patients with BRAF mutation. Targeted therapies have neutralized the negative impact of BRAF mutation and have even improved the prognosis over patients with wild-type BRAF. (Long *et al.*, 2011)

The BRAF inhibitors are small molecules that target the mutated BRAF either by binding into an ATP binding pocket of an activated BRAF or into the hydrophobic binding site next to the ATP binding pocket, which stabilizes the BRAF into its inactive conformation (Savoia *et al.*, 2019). Sorafenib was the first non-selective BRAF inhibitor that targeted also multiple tyrosine kinases and RTKs, but it failed to show improvement in the progression-free survival (PFS) and other efficacy endpoints in the phase 3 trial (McCain, 2013). In 2011 vemurafenib, the first inhibitor targeting the ATP-binding domain of mutated $BRAF^{V600E/D/R}$, became on the market (Savoia *et al.*, 2019; McCain, 2013). Dabrafenib is a $BRAF^{V600E/K/D}$ inhibitor that binds into the ATP binding pocket of an activated BRAF. It was approved by the U.S. Food and Drug Administration (FDA) in 2013, and it is used for the treatment of patients with unresectable or metastatic melanoma. (Savoia *et al.*, 2019) Dabrafenib showed a favorable effect on PFS compared to the dacarbazine (5.1 months for dabrafenib vs. 2.7 months for dacarbazine; $p < 0.0001$), although the effect on overall survival (OS) was not statistically significant (Hauschild *et al.*, 2012).

Trametinib is a reversible small molecule inhibitor of MEK1 and MEK2 kinases. It was first approved by the FDA in 2013 for the treatment of unresectable or metastatic melanoma with $BRAF^{V600E}$ or $BRAF^{V600K}$ mutation. Trametinib can be used as a monotherapy, but it is more often combined with dabrafenib. (Savoia *et al.*, 2019) The combination was approved in 2018 by the FDA for the treatment of unresectable or metastatic melanoma with $BRAF^{V600E/K}$ mutations (Kun *et al.*, 2021). The combination has been shown to improve and prolong the effect of the treatment compared to the dabrafenib monotherapy, which is observed as longer PFS (median PFS was 9.4 months for dabrafenib and trametinib combination vs. 5.8 months for dabrafenib monotherapy; $P < 0.001$), better OS (median OS was 25.1 months for dabrafenib and trametinib combination vs. 18.7 months for dabrafenib monotherapy; $P = 0.0107$) and delayed emergence of treatment resistance (Kun *et al.*, 2021; Long *et al.*, 2015, 2017; Flaherty *et al.*, 2012). Additionally, the combination has shown fewer adverse events compared to dabrafenib monotherapy (Flaherty *et al.*, 2012; Long *et al.*, 2014a). Thus, the combined treatment with dabrafenib and trametinib has become the standard of care for melanoma patients harboring BRAF mutations (Long *et al.*, 2015; Kun *et al.*, 2021; Long *et al.*, 2017).

1.3.4 Resistance to BRAF and MEK inhibitors in melanoma

BRAF inhibition alone is an effective treatment for BRAF mutant melanoma, but resistance occurs rapidly through different mechanisms. The most common driver of BRAF inhibitor resistance is the reactivation of the MAPK pathway through activating mutations in MEK1/2. In addition, *BRAF* amplification, aberrant BRAF slicing (BRAF^{V600E} splice variants), upregulation of RTKs, and activating mutations in *NRAS* have been found to drive the resistance to BRAF inhibitors through the MAPK pathway reactivation. (Long *et al*., 2014; Marin-Bejar *et al*., 2021; Poulikakos *et al*., 2011; Shi *et al*., 2012, 2014) BRAF inhibitor resistance can also emerge independently from the MAPK pathway, for example, through RTK-mediated activation of alternative survival pathways, such as the PI3K-AKT pathway (Nazarian *et al*., 2010; Yang *et al*., 2021; McCain, 2013). Also, activating genetic mutations in the PI3K-PTEN-AKT pathway members have been discovered in 22 % of progressive melanomas (Shi *et al*., 2014). The enrichments of the Mammalian target of rapamycin (mTOR) signaling and other stress-response signatures have been found in melanoma cells escaping BRAF inhibition (Yang *et al*., 2021). In addition, researchers have found that BRAF inhibitor-resistant cells have enriched EMT pathways and mesenchymal-like dedifferentiated gene signatures (Yang *et al*., 2021). The tumor microenvironment has also been found to contribute to the emergence of BRAF inhibitor resistance (Straussman *et al*., 2012).

As with BRAF inhibitor monotherapy, the most common resistance mechanism to MEK inhibitor monotherapy is the reactivation of the MAPK pathway. This reactivation can happen after alterations or genetic mutations occur in the components of the signaling cascade, such as RAS, RAF, Neurofibromin-1, or MEK1/2. (Caunt *et al*., 2015; Kozar *et al*., 2019) For example, mutations in MEK1/2 can result in their constitutive activation or the MEK inhibitor binding site may undergo structural changes that can prevent the drug binding (Patel *et al*., 2020). Importantly, several RTKs upstream of the MAPK pathway have been shown to mutate in response to MEK inhibition (Caunt *et al*., 2015). RTKs are shared by multiple signaling pathways, through which they can promote resistance to MEK inhibition independently from the MAPK pathway (Kun *et al*., 2021). The most mutated signaling pathways contributing to MEK inhibitor resistance include PI3K and STAT (Caunt *et al*., 2015; Kun *et al*., 2021; Dai *et al*., 2011; Halilovic *et al*., 2010). Moreover, it has been discovered that alterations in the Hippo pathway promote adaptive resistance to MEK inhibition (Kun *et al*., 2021; Lin *et al*., 2015). Indeed, it has been shown that the inhibition of one pathway often shifts the cells to use other pathways to drive cell proliferation and survival (Kun *et al*., 2021).

Despite that many BRAF-mutant tumors have a good response to MEK and BRAF inhibitors, eventually, over 50 % of patients treated with a monotherapy develop tumor recurrence only after 6 to 8 months of treatment (Patel *et al*., 2020; Long *et al*., 2014b; Hauschild *et al*., 2012; Welsh *et al*., 2016). Therefore, BRAF and MEK inhibitors are often combined to achieve a more sustained effect (Savoia *et al*., 2019; Patel *et al*., 2020; Long *et al*., 2014b). However, 50 % of patients treated with the combination of dabrafenib and trametinib developed resistance at 9–10 months of treatment (Long *et al*., 2014a). There is also a population of patients with BRAF-mutant melanoma who carry intrinsic resistance mechanisms to monotherapy and combination therapy, and they show no clinically observed response to these treatments (Patel *et al*., 2020).

Resistance to the combination of BRAF and MEK inhibitors includes very similar resistance mechanisms to resistance to BRAF inhibitor monotherapy. However, it has been shown that tumors resistant to the combination treatment carry a greater magnitude of genetic alterations, and the alterations are more frequently found in combination with each other (Moriceau *et al*., 2015). As in resistance to BRAF or MEK inhibitor monotherapies, the most common resistance mechanism to the combined BRAF/MEK inhibition involves the reactivation of the MAPK pathway. The MAPK pathway can be reactivated, for example, by *BRAF* amplification, gain-of-function mutations in $BRAF^{V600E/K}$, *MEK1*, *MEK2*, *KRAS*, or *NRAS*, or by deletion of Dual specificity protein phosphatase 4 (*DUSP4*) (Moriceau *et al*., 2015; Hugo *et al*., 2015; Villanueva *et al*., 2013; Long *et al*., 2014a). In contrast to the resistance to BRAF inhibitor monotherapy, alternative BRAF splicing does not seem to be a resistance mechanism to the combination treatment (Long *et al*., 2014a).

The resistance mechanisms that do not involve the MAPK pathway are proposed to be common in BRAF/MEK inhibition resistance because numerous resistance mechanisms to BRAF inhibitor monotherapy remain sensitive to MEK inhibitors, or combined BRAF/MEK inhibition (Long *et al*., 2014a). Indeed, genetic changes are often found in the parallel PI3K-AKT pathway (Wang *et al*., 2021). Genetic alterations found in this pathway include loss-of-function mutations or deletions in *PTEN*, *SOS1*, *AXL*, MET Proto-Oncogene (*MET*), *EGFR*, *SOS2*, Rac Family Small GTPase 2 (*RAC2*), and Phosphoinositide-3-Kinase Regulatory Subunit 1 (*PIK3R1*) (Long *et al*., 2014a; Wang *et al*., 2021; Moriceau *et al*., 2015; Hugo *et al*., 2015). For example, dysfunctional PTEN may result in the overactivation of the PI3K-AKT pathway that drives the development of resistance. However, it is known that mutations in *PTEN* alone are not sufficient to cause resistance and additional changes are usually found in the phosphorylation of AKT. (Patel *et al*., 2020) Mutations have been also discovered in genes that are important for cell cycle regulation, such as

Retinoblastoma 1 (*RB1*), Tumor protein 53 (*TP53)*, and *CDKN2A* (Moriceau *et al*., 2015; Long *et al*., 2014a; Hugo *et al*., 2015).

It has been found that 20 % of resistant melanomas have no resistance driving single-nucleotide alterations or BRAF amplifications that could explain the emergence of resistance. These melanoma cells may use non-genetic resistance mechanisms to evade the combination treatment. (Marin-Bejar *et al*., 2021) The non-genetic resistance mechanisms to BRAF/MEK inhibition can manifest alone or in combination with genetic resistance (Moriceau *et al*., 2015). Several transcriptional mechanisms have been identified, including overexpression of mutant NRAS mRNA and protein (Moriceau *et al*., 2015), overexpression of wildtype *NRAS* and *KRAS*, and up- and downregulation of *PTEN*, *CDKN2A*, and *DUSP4* (Hugo *et al*., 2015). The combination and monotherapy-resistant cells can also adopt different metabolic pathways and transcriptional states that are more tolerant to the treatment. The resistant melanoma cells can change toward a dedifferentiated cell state that has high AXL expression and low Microphthalmia-associated transcription factor (MITF) and SRY-box transcription factor 10 (SOX10) expressions. (Yang *et al*., 2021) Interestingly, it has been shown that melanoma cells with high MITF expression are more responsive to the therapy than the cells with low MITF expression. The low MITF expression has also been associated with an invasive gene signature. (Hoek *et al*., 2008; Konieczkowski *et al*., 2014; Kun *et al*., 2021)

Studies have shown that increased activation of YAP/TAZ-TEAD may function as a non-genetic resistance mechanism to targeted therapies in melanoma (Hugo *et al*., 2015; Kim *et al*., 2016; Lin *et al*., 2015; Fisher *et al*., 2017). A previous study has shown that the *YAP1* gene signature was enriched without simultaneous mRNA over-expression in MAPK pathway inhibition-resistant melanoma tumors and cell lines. These resistant cell lines had elevated YAP1 and phospho-YAP1 protein levels in the cytoplasm and/or nucleus compared to the treatment naïve parental cell lines. Interestingly, *YAP1* knockdown resensitized the cells to BRAF or BRAF/MEK inhibition. (Hugo *et al*., 2015) In another study, *YAP1* knockdown did not increase the responsiveness of melanoma cells to cytotoxic chemotherapy but improved the response to vemurafenib and trametinib. *YAP1* and *TAZ* overexpressions also decreased sensitivity to vemurafenib and trametinib in HCC364 lung adenocarcinoma cells. (Lin *et al*., 2015) Lastly, it has been suggested that downregulations of MITF and SOX10 in treatment-resistant melanoma cells are driven by YAP overexpression, and it was shown that YAP expression affected the levels of EGFR, c-MYC, phosphorylated ERK (pERK), and phosphorylated AKT in melanoma cells treated with vemurafenib (Kim *et al*., 2016).

Changes in the tumor microenvironment and intra-tumoral immunity have been found in combination-resistant cells. An analysis of gene enrichment data of resistant and matched baseline tumors revealed recurring enrichments in signatures associated with Nuclear factor kappa B (NFκB) signaling, inflammation, and monocyte functions. Also, over-expression of MET proto-oncogene (*MET*) and Interleukin 8 (*IL-8*) genes, macrophage markers (Cluster of Differentiation 163 (CD163) and CD163 Molecule Like 1 (CD163L1)), and genes involved in leukocyte function (e.g., Chemokine (C-C motif) ligand 8 (*CCL8)* and Colony Stimulating Factor 3 Receptor (*CSF3R*)) have been found. The resistant tumors may also express Cluster of differentiation 8 (CD8) T-cell deficiency and exhaustion. Additionally, down-regulation of immune response modulation gene *CTLA4*, antigen-presenting genes (e.g., Major histocompatibility complex, class I, A and B (*HLA-A* and *HLA-B*), Transporter associated with antigen processing 1 (*TAP1*), and β2 microglobulin (*B2M*)), and Wingless-related integration site (Wnt) signaling genes (e.g., Lymphoid enhancer-binding factor 1 (*LEF1*), Wnt family member 10A and 11 (*WNT10A* and *WNT11*), and Frizzled-6 (*FZD6*)) have been discovered. Also, epigenetic mechanisms, such as changes in DNA methylation have been found. (Hugo *et al*., 2015)

1.4 Summary and the research project

Metastasized melanoma is an aggressive skin cancer with a high mortality rate. Over half of the metastasized melanomas are driven by genetic mutations in the MAPK pathway kinase BRAF. The current standard of care in BRAF-mutant melanoma targets the BRAF and the downstream kinase MEK. Unfortunately, resistance to these compounds emerges rapidly and inexorably. Hence, it is of utmost importance to find novel therapy options for patients developing resistance. One proposed resistance mechanism has been the activation and nuclear localization of the Hippo pathway effector YAP, the co-activator of TEAD transcription factors. YAP-TEAD transcriptionally mediates resistance to targeted therapies by restoring cell proliferation, inhibiting apoptosis, and increasing the cells' invasive and metastatic capacity. Thus, the disruption of YAP-TEAD interaction provides a novel target to prevent the emergence of treatment resistance to BRAF/MEK inhibition.

The rationale for this research project is to assess if combined inhibition of BRAF and MEK activates YAP in a BRAF-mutant melanoma cell line A375, and whether a triple combination of BRAF, MEK, and TEAD inhibitors is more efficacious than the BRAF/MEK inhibition. The study aims to find a new resistance mechanism to targeted therapies in the A375 cell line and to find a new indication for TEAD inhibitor treatment in preventing the emergence of treatment resistance to targeted BRAF/MEK inhibition.

The study is conducted by using a combination of the BRAF inhibitor dabrafenib and the MEK inhibitor trametinib and their effect in ERK phosphorylation, cell proliferation, apoptosis, senescence, cellular morphology, and YAP-TEAD activation is measured in A375 cells. The effect of combined dabrafenib and trametinib treatment is assessed on treatment days 3, 7, and 10, as well as after a 14-week continuous treatment. For the triple combination treatment, two novel TEADi, Compound A (Orion Pharma) and VT-103 (Tang *et al*., 2021) are used and the cell proliferation, apoptosis, senescence, cell morphology, and YAP-TEAD activation in the cells are measured.

2 RESULTS

2.1 BRAF/MEK inhibition reduces cell growth and ERK phosphorylation in A375 cells

To study the effect of dabrafenib and trametinib treatment on BRAF mutant melanoma, A375, a human metastatic melanoma cell line harboring $BRAF^{V600E}$ mutation, was used. First, a dose-response with 1 nM–10 µM concentrations of dabrafenib or trametinib was performed to study the potency of these compounds in inhibiting the growth of A375 cells. The IC50 values for dabrafenib and trametinib were 3.6 nM and 2.3 nM, respectively (Figure 4. A). The IC50 value represents the minimal concentration of a compound that is required for half-maximal inhibition in cell proliferation. During the dose-response assay, the cell number decreased dose-dependently, but no cell death was observed.

To identify the minimum concentrations of dabrafenib and trametinib that inhibit A375 cell growth when used in combination, 5 concentrations (1 nM, 3 nM, 10 nM, 30 nM, and 100 nM) were selected based on the dose-response curves of each compound. The minimum combination concentrations having a maximal inhibitory effect were selected to avoid unspecific and toxicological effects. Especially, the concentration of trametinib was selected to be as low as possible because MEK inhibitors block the MAPK pathway also in healthy tissues which contributes to their bad tolerability among patients (Sullivan and Flaherty, 2013).

The number, shape, size, and intensity of nuclei and the confluency of the cells were used to evaluate the optimal concentrations for combination treatment. The addition of 30 nM dabrafenib reduced the cell number by 79 % showing near maximal effect (Figure 4. B), and it had a moderate effect on the nuclear roundness (Figure 4. C–D). This concentration was also near the IC95 value of dabrafenib (23.7 nM) that was obtained from the dose-response curve (Figure 4. A). The IC95 represents the minimal concentration of a compound that is required for maximal inhibition in cell proliferation. The 1 nM concentration of trametinib reduced the cell number by 51 % (Figure 4. B) without affecting nuclear roundness (Figure 4. C–D). However, when 1 nM trametinib was combined with 30 nM dabrafenib the cell number was inhibited by 87 % (Figure 4. B) and there was a dramatic effect on nuclear roundness (Figure 4. C–D). Indeed, 30 nM dabrafenib in combination with 1 nM trametinib was more efficacious than dabrafenib or trametinib alone, and the combination showed a maximal inhibitory effect. These concentrations were also in line with the concentrations used previously in the literature (Lin *et al*., 2015; Marin-Bejar *et al*., 2021). In follow-up studies, a combination of 30 nM dabrafenib and 1 nM trametinib (hereby termed DT) was used.

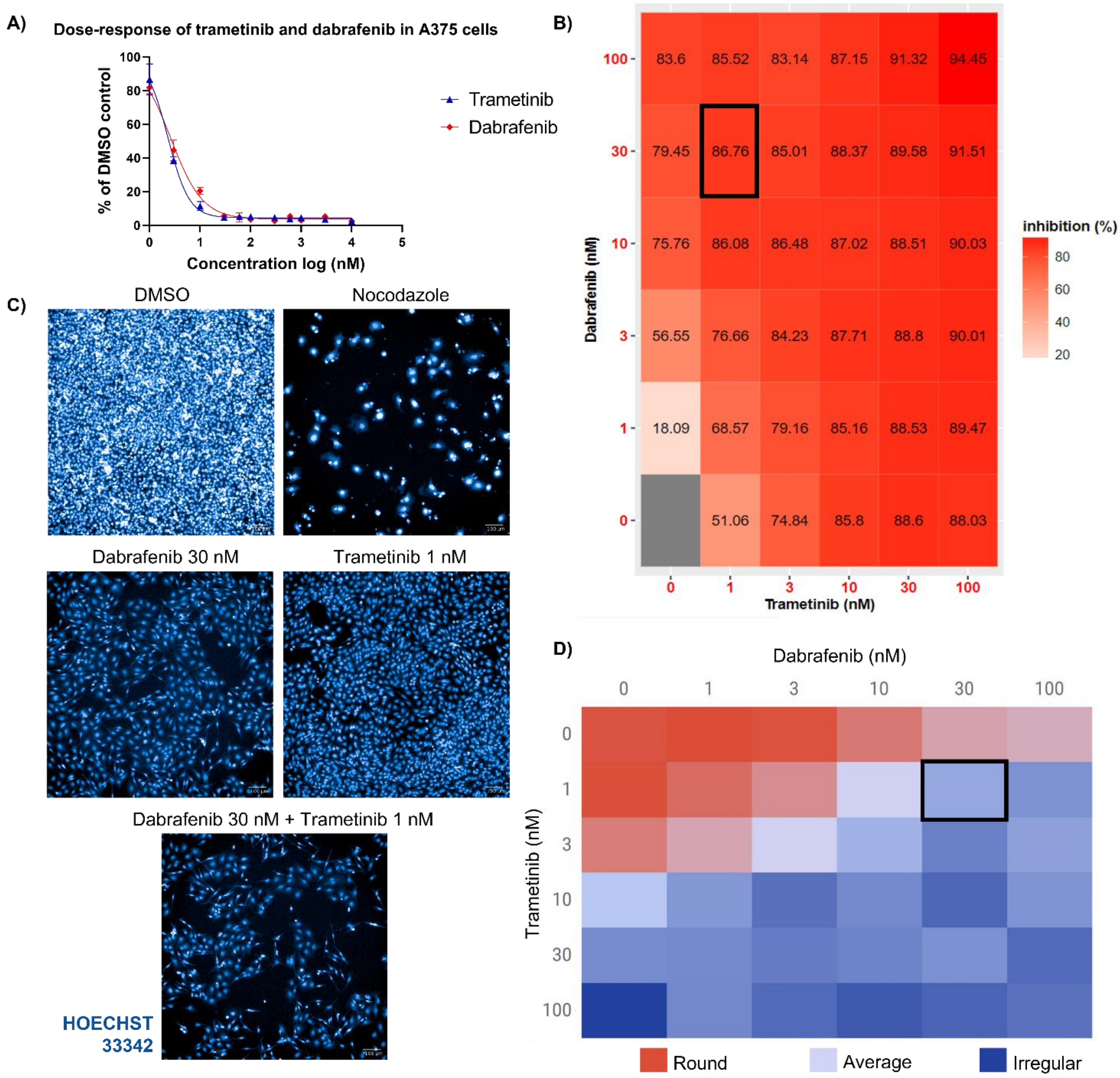

Figure 4. Dabrafenib and trametinib for inhibition of cell growth in A375 cells A) Dose-response curve. Cells were incubated for 4 days with the compounds. The IC50 values for dabrafenib and trametinib were 3.6 nM and 2.3 nM, respectively. Data are shown as means ± s.e.m.; *n* = 4 biological replicates. B) Inhibition percentage with 1–100 nM dabrafenib and trametinib alone or in combination. The data are visualized with SynergyFinder 3.0 web application (Ianevski *et al.*, 2022). Data are shown as means; *n* = 4 biological replicates. C) Immunofluorescence images for HOECHST 33342 staining showing nuclear morphology and cell number after a 3-day incubation with 30 nM dabrafenib and 1 nM trametinib alone or in combination. DMSO and nocodazole were used as controls. Bars 100 µm, 10x magnification. D) Heatmap showing the nuclear roundness in response to different concentrations of dabrafenib and trametinib monotherapy or combination therapy. Red represents round nuclear morphology and blue irregular morphology. The data are visualized with Spotfire 12 Data visualization and Analytics Software (TIBCO).

To further study the effect of dabrafenib and DT treatment on cell growth and the MAPK pathway, the cells were treated with 30 nM dabrafenib (hereby dabrafenib) or DT for up to 10 days. The number of cells in each treatment was calculated with DAPI staining and the MAPK pathway activity was measured with an antibody against pERK. Dabrafenib decreased ERK phosphorylation by 95 % (Figure 5. A–B) and substantially decreased the cell number compared to the control (DMSO) after 3 days of treatment (Figure 5. C). Unfortunately, the activation of ERK could not be measured from the control wells on treatment days 7 and 10 because the wells became too confluent to obtain reliable data. Also, different time points could not be compared to each other due to different cell numbers and culture times. On the 10th day of dabrafenib treatment, 30 % of the cells were pERK positive (Figure 5. A–B) and the cell number was significantly lower than in control wells (Figure 5. C). Similarly, a 3-day DT treatment decreased ERK phosphorylation by 93 % (Figure 5. A–B) and dramatically reduced the cell number compared to the control (Figure 5. C). After 10 treatment days with DT, the proportion of pERK-positive cells was only 16 % (Figure 5. A–B) and the cell number was significantly lower compared to the control (Figure 5. C). Thus, the initial responses to dabrafenib and DT treatments were very similar, but DT treatment led to more pronounced MAPK pathway inhibition. These results confirmed that *in vitro* double inhibition of BRAF and MEK is more efficacious than BRAF inhibition alone.

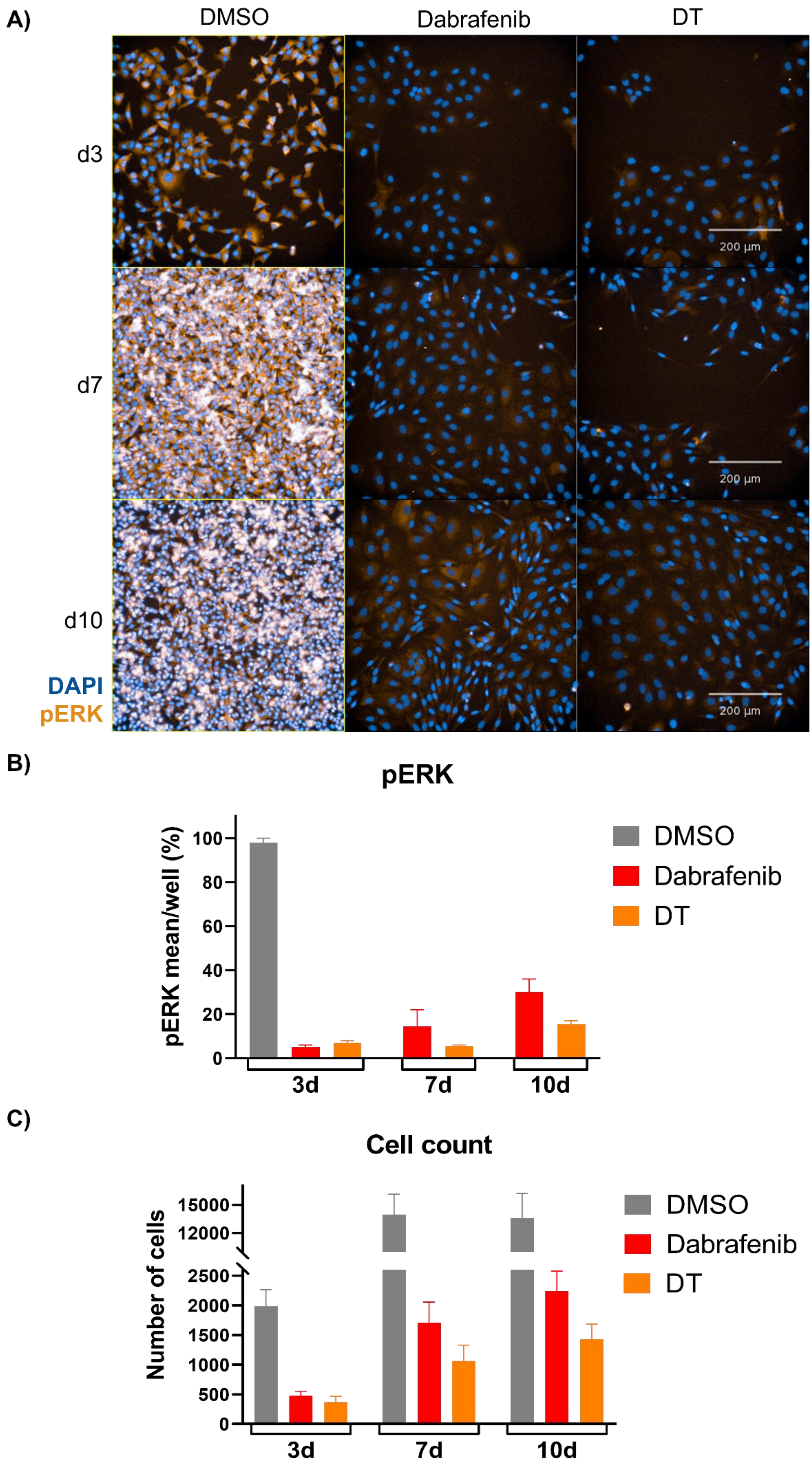

A)
DMSO
Dabrafenib
DT
d3
d7
d10
DAPI
pERK
200 µm
200 µm
200 µm
B)
pERK
pERK mean/well (%)
100
80
60
40
20
0
3d
7d
10d
DMSO
Dabrafenib
DT
C)
Cell count
Number of cells
15000
12000
2500
2000
1500
1000
500
0
3d
7d
10d
DMSO
Dabrafenib
DT

Figure 5. The activation of the MAPK pathway and cell count of A375 cells under 30 nM dabrafenib alone or in combination with 1 nM trametinib. A–B) Immunofluorescence images for phosphorylated ERK (orange) and DAPI (blue) (A) and their quantification (B). The cells with pERK intensity >1200 were considered pERK positive. Data are shown as means ± s.e.m.; *n* = 2 biological replicates. Bars 200 μm, 20x magnification. C) Quantification of the number of DAPI-positive cells. Data are shown as means ± s.e.m.; *n* = 12 biological replicates.

2.2 BRAF/MEK inhibition reduces cell proliferation without affecting apoptosis and senescence in A375 cells

The reduced cell number in dabrafenib and DT-treated wells can be explained by the inhibition of cells' proliferative capacity, induction of apoptosis, or cellular senescence. Thus, the cells were stained for markers of these processes.

First, the Ki67 antibody was used to study the proliferation in A375 cells treated with dabrafenib or DT for up to 10 days. Ki67 is an antigen present in all active phases of the cell cycle and absent in quiescent cells (G0). Thus, the Ki67 antibody can be used to determine proliferating cancer cells (Li *et al*., 2015b). The treatment with either dabrafenib or DT distinctively decreased the proportion of Ki67-positive cells (Figure 6. A). After 3 days of treatment, the proportion of Ki67-positive cells had decreased by 42 % in dabrafenib-treated cells and by 63 % in DT-treated cells compared to the control (82 % of control cells were Ki67-positive) (Figure 6. B). On treatment day 3, most control cells were Ki67-positive whereas in dabrafenib and DT treatment only single cells were Ki67-positive (Figure 6. A). On the 10th day of treatment, the proportions of Ki67-positive cells in dabrafenib and DT were 6 % and 10 %, respectively. (Figure 6. B) Thus, the decreased cell proliferation accounted for the reduction in cell number upon dabrafenib or DT treatment.

Next, it was studied if apoptosis contributed to the reduced cell number during dabrafenib or DT treatment. To study the apoptosis, Caspase-3/7 reagent was added into the growth medium of A375 cells together with dabrafenib or DT. During a 5-day incubation period, no excessive apoptosis was observed in the treatment groups compared to the DMSO control (Figure 6. C). Conversely, there were more apoptotic cells in the control group because these wells became over-confluent over time. (Figure 6. C) Thus, apoptosis did not contribute to the reduction in cell number in response to dabrafenib or DT treatment.

Finally, it was studied if the cells became senescent in response to the dabrafenib and DT treatment. A375 cells were incubated with dabrafenib or DT for two days and the cells were stained with β-galactosidase, a marker of senescence (Dimri *et al*., 1995). No difference was observed in the number of senescent cells between the treatments and control. This finding suggested that senescence did not contribute to the cell phenotype. (Figure 6. D)

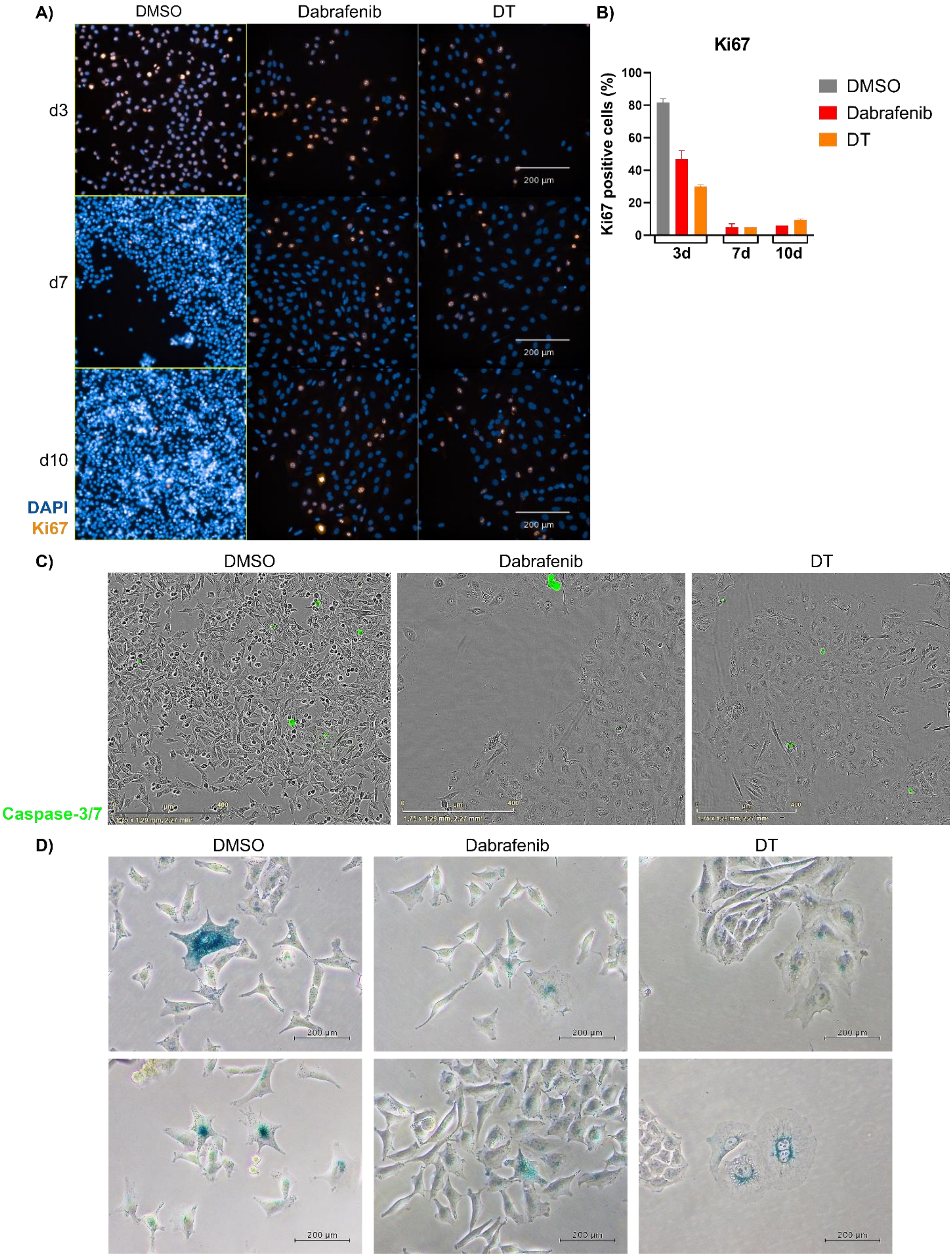

Figure 6. Proliferation, apoptosis, and senescence in A375 cells treated with 30 nM dabrafenib alone or in combination with 1 nM trametinib. A) Immunofluorescence images showing Ki67 positive cells (orange) on treatment days 3, 7, and 10. Nuclei are stained with DAPI (blue). Bars 200 µm, magnification 20x. B) Quantification of the immunofluorescence data showing the proportion of proliferating cells detected with the

Ki67 antibody. Cells with nuclear Ki67 intensity value >4500 were considered positive. Data are shown as means ± s.e.m.; n = 2 biological replicates. C) Apoptosis detected with Incucyte Caspase-3/7 Green Apoptosis Assay Reagent. The images were taken with Incucyte® S3 on the 4th day of treatment. Apoptotic cells are seen as light green. Bars 400 µm, 10x magnification. D) Light microscopy images of cells that were treated for 2 days with dabrafenib or DT and stained with Senescence β-Galactosidase Staining Kit. Senescent cells are stained blue. Bars 200 µm, 20x magnification.

2.3 BRAF/MEK inhibition induces morphological changes in A375 cells

The morphological changes induced by the administration of dabrafenib or DT were studied with phalloidin staining. Phalloidin is a toxin that binds to the filamentous actin (F-actin) (Kumari *et al*., 2020). The obtained immunofluorescence images were analyzed with Columbus software. The software was trained to identify three different morphological cell types: normal, large, and elongated.

The phalloidin staining showed that dabrafenib and DT treatments had induced drastic changes in the cell morphology (Figure 7. A). On treatment day 3 the proportion of cells with normal morphology noticeably decreased in the wells treated with dabrafenib or DT, and most of the cells became significantly enlarged and round (large phenotype) (Figure 7. A–B). On the 7th treatment day, approximately one-third of the treated cells exhibited large morphology and one-third had become elongated resembling the cells undergoing EMT (Kalluri and Weinberg, 2009) (Figure 7. A–B). These morphological changes persisted also on the 10th treatment day (Figure 7. A–B). These data suggested that treatment with dabrafenib or DT strongly affected the cell morphology, and the treatments might have induced an EMT-like phenotype switching (Pedri *et al*., 2022; Li *et al*., 2015a) in a proportion of cells.

To study if the treated cells were undergoing an EMT-like phenotype switching, the cells were stained with an antibody against vimentin, a type III intermediate filament expressed in mesenchymal cells, which overexpression is associated with an EMT-like phenotype switching and melanoma metastasis (Usman *et al*., 2021; Cristofani *et al*., 2022; Li *et al*., 2010; Pedri *et al*., 2022; Rad *et al*., 2016). The amount of vimentin increased after 3 days of dabrafenib and DT treatment compared to the control (Figure 7. C–D). The increase was more pronounced in DT cells (Figure 7. D). On the 7th and 10th treatment days, vimentin intensity remained higher in DT-treated cells than in dabrafenib-treated cells (Figure 7. C–D). Thus, the cells treated with dabrafenib or DT may undergo an EMT-like phenotype switching. Interestingly, the vimentin expression in DT-cells was higher than in dabrafenib-treated cells suggesting that more cells in the combination treatment might have been undergoing the phenotype switching than in dabrafenib treatment.

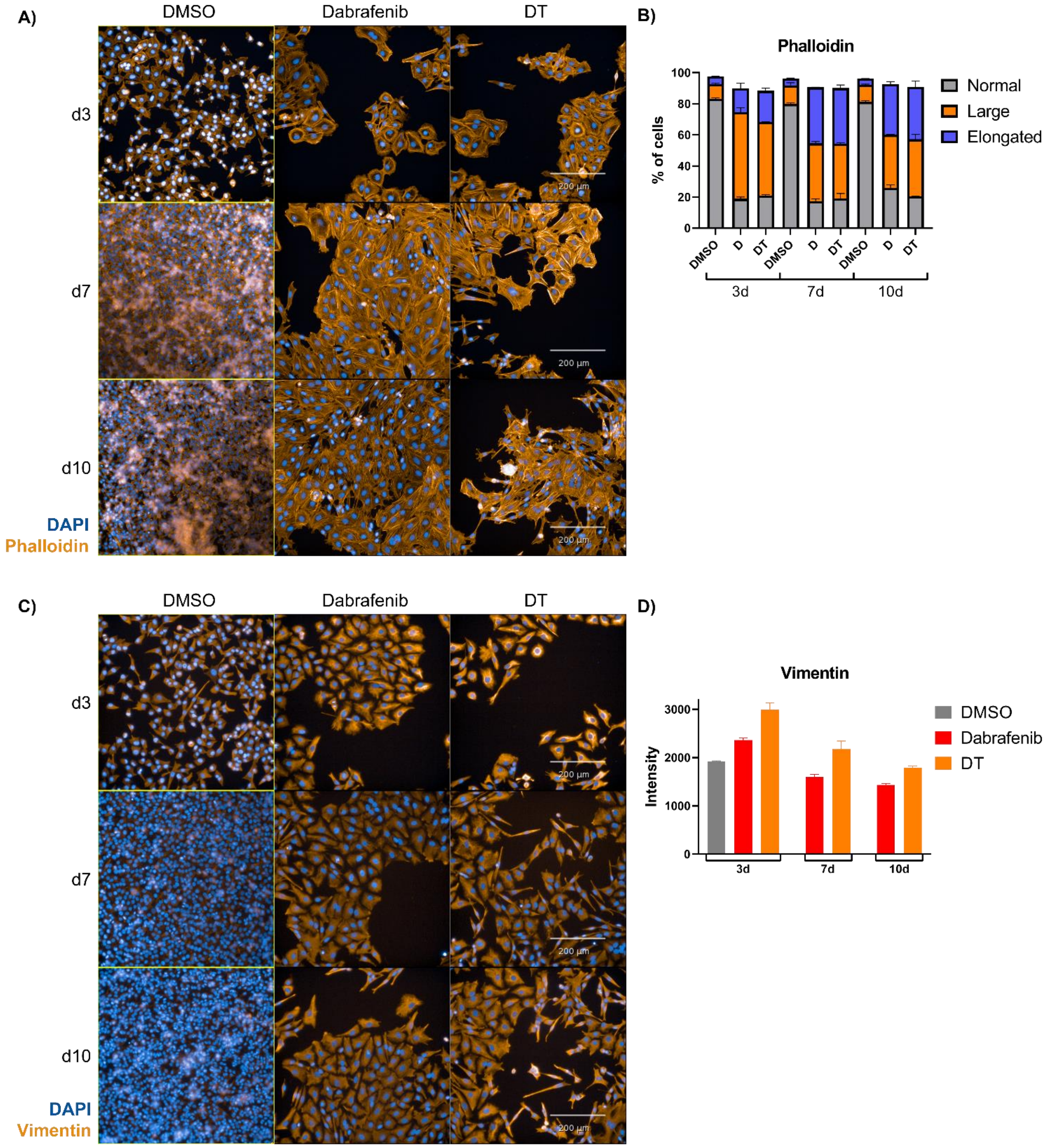

Figure 7. Cell morphology and EMT-marker vimentin expression in A375 cells treated with 30nM dabrafenib alone or in combination with 1nM trametinib. A) Immunofluorescence images for phalloidin staining (orange) and DAPI (blue). Bars 200 µm, magnification 20x. B) Quantification of different cell shapes identified with Columbus software. The cells in DMSO control were considered to express the normal phenotype. Data are shown as means ± s.e.m.; *n* = 2 biological replicates. C) Immunofluorescence images for vimentin (orange) and DAPI (blue). Bars 200 µm, magnification 20x. D) Quantification of vimentin intensity on a ring region around the nucleus. Data are shown as means ± s.e.m.; *n* = 2 biological replicates.

2.4 BRAF/MEK inhibition increases YAP1 nuclear localization and TEAD target gene expression

A previous study by Kim *et al.* has discovered that the nuclear localization of YAP increases in response to treatment with BRAF inhibitor vemurafenib. In addition, they showed that vemurafenib treatment induces actin cytoskeleton remodeling by increasing actin stress fiber formation and actomyosin tension, which leads to increased YAP/TAZ activation. This finding suggested that the Hippo pathway and actin cytoskeleton cooperatively contribute to the activation of YAP/TAZ in melanoma cell resistance to BRAF inhibition (Kim *et al*., 2016). To study if YAP/TAZ-TEAD were activated during dabrafenib or DT treatment, the nuclear localization of YAP1 was examined with a YAP1 antibody, and the expressions of *YAP1* and four YAP-TEAD target genes, *CYR61*, *CTGF*, *ANKRD1* (Ankyrin repeat domain 1), and *AMOTL2* (Angiomotin like 2) were measured by RT-qPCR during a 10-day incubation with the compounds.

After 3 days of treatment the proportion of cells with a high YAP1 nuclear to cytoplasmic (N/C) ratio, which indicated YAP1 nuclear localization and activation, was increased by 31 % in DT-treated cells and by 11 % in dabrafenib-treated cells compared to the control (43 % of control cells had YAP1 located into the nucleus) (Figure 8. A–B). The expressions of *CYR61* ($P < 0.0001$) and *CTGF* ($P = 0.0001$) were significantly increased in DT-treated cells compared to the control, while there was no significant difference in expressions of *AMOTL2* or *ANKRD1* (Figure 8. C). In addition, the expression of CYR61 was significantly higher ($P = 0{,}0148$) in DT-treated cells than in dabrafenib-treated cells (Figure 8. C). In dabrafenib-treated cells, the expressions of *CYR61* ($P = 0{,}0004$) and *CTGF* ($P = 0.0024$) were increased significantly compared to the control (Figure 8. C).

The N/C ratio of YAP1 could not be measured from the control wells at later time points because the wells became too confluent to obtain reliable data (Figure 8. A). In addition, different cell numbers and culture times prevented the comparison of YAP1 N/C ratio or gene expression data between different time points. On the 7th treatment day, the proportion of cells with a high YAP1 N/C ratio in dabrafenib- and DT-treated cells was 19 % and 32 %, respectively (Figure 8. B). The expressions of *CYR61* and *CTGF* were significantly increased in both, dabrafenib and DT-treated cells ($P < 0.0001$) compared to the control while the expressions of *ANKRD1* and *AMOTL2* were not significantly altered (Figure 8. D).

Finally, on the 10th treatment day, the proportion of cells with a high YAP1 N/C ratio was 13 % in dabrafenib-treated cells and 26 % in DT-treated cells. (Figure 8. B) The expressions of *CYR61*and *CTGF* remained significantly increased ($P < 0.0001$) in dabrafenib and DT treated cells compared to the control, and the expressions of *AMOTL2* and *ANKRD1* were not significantly altered (Figure 8. E). Additionally, *CYR61* expression was significantly higher ($P = 0.0067$) in DT-treated cells compared to dabrafenib-treated cells (Figure 8. E).

The expression of *YAP1* was not significantly altered between the treatment groups on any treatment day (Figure 8. C–E). This suggested that neither dabrafenib- nor DT-treatment directly affected *YAP1* expression, and the changes in YAP-TEAD target gene expression were not induced by changes in *YAP1* expression.

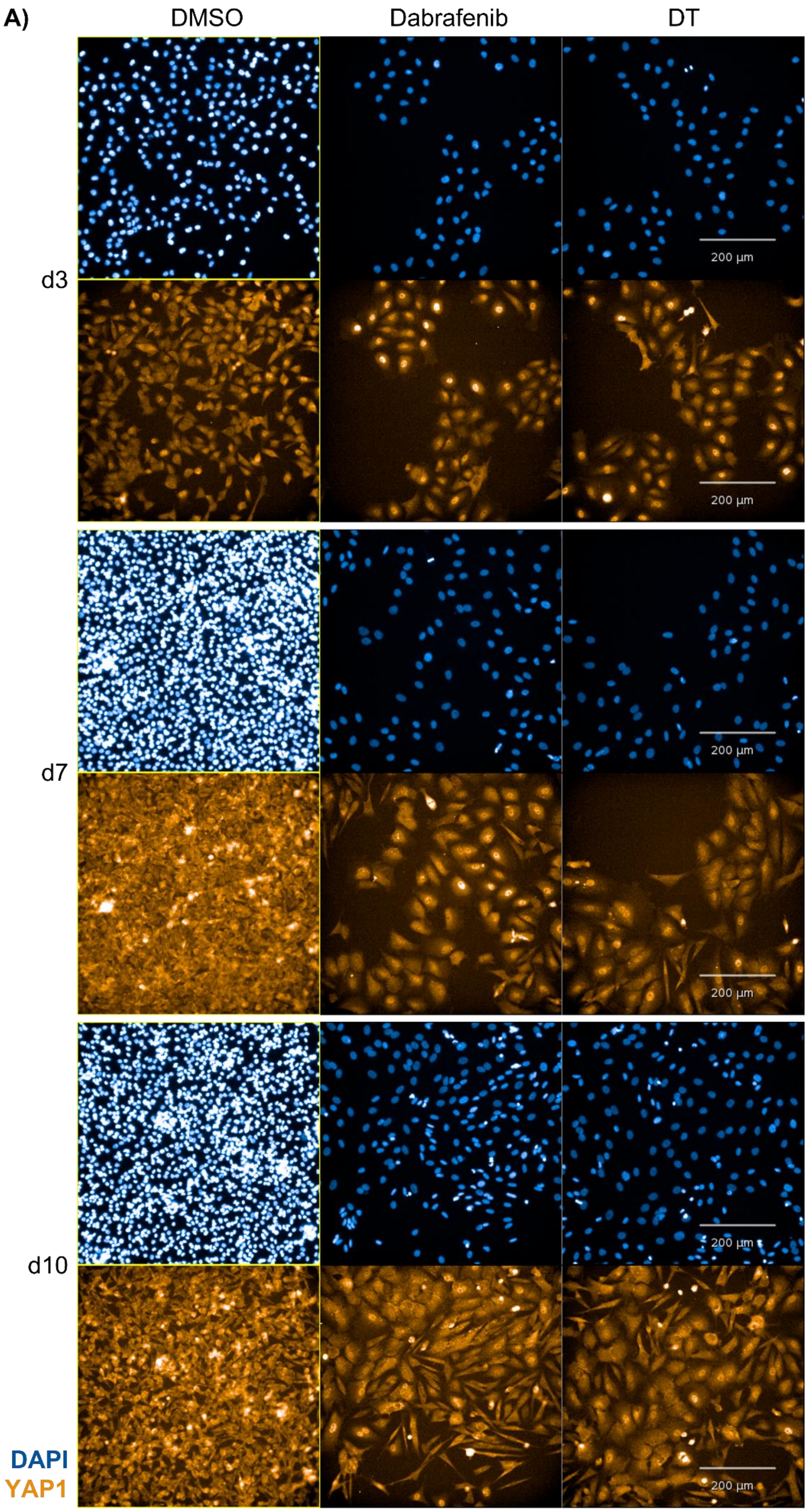
A)
DMSO
Dabrafenib
DT
d3
d7
d10
200 µm
DAPI
YAP1

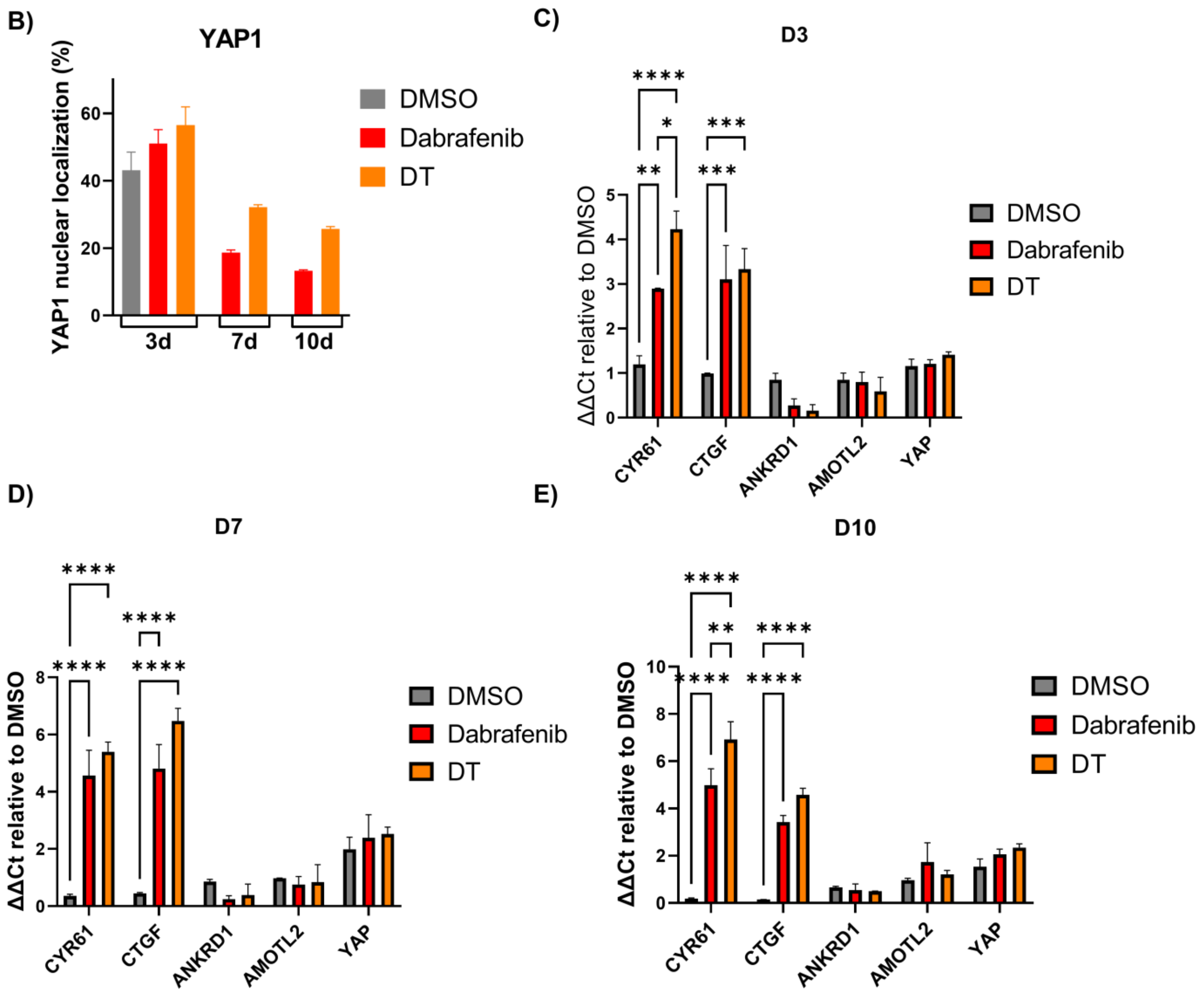

Figure 8. YAP-TEAD activation in A375 cells treated with 30 nM dabrafenib alone or in combination with 1 nM trametinib for up to 10 days. A) Immunofluorescence images for YAP1 (orange) and DAPI (blue). Bars 200 µm, magnification 20x. B) Quantification of YAP1 immunofluorescence data. The cells with YAP1 nuclear to cytoplasmic (N/C) ratio >1.3 were considered to have YAP1 located in the nucleus. Data are shown as means ± s.e.m.; *n* = 2 biological replicates. C–E) Expressions of YAP-TEAD target genes and *YAP1* on days 3 (C), 7 (D), and 10 (E) of dabrafenib- or DT-treatment. Data are shown as means ± s.e.m.; *n* = 2 biological replicates, 2 technical replicates. *GAPDH* was used as a housekeeping gene and the data were normalized to a biological replicate of DMSO on treatment day 3.

2.5 Long-term BRAF/MEK inhibition suppresses ERK phosphorylation, but has a minimal effect on cell growth and proliferation

Next, the A375 cells were cultured in a medium containing dabrafenib (A375-D) or DT (A375-DT) until they resumed proliferation. After 14 weeks of treatment, cell growth inhibition was evaluated using a dose range of 1 nM–10 µM dabrafenib and trametinib. The growth of A375-DT cells was inhibited at higher concentrations of dabrafenib (IC50 = 13.2 nM) (Figure 9. A) and trametinib (IC50 = 22.1 nM) (Figure 9. B) compared to parental cells (dabrafenib IC50 = 3.6 nM, trametinib

IC50 = 2.3 nM) (Figure 9. A–B). In addition, dabrafenib inhibited cell growth only partially even at high micromolar concentrations (Figure 9. A). In A375-D cells the effect was very modest with a partial inhibition and an IC50 of 8.6 nM for dabrafenib (Figure 9. A) and an IC50 of 9.2 nM for trametinib (Figure 9. B). Taken together, these findings suggested that A375-DT and A375-D cells began to show resistance to the treatment with DT or dabrafenib, and this was more prominent in A375-DT cells. However, it must be noted that A375-D and A375-DT cells were not entirely resistant cell lines to dabrafenib or trametinib.

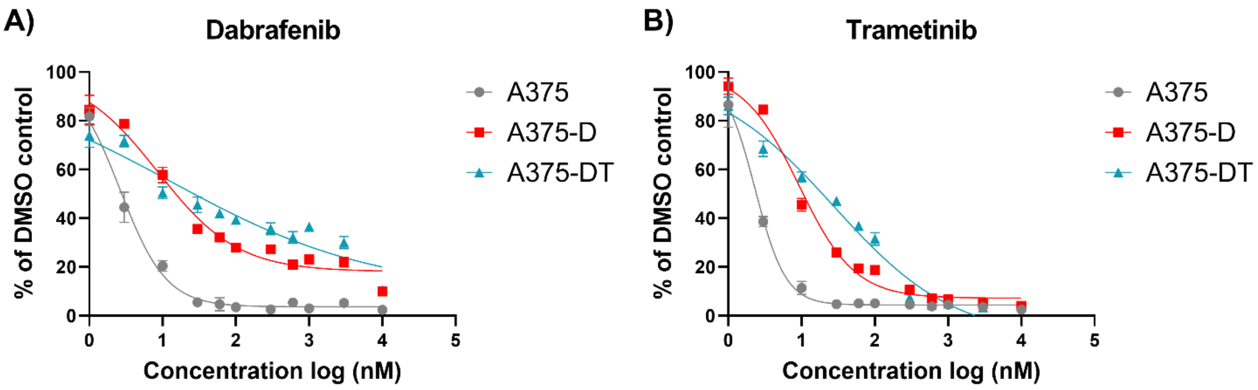

Figure 9. Dose-response curves for dabrafenib and trametinib in A375 parental cells and A375 cells treated with 30 nM dabrafenib (A375-D) or 30 nM dabrafenib and 1 nM trametinib (A375-DT) for 14 weeks. The parental cells were treated with dabrafenib or trametinib for 4 days, and the A375-D and A375-DT cells were treated for 6 days. Data are shown as means ± s.e.m.; *n* = 4 biological replicates. A) The IC50 values for dabrafenib in A375, A375-D, and A375-DT cells were 3.6 nM, 8.6 nM, and 13.2 nM, respectively. B) The IC50 values for trametinib in A375, A375-D, and A375-DT cells were 2.3 nM, 9.2 nM, and 22.1 nM, respectively.

To confirm that A375-D and A375-DT cells were proliferating under long-term dabrafenib and DT treatment, the proportions of proliferating cells in parental, A375-DT, and A375-D cells were assessed with the Ki67 antibody (Figure 10. A). In addition, the cells were stained with pERK antibody to study the MAPK pathway activation (Figure 10. B). The proportion of proliferating cells was 15 % lower in A375-D cells and 22 % lower in A375-DT cells than in parental cells (87 % of the parental cells were Ki67-positive) (Figure 10. C). These differences were also statistically significant (dabrafenib: P = 0.0274; DT: P = 0.0047) (Figure 10. C). Thus, the proportion of proliferating cells had recovered near the treatment naïve level in both cell lines.

As expected, the proportion of pERK-positive cells was 83 % less in A375-DT cells than in parental cells (98 % of parental cells pERK-positive) (Figure 10. D). This difference was statistically significant (P <0.0001) (Figure 10. D). The proportion of pERK-positive cells was also significantly higher in A375-D cells ($P<0.0001$) than in the A375-DT cells (Figure 10. D). In A375-D cells the proportion of pERK-positive cells was 41 % less compared to parental cells (Figure 10. D).

Taken together, these results showed that A375-DT and A375-D cells were able to continue proliferation despite the presence of compounds, suggesting that the cells had adapted to the treatments. More importantly, these results showed that the MAPK pathway was reactivated in A375-D cells while in A375-DT cells the MAPK pathway activation remained low. Together these findings suggested that A375-D cells used resistance mechanisms involving the MAPK pathway reactivation while A375-DT cells relied on other resistance mechanisms.

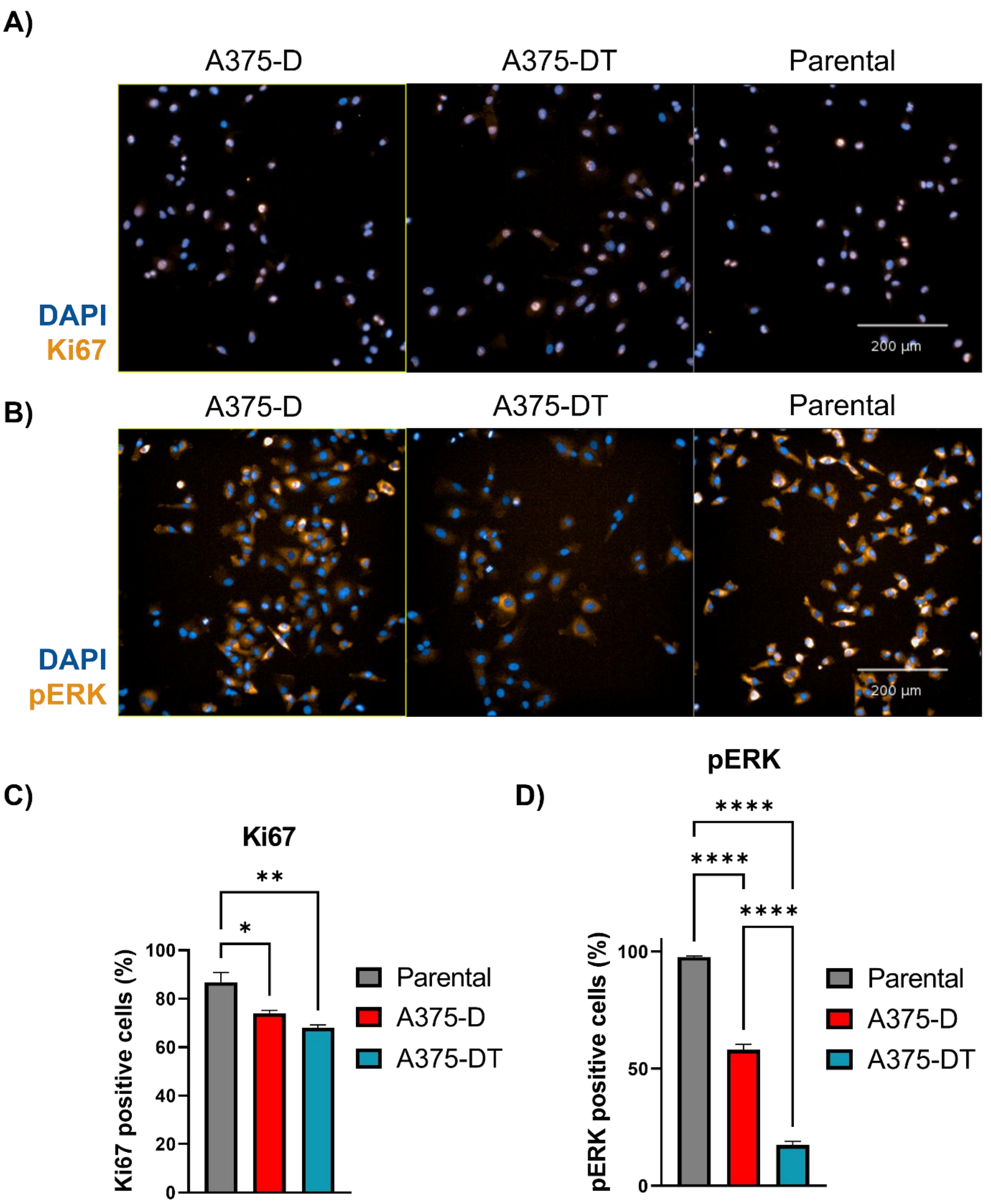

Figure 10. Proliferation and the MAPK pathway activation in parental, A375-D, and A375-DT cells. A) Immunofluorescence images showing Ki67 positive cells (orange) and DAPI (blue). B) Immunofluorescence images for phosphorylated ERK (orange) and DAPI (blue). Bars 200 µm, magnification 20x. C) Quantification of immunofluorescence data showing the proportion of proliferating cells detected with Ki67 antibody. Cells with nuclear Ki67 intensity value >4500 were considered positive. D) Quantification of immunofluorescence data showing the proportion of cells with phosphorylated ERK. The cells with pERK intensity >1200 were considered pERK positive. Data are shown as means ± s.e.m.; *n* = 3 biological replicates.

2.6 Long-term BRAF/MEK inhibition induces a distinctive cellular morphology

Next, to study the cellular morphology and EMT-like phenotype switching in parental, A375-D, and A375-DT cells, the cells were stained with phalloidin and an antibody against vimentin (Figure 11. A–B). The morphology between cell types was dramatically different. (Figure 11. A, C). While the A375-D cells had mostly reverted to the normal phenotype, the A375-DT cells mainly expressed the large phenotype (Figure 11. A, C). In contrast to the cells that had been in the DT combination treatment for 10 days, the A375-DT cells had mostly lost the elongated phenotype (Figure 7. A–B and Figure 11. A, C). The cell lines did not have statistically significant differences in vimentin expression ($P = 0.0670$) indicating that there was no ongoing EMT-like phenotype switching in A375-D and A375-DT cells (Figure 11. D).

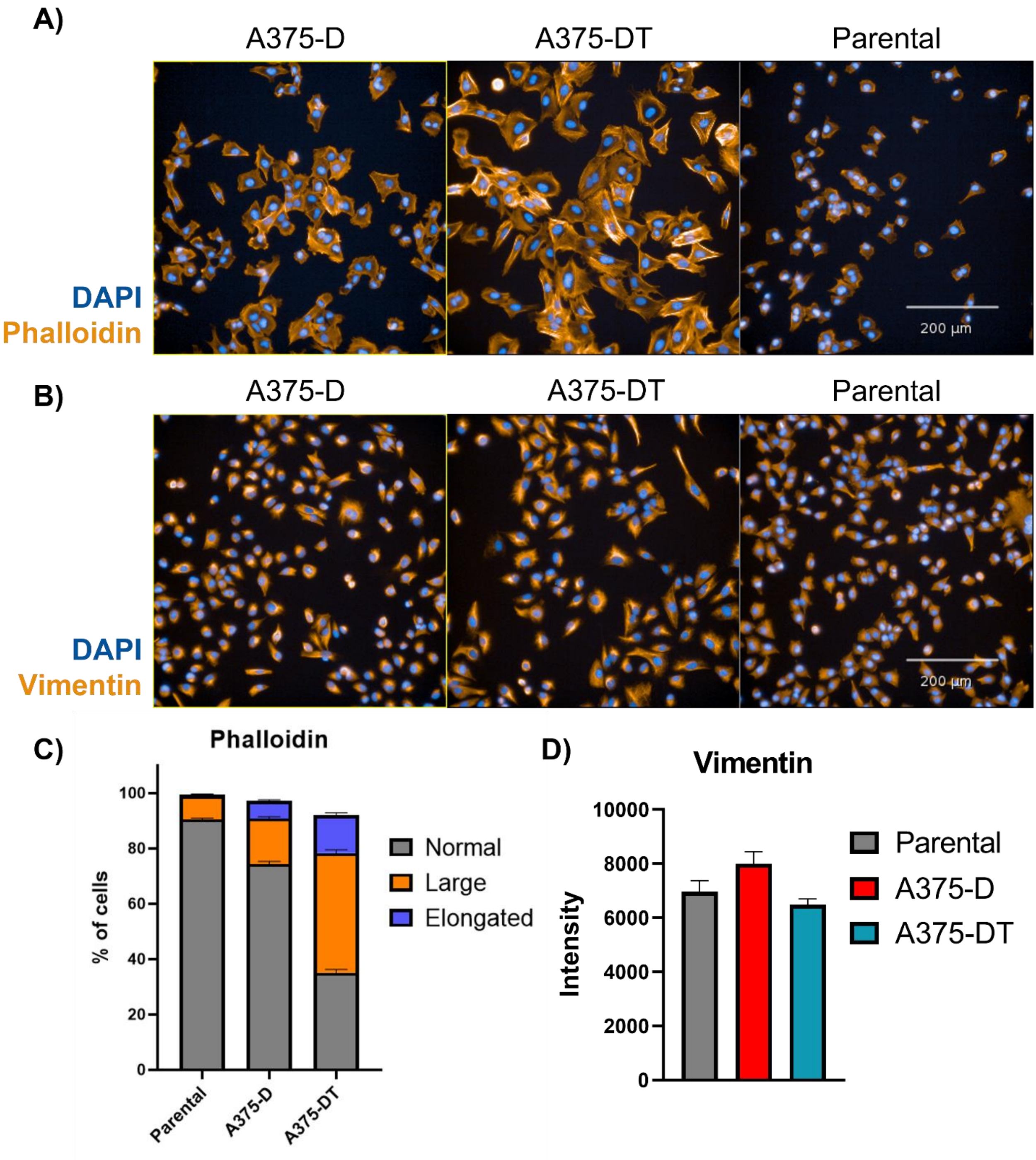

Figure 11. Cellular morphology and vimentin expression in A375, A375-D, and A375-DT cells. A) Immunofluorescence images of cells stained for phalloidin (orange) and DAPI (blue). B) Immunofluorescence images for vimentin (orange) and DAPI (blue). Bars 200 µm, magnification 20x. C) Quantification of different cell morphologies identified with Columbus software. Data are shown as means ± s.e.m.; *n* = 4 biological replicates. D) Quantification of vimentin intensity on a ring region around the nucleus. Data are shown as means ± s.e.m.; *n* = 3 biological replicates.

2.7 Long-term BRAF/MEK inhibition induces the activation of YAP-TEAD

Next, to study if YAP-TEAD activation was enhanced in A375-DT cells, the cells were stained with YAP1 antibody (Figure 12. A), and the expressions of *YAP1* and four YAP-TEAD target genes were studied by RT-qPCR. The YAP1 immunostaining showed that the proportion of cells with a high YAP1 N/C ratio was 79% higher in A375-DT cells compared to parental cells (YAP1 was located in the nucleus in 24 % of parental cells) (Figure 12. B). This difference was also statistically significant ($P = 0.0142$) (Figure 12. B). Total *YAP1* expression was not significantly altered between these two cell lines. (Figure 12. C)

The expression of YAP-TEAD target gene *ANKRD1* was 8 times higher in A375-DT cells compared to parental cells (Figure 12. C). Indeed, this increase was statistically significant ($P < 0.0001$) (Figure 12. C). In addition, *CYR61* expression had increased significantly ($P < 0.0001$) in A375-DT cells compared to the parental cells (Figure 12. C). However, there were no significant differences in the expressions of *CTGF* and *AMOTL2* between the cell lines (Figure 12. C).

These results suggested that YAP-TEAD was activated in A375-DT cells. Moreover, the aforementioned results (see section 2.4, Figure 8) showed increased YAP-TEAD activation also in parental cells during a 10-day treatment period with DT. Together these results suggested that YAP-TEAD activation was a rapid response to the initiation of DT treatment and the activation remained increased after long-term treatment.

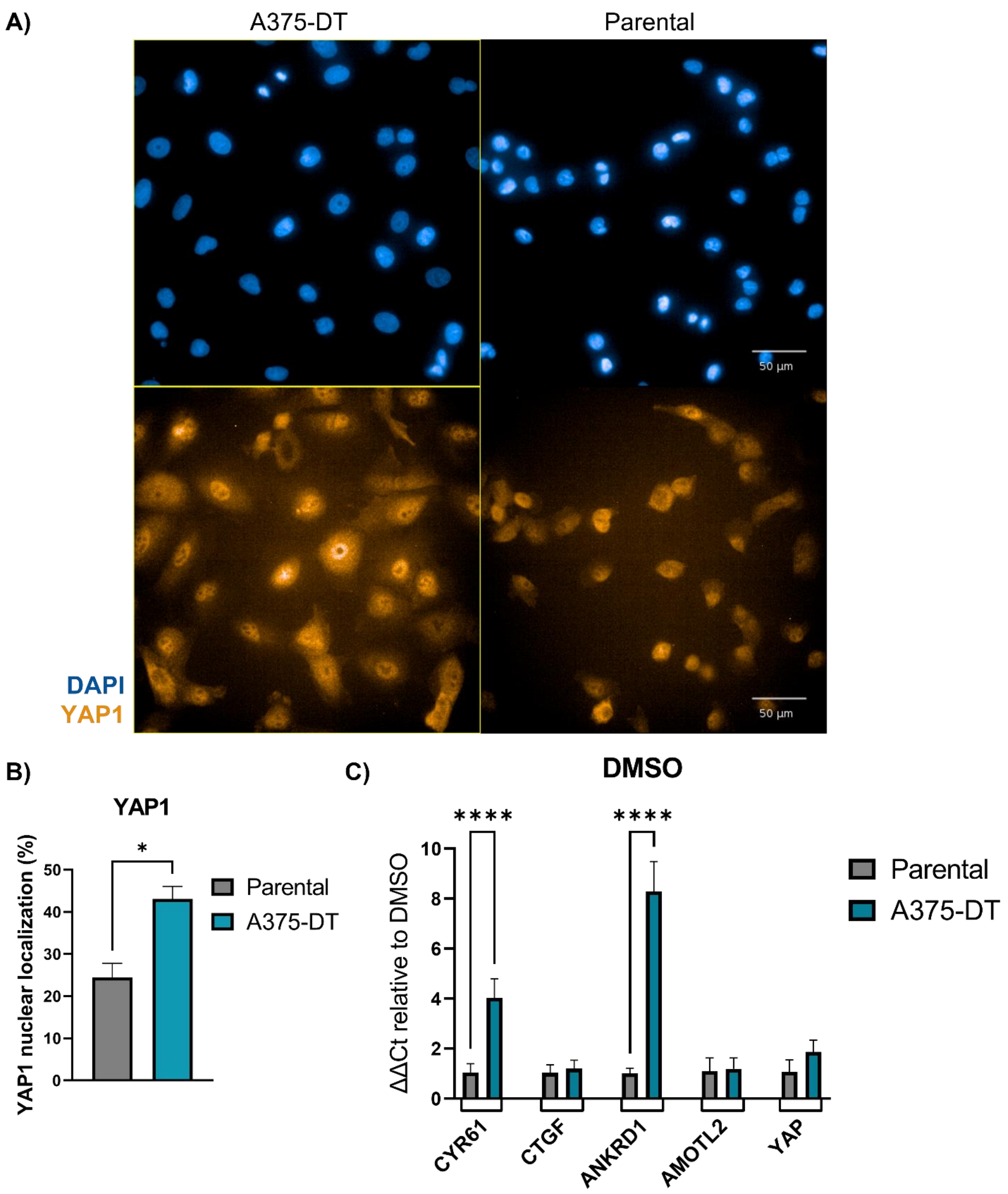

Figure 12. YAP1 subcellular localization and the expressions of *YAP1* and YAP-TEAD target genes in A375 and A375-DT cells. A) Confocal microscopy images for YAP1 (orange) and DAPI (blue). Bars 50 µm, magnification 63x. B) Quantification of the confocal microscopy data of YAP1. The cells with YAP1 nuclear to cytoplasmic (N/C) ratio > 1.3 were considered to have YAP1 located in the nucleus. Data are shown as means ± s.e.m.; *n* = 3 biological replicates. C) The expressions of YAP-TEAD target genes and *YAP1*. Data are shown as means ± s.e.m.; *n* = 3 biological replicates, 2 technical replicates. *GAPDH* was used as a housekeeping gene and the data were normalized to the mean of parental cells' DMSO control.

2.8 TEADi decrease the YAP-TEAD activation in A375-DT cells

To study if TEADi affected the activation of YAP-TEAD in A375-DT cells, two TEADi, Compound A (Orion Pharma) and VT-103 (Tang *et al*., 2021), which are known to bind TEAD and inhibit YAP-TEAD transcriptional activity, were used. The YAP1 nuclear localization in A375-DT cells treated with 10 µM TEADi was assessed with the YAP1 antibody (Figure 13. A). The YAP1 immunostaining showed that the proportion of cells with a high YAP1 N/C ratio was 24 % less in the cells treated with Compound A than in the control cells and the cells treated with VT-103 (Figure 13. B) (42 % of control cells had YAP1 located in the nucleus). This decrease was statistically significant (Compound A vs. control: P = 0.0186; Compound A vs. VT-103: P = 0.0172) (Figure 13. B). Surprisingly, Compound A decreased YAP1 nuclear localization while VT-103 did not affect it.

To confirm if TEADi binding to TEAD was successful, the YAP-TEAD target gene expression in parental and A375-DT cells was studied during 10 µM TEADi treatment. The cells were treated with TEADi for 6h and the cells' RNA was extracted. The expressions of YAP1 and four YAP-TEAD target genes were studied by RT-qPCR.

After the addition of TEADi, the expressions of all four YAP-TEAD target genes decreased in both parental and A375-DT cells. In parental cells, Compound A significantly decreased the expressions of CYR61 (P = 0.0012), CTGF (P = 0.001), ANKRD1 (P = 0.0006), and AMOTL2 (P = 0.0016) while VT-103 decreased only CTGF (P = 0.0414) expression significantly (Figure 13. C). In A375-DT cells Compound A decreased CYR61 (P = 0.0011) and ANKRD1 (P < 0.0001) expressions significantly, and similarly VT-103 decreased CYR61 (P < 0.0001) and ANKRD1 (P < 0.0001) expressions significantly (Figure 13. D). The decreases in CTGF and AMOTL2 expressions were not statistically significant with either compound (Figure 13. D). The YAP1 expression was not significantly altered by TEADi in parental or A375-DT cells (Figure 13. C–D).

Taken together, these results suggested that inhibition of TEAD with Compound A and VT-103 was successful in both cell lines. Target gene expression of all measured genes decreased in both cell lines even if the decrease was not statistically significant in all of the genes (Figure 13. C–D). As expected, TEADi did not affect YAP1 expression in either cell line, which further suggested that the decrease in YAP-TEAD target gene expression was not caused by diminished cellular YAP1 (Figure 13. C–D).

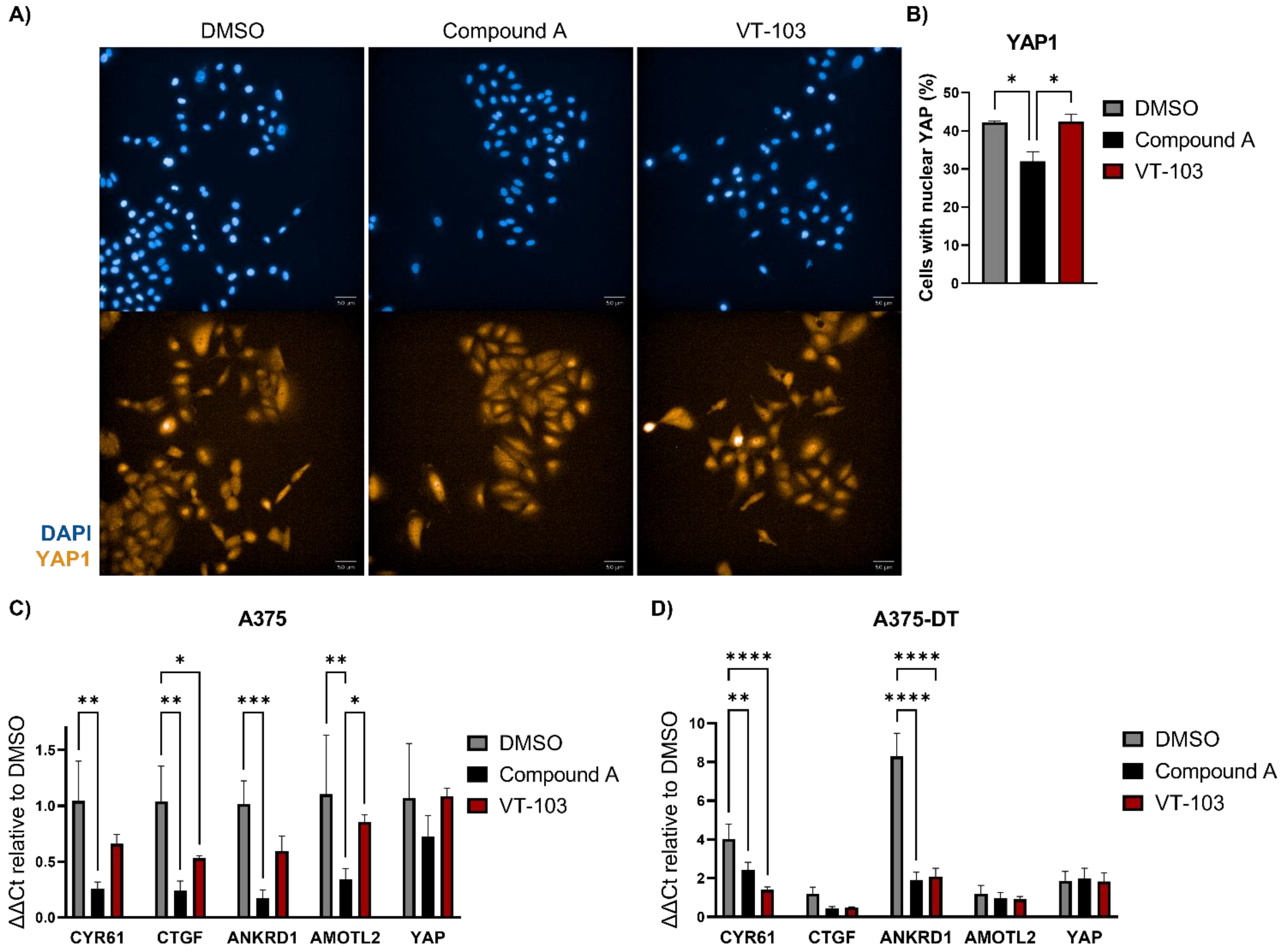

Figure 13. YAP-TEAD activation during 10 µM TEADi treatment. A) Immunofluorescence images for YAP1 (orange) and DAPI (blue) in A375-DT cells after triple combination treatment with DT and Compound A or VT-103. Bars 50 µm, magnification 20x. B) Quantification of YAP1 immunofluorescence data. The cells with YAP1 nuclear to cytoplasmic (N/C) ratio >1.3 were considered to have YAP1 located in the nucleus. Data are shown as means ± s.e.m.; n = 3 biological replicates. C–D) The expressions of YAP-TEAD target genes and YAP1 in parental A375 cells (C) and A375-DT cells (D) after 6 h TEADi treatment. Data are shown as means ± s.e.m.; n = 3 biological replicates, 2 technical replicates. GAPDH was used as a housekeeping gene and the data were normalized to the mean of parental cells' DMSO control.

2.9 TEADi have a modest effect on cell growth and proliferation

To assess whether the increased YAP-TEAD activity observed in A375-DT cells contributed to the differences in cell growth, the A375-DT cells were treated with TEADi. First, a dose range of 1 nM–10 µM TEADi was used to evaluate the effect of TEAD inhibition on the growth of A375 cells. The dose-response analysis showed that TEADi alone did not reduce the number of A375 cells (Compound A: IC50 = ND; VT-103: IC50 = 37.0 nM) (Figure 14. A). This result was expected because YAP-TEAD activation was modest in parental cells and YAP-TEAD is often activated as a response to targeted therapies.

Next, a dose range of 1 nM–10 µM TEADi was used to evaluate the effect of TEAD inhibition and simultaneous DT treatment on parental A375 cells. With both inhibitors, Compound A and VT-103, there was a modest decrease in cell number with the highest concentrations of TEADi when the data were normalized to the DT treatment alone (Compound A: IC50 = 14.8 nM; VT-103: IC50 = 24.3 nM) (Figure 14. B–C). The same dose range of TEADi in combination with DT in A375-DT cells led to a more pronounced inhibition in cell growth (Compound A: IC50 = 34.0 nM; VT-103: IC50 = 12.8 nM) (Figure 14. B–C). Indeed, there was a significant decrease in the growth of A375-DT cells observed with a 3 µM concentration of Compound A (P= 0.0046) and VT-103 (P=0.0005) compared to the parental cells (Figure 14. B-C). However, the effect in A375-DT cells was quite modest, in line with the modest YAP-TEAD activation (see section 2.7, Figure 12.).

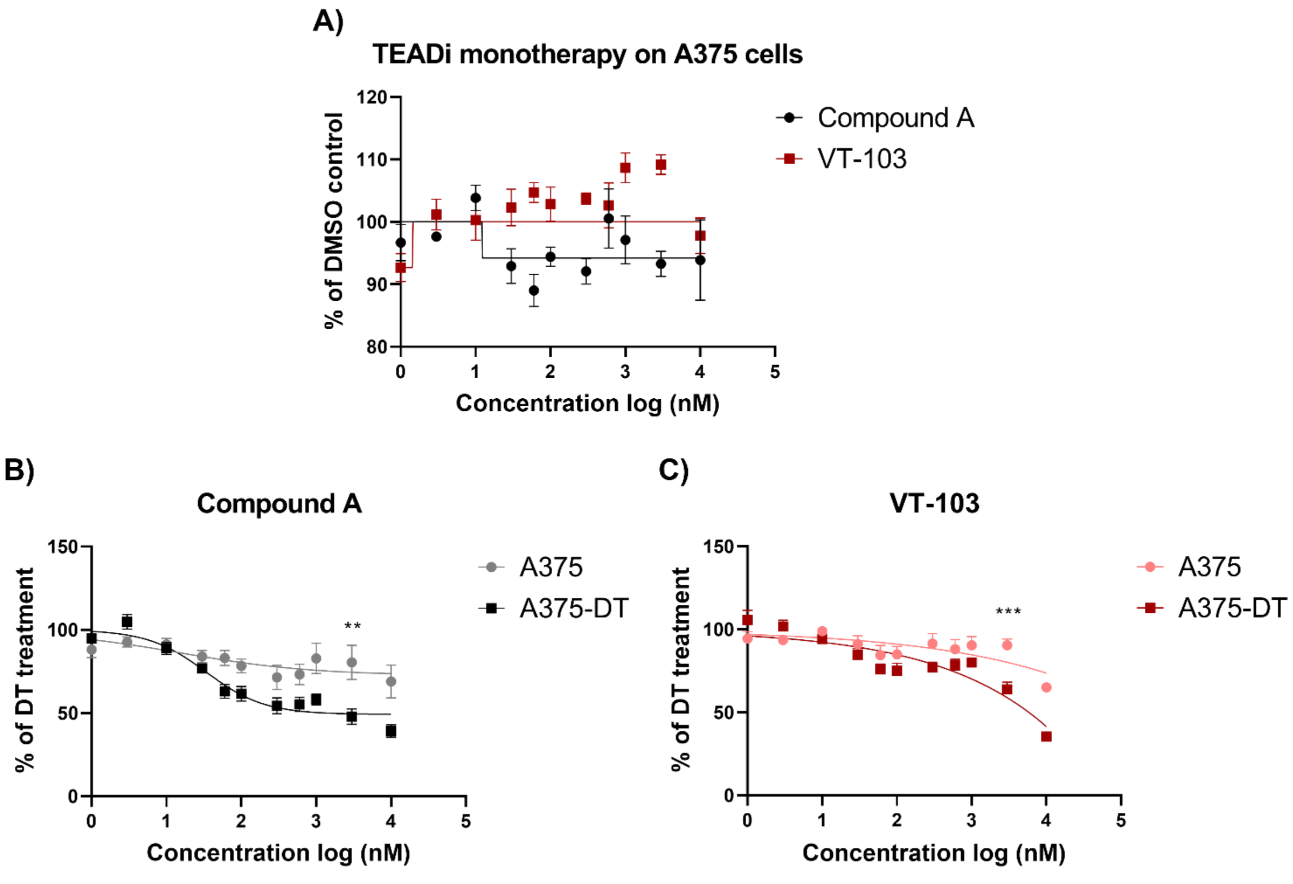

Figure 14. Dose-response curves for TEAD inhibitors (TEADi), Compound A and VT-103, in A375 and A375-DT cells. A) TEADi in treatment naïve parental A375 cells. The cells were treated for 4 days with the compounds. Data are shown as means ± s.e.m.; *n* = 4 biological replicates. B) Compound A in combination with the DT treatment on parental and A375-DT cells (P = 0.0046). The cells were treated for 6 days with the compound. C) VT-103 in combination with the DT treatment on parental and A375-DT cells (P = 0.0005). The cells were treated for 6 days with the compound. Data are shown as means ± s.e.m.; *n* = 8 biological replicates for A375 cells and *n* = 12 biological replicates for A375-DT cells.

The effect of 10 µM TEADi in cell proliferation, apoptosis, and senescence was further studied in A375-DT cells. As previously, the TEADi effect on cell proliferation in A375-DT cells was studied with Ki67 antibody (Figure 15. A). In the cells treated with Compound A, 8 % fewer cells were Ki67 positive than in the control cells treated with DMSO (89 % of control cells were Ki67-positive) (Figure 15. B). Similarly, in the cells treated with VT-103, 13 % fewer cells were Ki67 positive than in the control (Figure 15. B). Thus, TEADi decreased cell proliferation only modestly.

Next, apoptosis in A375-DT cells was studied with a Caspase-3/7 apoptosis reagent, using 10 µM TEADi on top of DT treatment and staurosporine as a positive control. Apoptosis was followed for 5 days. Cells in staurosporine became apoptotic already after 12 h of treatment (Figure 15. C). Thus, the cell number in these wells remained low throughout the experiment. In all other conditions, only few apoptotic cells were detected on treatment day 5 (Figure 15. C). The A375-DT cells in the DT medium with Compound A or VT-103 had grown significantly less, yet there were no more apoptotic cells detected than in the cells in DMSO or DT + DMSO medium (Figure 15. C). Thus, these findings suggested that the reduced cell number in the dose-response analysis was not caused by increased apoptosis.

Finally, cellular senescence was studied with β-galactosidase staining in A375-DT cells treated with TEADi for two days. TEADi did not increase senescence in A375-DT cells compared to the DMSO control, suggesting that the reduction in cell number was not caused by increased senescence. (Figure 15. D).

Taken together, despite the modest effect TEADi had on cell proliferation, the partial inhibition in A375-DT cell number during the dose-response analysis was most likely caused by decreased cell proliferation while apoptosis and senescence did not play a big role.

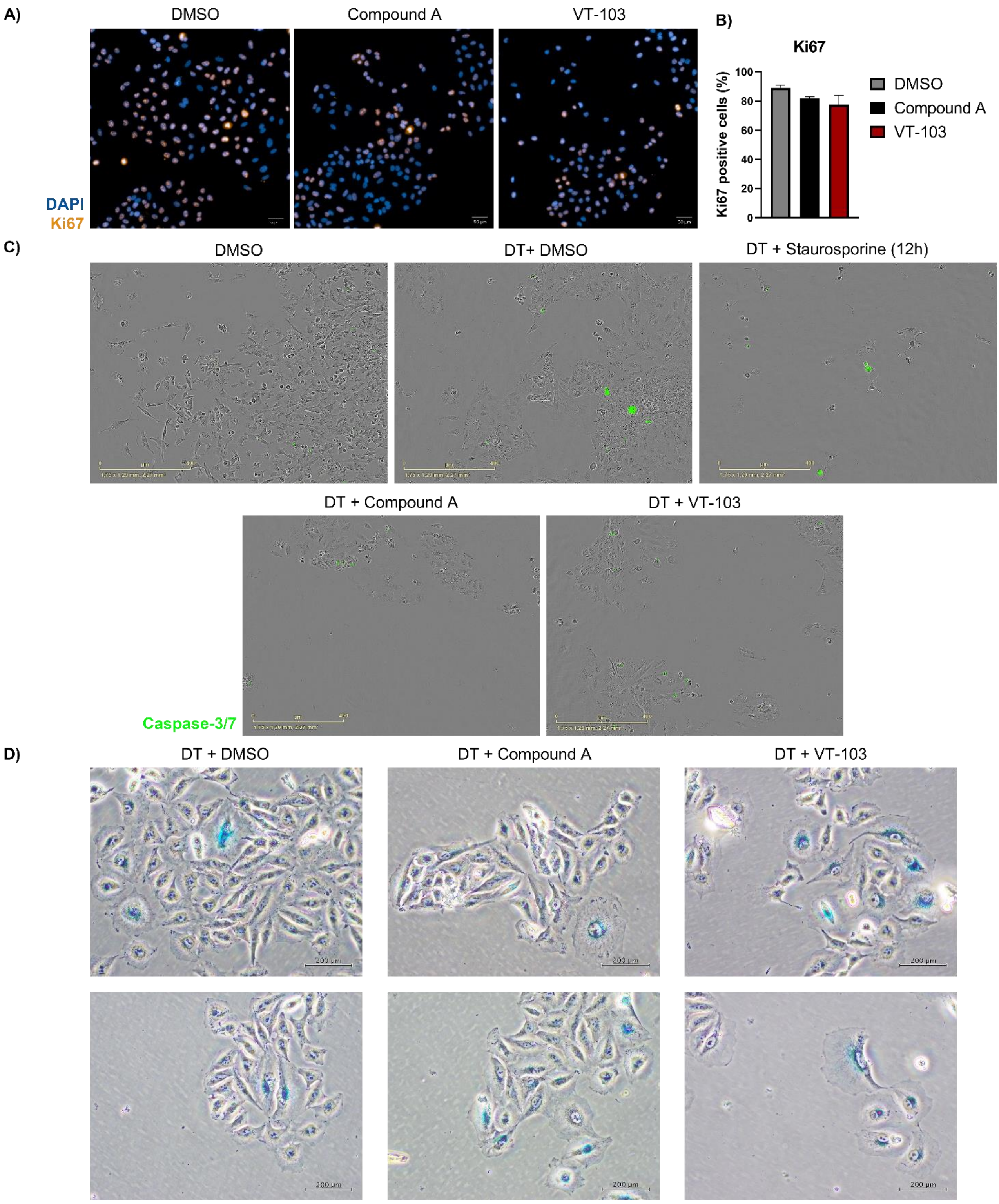

Figure 15. Proliferation, apoptosis, and senescence in A375-DT cells treated with 10 µM TEADi.
A) Immunofluorescence images showing Ki67-positive (orange) A375-DT cells under triple combination treatment with DT and Compound A or VT-103. Nuclei are stained with DAPI (blue). Bars 50 µm, magnification 20x. B) Quantification of the immunofluorescence data showing the proportion of Ki67-positive cells. Cells with nuclear Ki67 intensity value > 4500 were considered positive. Data are shown as means ± s.e.m.; *n* = 3 biological replicates. C) Apoptosis detected with Incucyte Caspase-3/7 Green Apoptosis Assay Reagent in A375-DT cells treated with DMSO, DT, and DMSO, or triple combination with DT and Compound A or VT-103. Images are taken with Incucyte® S3 and the apoptotic cells are seen as light green. Bars 400 µm, 10x magnification. D) Light microscopy images of cells treated for 2 days with DT in

combination with Compound A or VT-103 and stained with Senescence β-Galactosidase Staining Kit. Senescent cells are stained blue. Bars 200 μm, 20x magnification.

2.10 TEADi have no effect on cellular morphology or vimentin expression in A375-DT cells

Finally, to study if TEADi induced changes in cellular morphology or vimentin expression, the A375-DT cells were treated with 10 μM Compound A or VT-103 for 3 days, and the cells were stained with phalloidin (Figure 16. A) or vimentin antibody (Figure 16. B). The phalloidin staining did not show significant changes in cellular morphology between DMSO control, Compound A, and VT-103 treatment (Figure 16. C). Moreover, the vimentin staining did not show a significant difference in vimentin intensity between control and TEADi-treated cells (Figure 16. D). These results suggested that TEADi did not affect the morphology of A375-DT cells and TEAD inhibition did not reverse the morphological changes induced by long-term DT treatment. Also, the addition of TEADi did not induce or reduce EMT-like phenotype switching in A375-DT cells. However, it remains to be determined if YAP-TEAD activation contributed to the changes seen in cellular morphology and vimentin expression during the 10-day incubation with DT and if the addition of TEADi could have prevented these changes.

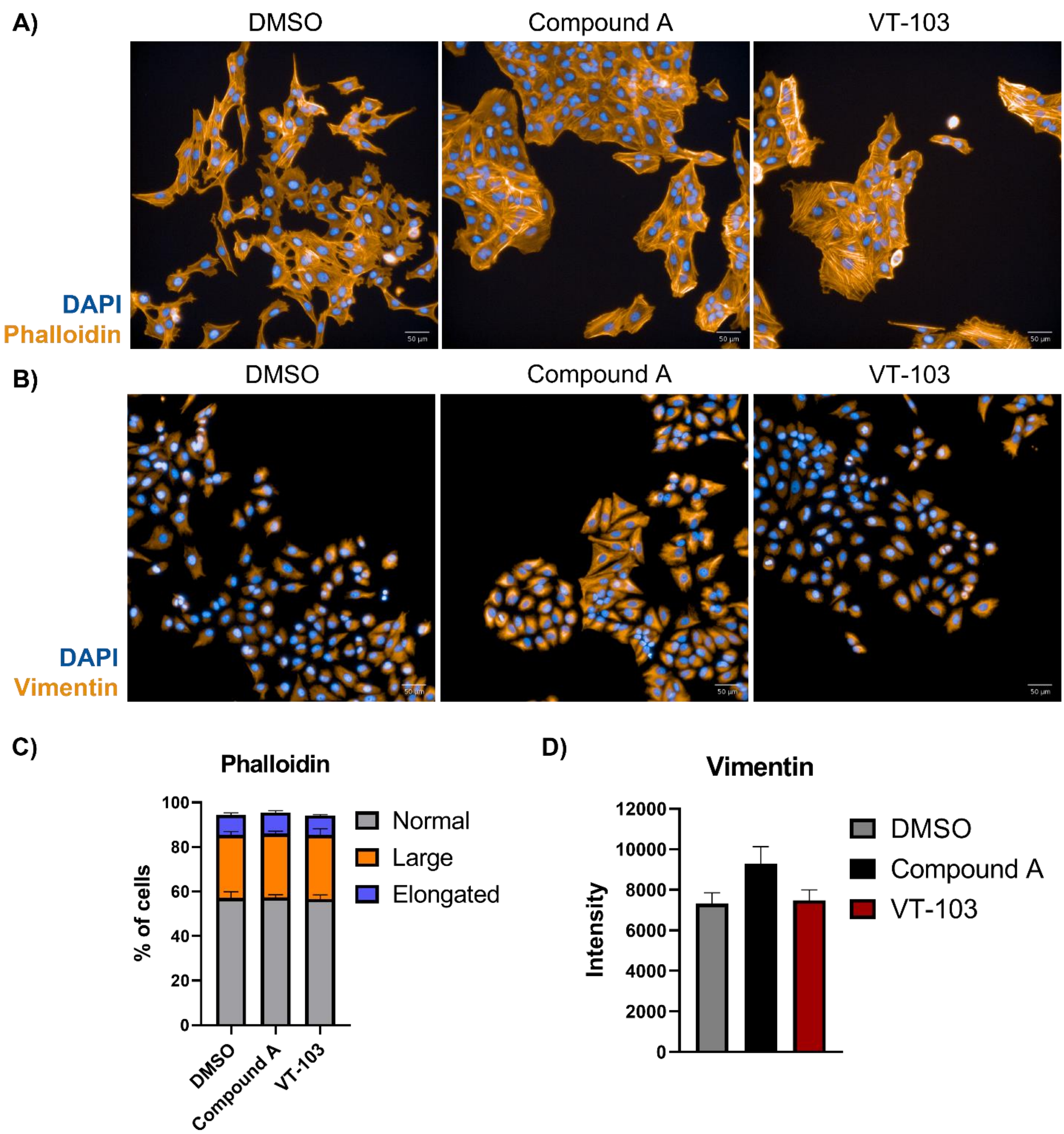

Figure 16. Cell morphology and vimentin expression in A375-DT cells after triple combination with DT and Compound A or VT-103. A) Immunofluorescence images of cells stained for phalloidin (orange) and DAPI (blue). Bars 50 µm, magnification 20x. B) Immunofluorescence images for vimentin (orange) and DAPI (blue). Bars 50 µm, magnification 20x. C) Quantification of different cell morphologies identified with Columbus software. Data are shown as means ± s.e.m.; n = 4 biological replicates. D) Quantification of vimentin intensity on a ring region around the nucleus. Data are shown as means ± s.e.m.; n = 3 biological replicates.

3 DISCUSSION

This study assesses whether a triple combination of the current standard of care, dabrafenib and trametinib, together with TEADi is more effective in A375 melanoma cells to prevent cell growth compared to dabrafenib and trametinib treatment. The minimum concentrations of dabrafenib and trametinib, having a maximal inhibitory effect, are selected, and later combined with two novel TEADi, Compound A (Orion Pharma) and VT-103 (Tang *et al*., 2021) in A375-DT cells. First, the effect of DT on A375 cell growth, proliferation, apoptosis, senescence, cell morphology, and ERK phosphorylation, the marker of MAPK activation, are studied. The DT treatment decreases cell proliferation, and ERK phosphorylation, changes the cell morphology, and moderately increases YAP-TEAD activation. In long-term DT treatment, the ERK phosphorylation remains low, but the cell proliferation restores almost to the same level as the cell proliferation in parental treatment-naïve cells suggesting that the cells use resistance mechanisms not involving the MAPK pathway. In addition, the YAP-TEAD activation remains moderately increased in A375-DT cells. Combined DT and TEAD inhibitor treatment moderately and partially decreases the growth and proliferation of A375-DT cells. TEADi combined with DT decrease the YAP-TEAD activation in A375 and A375-DT cells, suggesting that the TEADi's binding to TEAD was successful. Taken together, these results suggest that YAP-TEAD is activated in A375 and A375-DT cells in response to the DT treatment, and the activation is used as a resistance mechanism. However, YAP-TEAD activation is modest, it is not essential for cell survival, and the cells likely rely on other resistance mechanisms that are more important for these cells than YAP-TEAD activation.

In response to dabrafenib and DT treatments, the A375 cells exhibit only few apoptotic cells while the majority of the cells adopt a drug-tolerant phenotype. Similarly, Yang *et al.* have shown that dabrafenib treatment induces apoptosis only in 8 % of A375 cells while most cells enter a quiescent state (Yang *et al*., 2021). In contrast, Schulz *et al.* and Joshi *et al.* have shown that BRAF and MEK inhibitor combination therapy induces apoptosis in BRAF-mutated cell lines (Joshi *et al*., 2015; Schulz *et al*., 2022). Thus, the cells' response to dabrafenib monotherapy or dabrafenib and trametinib combination therapy seems to be highly cell-line dependent. A similar conclusion has been presented by Yang *et al.* who demonstrated that melanoma cell lines had a dramatically different propensity for apoptosis in response to dabrafenib treatment (Yang *et al*., 2021).

Despite the low emergence of apoptosis, dabrafenib and DT treatments significantly reduce the number of A375 cells by decreasing cell proliferation. Similarly, previous studies have shown that dabrafenib treatment reduces cell proliferation and induces a G0/G1 cell cycle arrest (Fratangelo *et* *al*., 2018; Yang *et al*., 2021). Yang *et al.* have shown that almost half of the A375 cells escape dabrafenib treatment and begin to proliferate only after 3 days of treatment (Yang *et al*., 2021). Similarly, here the proportion of proliferating A375 cells is initially decreased by dabrafenib, but the cells rapidly restore the cell proliferation. The DT treatment more effectively inhibits cell proliferation, but even the combination treatment is not able to fully eradicate the population of proliferating cells, consistent with the results obtained by Yang *et al.* (Yang *et al*., 2021).

The reactivation of the MAPK pathway functions as one of the main resistance mechanisms to BRAF inhibitor monotherapy (Nazarian *et al*., 2010; Poulikakos *et al*., 2011; Johannessen *et al*., 2010; Lito *et al*., 2012; Hirata *et al*., 2015). Consistently, after the substantial decrease shown in the MAPK pathway activation, the A375 cells rapidly begin to reactivate this pathway only few days after the initiation of dabrafenib treatment. Similarly, Yang *et al.* have shown that the MAPK pathway activation was initially decreased but quickly rebounded in dabrafenib-treated A375 cells (Yang *et al*., 2021). The DT combination treatment, however, leads to a more pronounced and sustained MAPK pathway inhibition in A375 cells. A similar effect is also seen in melanoma patients in which the dabrafenib and trametinib combination therapy is more effective and durable in preventing MAPK pathway reactivation (Flaherty *et al*., 2012; Long *et al*., 2017). Thus, the results obtained here replicate the findings of previous studies.

The cell shape dramatically changes during the short treatment with dabrafenib or DT. Both treatments induce most of the A375 cells to express an enlarged or elongated morphology. Similarly, Kim *et al.* have discovered that the inhibition of BRAF with vemurafenib increases the number of actin stress fibers and enlarges the size of SKMEL28 and WM3248 melanoma cells (Kim *et al*., 2016). Interestingly, vimentin expression in A375 cells increases after three days of treatment in both treatment groups. The elongated morphology together with the increased vimentin expression suggests that dabrafenib and DT treatments may induce an EMT-like phenotype switching in a proportion of A375 cells. Indeed, previous studies have found that the MAPK pathway inhibition induced phenotype switching in melanoma cells and changed the cells' phenotype toward an invasive and drug-resistant phenotype (Konieczkowski *et al*., 2014; Müller *et al*., 2014; Rambow *et al*., 2018; Verfaillie *et al*., 2015). The phenotype switching from proliferative to invasive phenotype has also been associated with the activation of YAP-TEAD (Zhang *et al*., 2020; Verfaillie *et al*., 2015).

The activation of YAP-TEAD has been suggested as one of the non-genetic resistance mechanisms to targeted therapies in melanoma and other cancers (Lin *et al*., 2015; Nguyen and Yi, 2019;

Verfaillie *et al*., 2015). Increased activation of YAP-TEAD provides the cells with a survival advantage by inhibiting apoptosis, restoring cell proliferation, and increasing the invasive and metastatic capacity of the cells (Nallet-Staub *et al*., 2014; Kim *et al*., 2016; Fisher *et al*., 2017). Here, short treatment with dabrafenib or DT did not affect the *YAP1* expression. Similarly, in response to BRAF inhibitor treatment, Hugo *et al.* did not find changes in YAP1 mRNA expression (Hugo *et al*., 2015). Dabrafenib and DT treatments increase the nuclear localization of YAP1. The nuclear localization of YAP1 is moderately higher in DT-treated cells than in dabrafenib-treated cells. Also, the expressions of YAP-TEAD target genes *CYR6*1 and *CTGF* increase significantly in dabrafenib- and DT-treated cells, and the expressions of these genes are higher in DT-treated cells. These results suggest that the YAP-TEAD is moderately activated in both cell lines in response to the treatments and the activation is higher in DT-treated cells. The lower activation of YAP-TEAD in dabrafenib-treated cells might occur because the cells rely more on the reactivation of the MAPK pathway as a resistance mechanism whereas DT-treated cells must harness other resistance mechanisms, such as YAP-TEAD activation.

After 14 weeks of dabrafenib (A375-D cells) and DT (A375-DT cells) treatments, the cells begin to show resistance to the given concentrations of drugs, which is shown as increased IC50 values for dabrafenib and trametinib in these cell lines. In a previous study, a dabrafenib-resistant A375 cell line had an IC50 value of 110.5 μM (Cordaro *et al*., 2017) whereas here the IC50 values for dabrafenib in A375-D and A375-DT cells were 8.6 nM and 13.2 nM, respectively. Thus, it is important to note that these cell lines are not truly resistant to dabrafenib or trametinib. The proportion of proliferating cells in these cell lines recovers nearly to the level of treatment-naïve parental cells. The activation of the MAPK pathway is significantly higher in A375-D cells compared to the A375-DT cells, which confirms that the resistance for long-term dabrafenib treatment is mostly driven by the MAPK pathway reactivation. Therefore, to prevent the MAPK pathway reactivation in patients, trametinib is combined with dabrafenib, and a more sustained effect is achieved (Long *et al*., 2015; Robert *et al*., 2015). However, the recovered cell proliferation in A375-DT cells without simultaneous MAPK pathway reactivation suggests that these cells must activate other resistance mechanisms to survive under the treatment. This result is in line with the clinical observations where patients, despite the combined BRAF and MEK inhibition, relapse (Long *et al*., 2014a, 2017; Robert *et al*., 2015).

Vemurafenib-resistant melanoma cells, SKMEL28 and WM3248, have been observed to express a flat and enlarged morphology (Kim *et al*., 2016). Another study has found that melanoma cell lines resistant to a BRAF inhibitor exhibit more elongated and fibroblast-like shape compared to the parental cells (Wang *et al*., 2015). Moreover, dabrafenib-resistant melanoma cell lines, including A375, have been found to change their cellular phenotype toward mesenchymal type (Cordaro *et al*., 2017). In contrast, the morphology of A375-D cells mostly reverts to the normal morphology expressed by the parental A375 cells. This finding may be explained by the fact that the A375-DT and A375-D cell lines were not entirely resistant to the treatments. For example, in their study, Kim *et al.* created a resistant cell line by treating the cells with a 2 μM concentration of vemurafenib for 2 months (Kim *et al*., 2016). Conversely, here the A375-D cell line was created by treating the cells with a low 30 nM concentration of dabrafenib for 14 weeks. This low dabrafenib concentration is not enough to induce the development of truly resistant cells. Instead, it is more probable that the A375-D cells only adapted for the treatment. As Yang *et al.* have shown, a small population of A375 cells escapes the dabrafenib treatment in the early stages of treatment. They also showed that these escaping cells out-proliferate the non-escapees as the treatment progresses and suggested that after long-term treatment the descendants of the escapees may dominate the population. (Yang *et al*., 2021) Interestingly, the data presented here support this hypothesis. Likely few dabrafenib-resistant cells escape the treatment, re-enter into proliferation, and adapt to the treatment. These adapting cells later outgrow the non-escapees and form a morphologically homogenous cell population that expresses the normal morphology. However, this hypothesis should be validated by sorting or labeling the escaping cells. Interestingly, A375-DT cells mainly express an enlarged and round phenotype while the proportion of elongated cells has diminished. Given the extent of the cell lines' MAPK pathway activation, the different morphologies between A375-D and A375-DT cells suggest that the cellular morphology might be attributed to the activation of ERK. However, the relationship between ERK activation and cellular morphology should be further studied.

A previous study has found that the expressions of markers associated with an EMT-like phenotype switching, such as increased vimentin expression in the perinuclear region, are increased in dabrafenib-resistant cells while the expression of epithelial marker E-cadherin is decreased (Cordaro *et al*., 2017). Here, the vimentin expression is not altered between the A375, A375-D, and A375-DT cell lines. Taking into consideration that the cell lines had lost the elongated morphology, the unchanged vimentin expression between the cell lines supports the previous hypothesis that elongated cells are undergoing an EMT-like phenotype switching to a more invasive state. However, to confirm this hypothesis, more studies on elongated cells are needed.

The A375-DT cells show higher YAP-TEAD activation than parental A375 cells. The higher YAP-TEAD activation is observed as increased YAP1 nuclear localization and increased expressions of YAP-TEAD target genes *ANKRD1* and *CYR61*. Similarly, Kim *et al*. have found an increase in the expressions of *ANKRD1*, *CTGF*, and *CYR61* in melanoma cells resistant to vemurafenib (Kim *et al*., 2016). The *YAP1* expression is not altered in A375-DT cells. Taken together, the results obtained here suggest that DT combination and vemurafenib monotherapy induce a similar kind of response in YAP-TEAD activation. In addition, the results confirm that YAP-TEAD activation is a rapid response to the initiation of the DT treatment and the activation remains increased after a longer treatment period.

The inhibition of TEAD with Compound A moderately decreases YAP1 nuclear localization in A375-DT cells while VT-103 does not affect YAP1 nuclear localization. Most previously developed TEADi have not demonstrated a similar effect on YAP1 subcellular localization (Gridnev *et al*., 2022; Li *et al*., 2020). Recently, Sun *et al.* discovered that pan-TEAD inhibitor MGH-CP1 reduces YAP/TAZ nuclear localization. They suggested that this reduction is caused by TEAD-induced inhibition of TEAD-YAP/TAZ interaction that leads to impaired YAP and TAZ nuclear retention. (Sun *et al*., 2022) However, further studies are needed to determine the mechanism of if and how TEADi, like Compound A, inhibit the YAP1 shuttle to the nucleus.

VT-103 and Compound A decrease the expression of measured YAP-TEAD target genes (*CTGF*, *CYR61*, *ANKRD1*, and *AMOTL2*) in parental and A375-DT cells, confirming that the TEADi binding to TEAD is successful. However, the decrease is not statistically significant with all measured genes. Similarly, Tang *et al.* have shown inhibition in YAP-TEAD target gene expression with VT-103 (Tang *et al*., 2021). As expected, the expression of *YAP1* does not change in parental or A375-DT cells in response to TEAD inhibitor treatment, suggesting that the compounds do not mediate their effect by affecting *YAP1* expression. Taken together, both inhibitors decrease the YAP-TEAD transcriptional activity and successfully bind to TEAD.

Compound A and VT-103 alone do not affect the growth of parental A375 cells, as expected, because YAP-TEAD activation in parental A375 cells is low. This finding suggests that YAP-TEAD is not required for the survival and growth of treatment-naïve A375 cells. Similarly, inhibition of TEAD (Kurppa *et al*., 2020) or knockdown and overexpression of *YAP* (Nallet-Staub *et al*., 2014) have shown no effect on the growth of treatment-naïve cancer cell lines without Hippo pathway alterations. Simultaneous administration of TEADi with DT on parental A375 cells inhibits the growth of these cells more than DT combination alone, but the additional inhibition in cell growth is modest. A more notable inhibition in cell growth is achieved by administering TEADi with DT on A375-DT cells. These results suggest that YAP-TEAD is activated in A375-DT cells and parental A375 cells in response to DT treatment. The inhibition seen in the growth of A375-DT cells and DT-treated A375 cells, but not in treatment-naïve A375 cells also suggests that both cell lines use YAP-TEAD activation as a resistance mechanism. Given that the TEAD inhibition-induced reduction in cell growth and YAP-TEAD activation in these cells are modest, the YAP-TEAD activation as a resistance mechanism is not likely essential for survival in most of the A375 and A375-DT cells. Instead, these cells probably use multiple different resistance mechanisms. However, there may be a subpopulation of cells with a higher dependency on YAP-TEAD activation, but further analyses are needed to identify these different cell subpopulations.

Further studies in A375-DT cells revealed that the decrease in cell growth induced by the simultaneous DT and TEAD inhibitor treatment is caused by a modest decrease in cell proliferation. Interestingly, the addition of TEADi does not induce apoptosis or senescence in A375-DT cells. A previous study by Lin *et al.* has shown that *YAP1* knockdown promotes apoptosis upon RAF and MEK inhibitor treatments in melanoma, NSCLC, thyroid cancer, and colon cancer models with $BRAF^{V600E}$ mutation (Lin *et al*., 2015). Similarly, Kurppa *et al.* have shown that combined treatment with osimertinib, trametinib, and TEAD inhibitor increased apoptosis in EFGR-mutant NCSLC cells compared to the osimertinib and trametinib treatment (Kurppa *et al*., 2020). This difference between the occurrence of apoptosis may be explained by the cells' different dependencies on YAP-TEAD activation as a resistance mechanism which is shown as different levels of YAP-TEAD activation in the cells. Indeed, the activation of YAP1 in response to combined osimertinib and trametinib treatment in EFGR-mutant NCSLC cells was high (> 80 % of cells had high YAP activation) (Kurppa *et al*., 2020) whereas the YAP-TEAD activation in A375-DT cells was modest. Interestingly, a recent study by Sun *et al.* has found that YAP-TEAD inhibition prevented cell proliferation without the induction of cell death in a YAP-dependent liver cancer cell line. Sun *et al.* also discovered that the inhibition in cell proliferation was caused by a delay in cell cycle progression. The cell cycle progression was temporally arrested in G1 and G2/M stages and continued proliferation after the TEADi withdrawal. (Sun *et al*., 2022) Thus, more studies are needed to analyze the cell cycle progression in A375-DT cells and if the cells resume cell proliferation after TEAD inhibitor withdrawal. Altogether, these findings suggest that the role of YAP-TEAD activation and the effect of TEADi might be highly cancer and cell-line-specific. In cell lines with higher dependency on YAP-TEAD activation, the TEADi may induce apoptosis and/or inhibition in cell proliferation while in cancer cell lines with lower YAP-TEAD activation and dependency, TEADi can merely inhibit cell proliferation.

Previous studies have suggested that YAP mediates EMT (Lehmann *et al*., 2016; Tang *et al*., 2016; Kurppa *et al*., 2020). The treatment with DT and TEADi does not affect A375-DT cell morphology or vimentin expression. This is expected because the vimentin expression is not increased in A375-DT cells compared to the parental cells. Moreover, the A375-DT cells express an enlarged and round morphology while the elongated cells, which were hypothesized to represent cells undergoing an EMT-like phenotype switching, are absent. Thus, if no ongoing EMT-like changes were occurring in the baseline, the TEADi had nothing to inhibit. It is also important to note that TEADi did not induce EMT-like phenotypic changes. These results suggest that the morphological changes in A375-DT cells are not driven by YAP-TEAD activation. However, the changes in cell morphology may contribute to the activation of YAP-TEAD. Previously it has been discovered that changes in actin cytoskeletal tension affect the YAP/TAZ localization and activation (Dupont *et al*., 2011). Similarly, Kim *et al.* have shown that increases in actin stress fibers and cytoskeletal tension induce the activation of YAP/TAZ in vemurafenib-resistant cells (Kim *et al*., 2016). Thus, more studies are needed to determine the relationship between A375 and A375-DT cell morphology, EMT-like phenotype switching, and YAP-TEAD activation.

All the findings above suggest that the A375 and A375-DT cell lines use YAP-TEAD activation as one of many resistance mechanisms to the combined BRAF and MEK kinase inhibition, and therefore, the inhibition of TEAD is not likely an effective treatment in these cell lines to prevent tumor growth. Interestingly, Zhang *et al*. have proposed that YAP inhibition in metastatic melanoma might be more efficacious in preventing metastasis than diminishing tumor growth (Zhang *et al*., 2020). Hence, more studies are needed to determine if TEAD inhibition affects the invasive capacity of A375 cells. In addition, a recent study by Sun *et al.* has proposed limitations for YAP-TEAD inhibitor treatment in cancer. The study discovered that the VGLL3-mediated transcriptional activation of the SOX4/PI3K/AKT signaling axis may promote cancer cell survival and lead to TEAD inhibitor resistance (Sun *et al*., 2022). Thus, more studies are needed to discover the therapeutic potential of TEAD inhibition in preventing treatment resistance to targeted therapies.

In this study, some experiments were conducted using a low number of replicates, and in the future, these experiments should be repeated to confirm the observations presented here. In the immunostainings, several cells were analyzed from each well. However, the statistical analyses were performed by comparing the mean values expressed by the cells in each well. Therefore, statistical analyses were performed for a low number of replicates and statistical analyses could not be performed for immunofluorescence data from the 10-day experiment. Thus, the immunostainings could have been analyzed by using different statistical methods. In addition, the apoptosis analysis for parental A375 cells lacked a positive control, and therefore, this experiment should be replicated by using a proper positive control, such as staurosporine.

The measurement of YAP-TEAD activation was performed using only four YAP-TEAD target genes (*CTGF*, *CYR61*, *ANKRD1*, and *AMOTL2*). The observed effect on YAP-TEAD target genes was modest in parental A375 cells and A375-DT cells. Especially after the 10-day incubation, only two YAP-TEAD target genes showed a modest increase in expression while the expression of two other genes remained unchanged. Thus, the results of YAP-TEAD activation are inconclusive, and the confirmation of YAP-TEAD activation would have required the analysis of many more YAP-TEAD target genes. The YAP-TEAD target gene signature is not exactly known, but two recent studies have described the signature. These signatures consisted of 22 (Wang *et al*., 2018b) and 124 genes (Pham *et al*., 2021). Therefore, the measurement of only 4 YAP-TEAD target genes is not enough to make definite conclusions about YAP-TEAD activation.

The A375-DT and A375-D cell lines were created by administering 30 nM dabrafenib alone or in combination with 1 nM trametinib for 14 weeks. This treatment gives rise to cell lines resistant to the given concentrations of treatment and as explained above, the cell lines were not entirely resistant to dabrafenib or trametinib. The creation of resistant cell lines would have required treatment with increasing concentrations of compounds during extended periods of time, ranging from 2 months to even a year (Fratangelo *et al*., 2018; Wang *et al*., 2018a; Xie *et al*., 2017; Mudianto *et al*., 2021; Kim *et al*., 2016). Therefore, it is justified that due to the time limitation set for the master's thesis research project, the cell lines were created using only one concentration of compounds. It is also important to note that the goal of this master's thesis was not to create resistant cell lines. In addition, during this short 14-week treatment, the cells already began to show resistance to the compounds.

In the future, an entirely DT-treatment-resistant A375 cell line should be created by gradually increasing the concentrations of compounds. In this new cell line, the same experiments should be conducted to find how YAP-TEAD activation changes in the cell lines with full-blown dabrafenib and trametinib resistance. It should be also studied if YAP-TEAD activity remains increased after the development of other resistance mechanisms, such as genetic changes, or if YAP-TEAD activation is used only as a primary mechanism to escape the treatment and if in later stages, its significance is decreased. In addition, it should be studied how TEAD inhibition affects the entirely resistant A375 cells and if YAP-TEAD inhibition could resensitize resistant cells to dabrafenib and trametinib treatments. Indeed, previously YAP and TAZ knockdown has been shown to resensitize vemurafenib-resistant melanoma cells to vemurafenib (Kim *et al*., 2016).

The research project was conducted using multiple analysis methods giving consistent results. Importantly, the results obtained here are also consistent with the previous studies. There is an experimentally validated consensus that the inhibition of the MAPK pathway with BRAF inhibitor monotherapy rapidly leads to the reactivation of the MAPK pathway using resistance mechanisms involving the MAPK pathway (Patel *et al*., 2020; Yang *et al*., 2021; Kemper *et al*., 2014). Here, a similar response was observed with dabrafenib monotherapy. The A375 cells quickly reactivate their MAPK pathway and continue proliferation. Previous studies have also found that when the BRAF inhibitor is combined with the MEK inhibitor, a more sustained MAPK pathway inhibition is achieved (Long *et al*., 2017; Flaherty *et al*., 2012). Similarly, A375 cells here showed more sustained MAPK pathway inhibition together with slower cell proliferation when treated with DT combination, yet after long treatment with DT, the cells begin to proliferate faster due to the activation of alternative resistance mechanisms. Noteworthy, the results with the A375 cell line are in line with the previous studies conducted in the same cell line (Fisher *et al*., 2017; Yang *et al*., 2021).

Melanoma cells have been shown to express different phenotypes in response to targeted therapies (Marin-Bejar *et al*., 2021; Rambow *et al*., 2018; Hoek *et al*., 2008; Kemper *et al*., 2014). Previous studies have shown increased YAP-TEAD activation, especially in the cells expressing an invasive gene expression profile (Zhang *et al*., 2020). In the future, it would be interesting to study more closely, how different treatment-induced melanoma cell phenotypes are expressed in A375 cells in response to DT treatment, for example by sorting the cells with FACS, and further study how TEADi treatment affects these different types of cells. It should also be confirmed if elongated cells are undergoing an EMT-like phenotype switching, for example by measuring SOX10, MITF, and AXL expression in these cells.

TEADi were administered simultaneously with DT only on A375-DT cells and the effect on cell morphology and vimentin expression was studied. A previous study has suggested that YAP is necessary for the invasion of A375 cells and other cell lines (Zhang *et al*., 2020). Therefore, more analyses about the cells' invasive capacity should be conducted, such as Matrigel and wound healing assays. In the future, it should be also studied if TEADi decrease the proportion of cells exhibiting elongated morphology when added simultaneously with DT on parental treatment-naïve A375 cells. Finally, it should be studied if TEADi could prevent the invasion in other melanoma cell lines, and more importantly the dissemination and formation of secondary tumors *in* vivo and in patients with BRAF-mutant melanoma.

The results here encourage the study of YAP-TEAD activation in other melanoma cell lines and tumor samples from patients. Indeed, here only one melanoma cell line was used, and to obtain information on how YAP-TEAD is activated in melanoma and if TEAD inhibition has relevance in melanoma treatment, other cell lines must be studied. Also, the effect of YAP-TEAD inhibition on the survival of other cancer types harboring MAPK pathway alterations must be studied to find new indications for TEAD inhibitor treatment. Finally, YAP-TEAD activation and the effect of TEAD inhibition on primary and recurrent tumors with different treatment histories, mutations, and cellular origins should be studied.

4 CONCLUSIONS

The development of compounds targeting the MAPK pathway has revolutionized the treatment of BRAF-mutant melanoma. The MAPK pathway inhibitors have a robust initial response to tumor growth, but eventually, most patients relapse. Therefore, there is an urgent need to study the resistance mechanisms used by BRAF-mutant melanomas and to develop new treatments that could prevent the emergence of treatment resistance. The Hippo pathway effectors YAP and TAZ in combination with TEAD transcription factors have been found to mediate resistance to targeted therapies in melanoma and other cancers, and thus, they provide a novel and intriguing drug target in combat against treatment resistance.

In this master's thesis, it was hypothesized that the combined inhibition of BRAF and MEK activates YAP in a BRAF mutant melanoma cell line A375, and thus a triple combination of BRAF, MEK, and TEAD inhibitor is more efficacious than the BRAF/MEK inhibition. The study aimed to find a new resistance mechanism to targeted therapies in the A375 cell line and aimed to find a new indication for TEAD inhibitor treatment in preventing the emergence of treatment resistance to targeted MAPK pathway inhibition. Several previous studies have combined TEAD inhibition or YAP knockdown with BRAF inhibitor treatment in melanoma cell lines. Here, the current standard of care, dabrafenib and trametinib, were both combined with TEADi. In addition, in this study, a novel TEAD inhibitor Compound A, developed by Orion, was studied first time in a melanoma cell line with a $BRAF^{V600E}$ mutation.

The results indicate that most A375 cells become tolerant to the dabrafenib and DT treatments and they resume cell proliferation and begin to show resistance to the compounds. The data shows modest YAP-TEAD activation in response to the initiation of dabrafenib and DT treatments. The 14-week treatment of A375 cells with DT (A375-DT cells) also shows a moderate increase in YAP-TEAD activation. The combined TEAD inhibitor and DT treatment on A375-DT or A375 cells, however, revealed that the inhibition of TEAD only moderately decreases cell growth. These findings suggest that YAP-TEAD activation is used as a resistance mechanism in A375 and A375-DT cells. However, the YAP-TEAD activation is not essential for the development of treatment resistance or the survival of the A375 and A375-DT cells upon DT treatment. Thus, TEAD inhibition is not an effective treatment in preventing the emergence of treatment resistance in A375 cells.

Identification of new resistance mechanisms paves the way for the use of new therapeutic strategies and drug combinations. This study brings forward the understanding of different resistance mechanisms used by melanoma cells. In addition, this study along with the previous studies suggests that the response to TEAD inhibition is highly dependent on the cell line. In a clinical context, this raises a concern about how to identify the patients who could benefit from the TEAD inhibitor treatment. Therefore, new means for the identification of this patient population are needed. So far, TEADi have been proven efficacious only in the treatment of a very narrow selection of tumors with pre-existing Hippo pathway alterations that inactivate this pathway. These cancers include NF2-mutant mesothelioma, but the population of these patients is small (Hu *et al*., 2022). Thus, this study participates in the important quest aiming to the identification of new patient populations who could benefit from the TEAD inhibitor treatment and helps to narrow down the population of cancer types with the potential to benefit from TEAD inhibition. The obtained results also highlight that it is important to find the best timing for the initiation of TEAD inhibitor treatment. The results reported here demonstrate that the addition of TEADi alone does not affect the treatment naïve cells, but it may still be beneficial to add TEADi before the initiation of DT treatment to reduce the population of escaping cells. In the future, it is also important to study how sequential treatment with DT and TEADi together with drug holidays contribute to patient outcomes.

To summarize, the A375 cell line was used to study the activation of YAP-TEAD as a resistance mechanism to the treatment with BRAF and MEK inhibitors. The results showed increased YAP-TEAD activation after short and long-term treatment with DT suggesting that YAP-TEAD is used as a resistance mechanism in the A375 cell line. However, the treatment with TEADi showed that the activation of YAP-TEAD is not essential for the growth of A375 cells upon DT treatment. Thus, inhibition of TEAD does not prevent the emergence of treatment resistance in this cell line and is not an effective treatment option. However, further studies in other melanoma cell lines are needed to confirm the relevance of YAP-TEAD activation as a mechanism of resistance to targeted therapies.

5 MATERIALS AND METHODS

5.1 Compounds

In this research project, dabrafenib and trametinib were used as a standard of care. Dabrafenib was purchased from MedChem Express and trametinib from AK Scientific. TEAD inhibitor VT-103 was synthesized by Orion according to an article published by Tang *et al.* in 2021 (Tang *et al.*, 2021). Compound A is a TEAD inhibitor developed and synthesized by Orion. Nocodazole (Sigma-Aldrich, M1404-2MG) and staurosporine (Sigma-Aldrich, S5921-1MG) were purchased and used as control compounds.

5.2 Cell lines

The human melanoma cell line A375 with $BRAF^{V600E}$ mutation was obtained from the American Type Culture Collection (ATCC, Manassas, VA, USA). The cells were cultured in Dulbecco's Modified Eagle's Medium (DMEM) supplemented with 10 % fetal bovine serum (FBS) and 1 % Penicillin-Streptomycin (hereby termed as complete culture medium). The cells were tested negative for the presence of mycoplasma with MycoAlert™ PLUS Mycoplasma Detection Kit. The cells were maintained in Corning® T-75 cell culture flasks (37˚C, 5 % CO_2).

The A375-D and A375-DT cell lines were derived from parental A375 cells. The cells were cultured for 14 weeks in the complete culture medium with 30nM dabrafenib (A375-D) or 30nM dabrafenib and 1nM trametinib (A375-DT). The cells were maintained in Corning® CellBIND® T-75 cell culture flasks (37˚C, 5 % CO_2).

All 3 cell lines were subcultured every 3–4 days when the cells reached 70–90 % confluency. The cells were washed once with 1x Dulbecco's Phosphate Buffered Saline (DPBS) and detached with 0.25 % Trypsin-EDTA. The detached cells were suspended into the complete culture medium to inactivate the trypsin, and the cell suspension was centrifuged (800 rpm, 5 minutes, 24°C). Finally, 150 000–250 000 A375 cells in the complete culture medium were seeded into new Corning® T-75 cell culture flask. The A375-D and A375-DT cells were resuspended into the complete culture medium with dabrafenib or DT, and the cells were split into new Corning® CellBIND® cell culture flasks in 1:3–1:10 ratios. The list of materials used in the cell culture is provided in Table 1.

Table 1. Material used in cell culture.

Material	Supplier	Catalog number
Dulbecco's Modified Eagle's Medium (DMEM)	ATCC	30-2002
Fetal Bovine Serum (FBS)	Sigma-Aldrich	F7524
Penicillin-Streptomycin	Gibco™ ThermoFisher Scientific	15140-122
Dulbecco's Phosphate Buffered Saline (DPBS)	Gibco™ ThermoFisher Scientific	14190-094
Trypsin-EDTA (0.5 %), no phenol red	Gibco™ ThermoFisher Scientific	15400-054
MycoAlert™ PLUS Mycoplasma Detection Kit	Lonza	LT07-710
Corning® 75 cm² U-shape cell culture flask	Corning	430641U
Corning® CellBIND® 75cm² U-shape cell culture flask	Corning	3290

5.3 Combination assay

The assay-ready LLC CellCarrier-384 Ultra microplates (Perkin Elmer, 6057302) were prepared using an acoustic dispenser Echo® 655 (Labcyte). The acoustic dispenser added dabrafenib and trametinib in 5 concentrations (final concentrations 1 nM, 3 nM, 10 nM, 30 nM, and 100 nM) into the microplate (4 replicates/concentration). In addition, 0.2 % DMSO (Sigma-Aldrich, D2650-100ML) and 0.05 mg/ml nocodazole (Sigma-Aldrich, M1404) were used as controls. Next, 1000 A375 cells were plated into each well containing DMSO, nocodazole, or different concentrations of trametinib and dabrafenib in combination or alone. The cell growth was followed for 4 days with Incucyte® S3 (Sartorius) (37 ˚C, 5 % CO_2). After 4 days, the cells were incubated in a fixing solution containing 3.7 % formaldehyde (Sigma Aldrich, 252549-1L), 1:10 000 HOECHST 33342 (InVitrogen, H3570), and 1x DPBS (Gibco™ ThermoFisher Scientific, 14200-067) for 15 minutes in room temperature. After the fixing, the cells were washed with 1x DPBS and imaged with Operetta CLS High-Content Analysis System (PerkinElmer) with Harmony software (PerkinElmer, 4.9.2137.273) using a 10x air objective. The number, shape, size, and intensity of nuclei were analyzed using Columbus™ Image Data Storage and Analysis system version 2.9.1 (Perkin Elmer).

5.4 Dose-response assay

The cell proliferation upon dabrafenib and trametinib treatments was determined in A375-D, A375-DT, and A375 parental cells. The cells were plated on Corning® CellBIND® 384-well Flat Clear Bottom Black Polystyrene microplate (Corning, 3770). Into each well, 200 cells were plated in the complete culture medium. On the following day, dabrafenib or trametinib were added on top of cells with Microlab Star automated liquid handler (Hamilton) in half logarithmic dilutions from 1 to 10 000 nM (4 replicates/concentration). In addition, 0.1 % DMSO (Sigma-Aldrich, D2650-100ML) and 0.05 ng/µl nocodazole (Sigma-Aldrich, M1404) were used as controls. The cells were placed into an incubator and their growth was followed for 4 (parental cells) or 6 (A375-D and A375-DT cells) days with Incucyte® S3 (Sartorius), and finally, the cells were fixed.

The cell proliferation in the presence of TEADi was studied in parental and A375-DT cells. First, 200 cells/well were plated on Corning® CellBIND® 384-well Flat Clear Bottom Black Polystyrene microplate (Corning, 3770). The A375-DT cells were plated in a complete culture medium with 30 nM dabrafenib and 1nM trametinib, and the A375 cells were plated in the complete culture medium with or without 30 nM dabrafenib and 1 nM trametinib. On the following day, VT-103 or Compound A was added on top of the cells with Microlab Star automated liquid handler (Hamilton) in half logarithmic dilutions from 1 to 10 000 nM. Also, 0.05 ng/µl nocodazole (Sigma-Aldrich, M1404) and 0.1 % DMSO (Sigma-Aldrich, D2650-100ML) were used as controls. Every plate contained 4 replicates for each TEADi concentration, and the experiments were repeated 1–3 times. The A375 cells in the complete culture medium were fixed after 4 days. A375-DT cells and A375 cells with dabrafenib and trametinib in the culture medium were fixed after 6 days of incubation.

The cells were fixed for 15 minutes at room temperature using a solution of 3.7 % formaldehyde (Sigma Aldrich, 252549-1L) and 1:10 000 HOECHST 33342 (InVitrogen, H3570) in 1x DPBS (Gibco™ ThermoFisher Scientific, 14200-067). After fixing, the cells were washed with 1x DPBS, and the plates were imaged with Operetta CLS High-Content Analysis System (PerkinElmer) with Harmony software (PerkinElmer, 4.9.2137.273) using a 10x air objective. The cell number was calculated with Columbus™ Image Data Storage and Analysis system version 2.9.1 (Perkin Elmer).

5.5 RNA extraction

To study the effect of dabrafenib and trametinib treatment on A375 cells' *YAP1* and YAP-TEAD target gene expression, 9 500 A375 cells/well were plated on a Corning® CellBind® Surface 6-well plate (Corning, 3335) in complete culture medium. On the following day, 0.2 % DMSO, 30 nM dabrafenib, or 30 nM dabrafenib in combination with 1 nM trametinib were added to the cells. The RNA samples were collected on treatment days 3, 7, and 10 (2 replicates/treatment at each time point). The culture medium with compounds was changed every 3 to 4 days.

To study the effect of TEADi treatment on *YAP1* and YAP-TEAD target gene expression, 200 000 A375 and A375-DT cells/well were plated on a Corning® CellBind® Surface 6-well plate (Corning, 3335). A375 cells were plated in the complete culture medium with 0.2 % DMSO, and A375-DT cells were plated in the complete culture medium with 30 nM dabrafenib and 1 nM trametinib. On the following day, 0.1 % DMSO or 10 µM Compound A or VT-103 were added to the cells (3 replicates/treatment). After 6 h of TEADi addition, the RNA samples were collected.

The RNA isolation was started by washing the cells once with 1x DPBS (Gibco™ ThermoFisher Scientific, 14190-094), and the RNA was isolated with the Macherey-Nagel Nucleospin® RNA kit (Macherey & Nagel, 740955.250) according to the manufacturer's protocol. Cell lysis was done without β-mercaptoethanol, and 70 % ethanol was added before the cell lysates were moved into NucleoSpin RNA columns. The RNA yield and purity were measured with DeNovix DS II FX Spectrophotometer/Fluorometer (DeNovix).

5.6 Complementary DNA synthesis and RT-qPCR

To synthesize complementary DNA (cDNA) from the A375 cells treated for 1, 7, or 10 days with 30 nM dabrafenib alone or in combination with 1 nM trametinib, 0.25 µg RNA was used from each sample because a small cell number led to low RNA yield. For the cDNA synthesis of A375 and A375-DT cells treated with TEADi, 1 µg RNA was used from each sample. The cDNA synthesis was performed with SensiFAST cDNA Synthesis Kit (Bioline, BIO-65054) according to the manufacturer's protocol without the optional step.

The quantitative real-time polymerase chain reaction (RT-qPCR) was performed according to the manufacturer's protocol by mixing 1.7 ng/µl cDNA with TaqMan® Fast Advanced Master Mix, TaqMan® Gene Expression Assay, and RT-PCR Grade Water (Invitrogen™ ThermoFisher Scientific, AM9935) into the end volume of 20 µl. The list of used TaqMan® gene expression assays is provided in Table 2. The RT-qPCR was performed using Quantstudio 6 Flex (Applied Biosystems™). The following program was used: 95°C for 20 s; 40 cycles of 95°C for 1 s and 60°C for 20 s. The fold changes were calculated using the ΔΔCt method (see 5.11). The RT-qPCR was performed with 2–3 biological replicates of which 2 technical replicates were prepared for each.

Table 2. TaqMan® gene expression assays used in the RT-qPCR.

Gene	Taqman®	Probe and dye label	Function
GAPDH	Hs02786624_g1	FAM-MGB	Housekeeping gene
YAP1	Hs00902712_g1	FAM-MGB	TEAD coactivator
CTGF	Hs00170014_m1	FAM-MGB	YAP-TEAD target gene
CYR61	Hs00155479_m1	FAM-MGB	YAP-TEAD target gene
ANKRD1	Hs00173317_m1	FAM-MGB	YAP-TEAD target gene
AMOTL2	Hs01048101_m1	FAM-MGB	YAP-TEAD target gene

5.7 Apoptosis assay

Into Corning® CellBIND® 96-well Flat Clear Bottom Black Polystyrene microplate (Corning, 3340), 320 A375 cells/well were plated in the complete culture medium. On the following day, the medium was changed to a new complete culture medium with 0.2 % DMSO (Sigma-Aldrich, D2650-100ML), or 30 nM dabrafenib alone or in combination with 1 nM trametinib (4 replicates/treatment). IncuCyte® Caspase-3/7 Green Apoptosis Assay Reagent (Essen BioScience, #4440) was added 1:2 000 into the cell culture medium to detect apoptosis. The cells were placed into Incucyte® S3 (Sartorius) (37 ˚C, 5 % CO2), and the confluency and green fluorescence for apoptosis were followed at 6 h intervals for 5 days using a 10x objective.

TEADi effect on A375-DT cells was studied by plating 320 cells/well into a Corning® CellBIND® 96-well Flat Clear Bottom Black Polystyrene microplate (Corning, 3340) in a complete culture medium with 30 nM dabrafenib and 1 nM trametinib or 0.2 % DMSO. On the following day, 10 µM VT-103 or Compound A, 0.1 % DMSO (Sigma-Aldrich, D2650-100ML), or 10 µM staurosporine (Sigma-Aldrich, S5921-1MG) were added onto the cells in complete culture medium with 30 nM dabrafenib and 1 nM trametinib (2 replicates/treatment). IncuCyte Caspase-3/7 Green Apoptosis Assay Reagent (Essen BioScience, #4440) was added 1:2 000 onto the cells, and the confluency and green fluorescence for apoptosis were followed with Incucyte® S3 (Sartorius) (37 ˚C, 5 % CO2) at 6 h intervals for 5 days using a 10x objective.

5.8 Senescence-associated β-galactosidase staining

Into each well of the Corning® CellBIND® 6-well plate (Corning, 3335), 11 875 A375 or A375-DT cells were plated. The A375 cells were plated in the complete culture medium, and the A375-DT cells were plated in the complete culture medium with 30nM dabrafenib and 1 nM trametinib. On the following day, 0.2 % DMSO (Sigma-Aldrich, D2650-100ML), or 30 nM dabrafenib alone or in combination with 1nM trametinib (2 replicates/treatment) were added to the A375 cells in the complete culture medium. On the A375-DT cells, 0.2 % DMSO (Sigma-Aldrich, D2650-100ML), or 10µM Compound A or VT-103 (2 replicates/treatment) were added in the complete culture medium with 30nM dabrafenib and 1nM trametinib. After 2-day incubation with the compounds, the cells were fixed and stained with Senescence β-Galactosidase Staining Kit (Cell Signaling Technology, 9860S) according to the manufacturer’s protocol. The X-Gal was diluted into DMSO (Sigma-Aldrich, D2650-100ML), and the pH of the staining solution was adjusted to 6.07 with NaOH (Sigma Aldrich, S8045) and HCl (Merck, 100317). The pH was measured using a SevenEasy pH meter (Mettler Toledo), which was calibrated with pH 4.005 (Hach, S11M002), pH 7.000 (Hach, S11M004), and pH 10.012 (Hach, S11M007) Certified Buffer Standard Solutions. The cells were incubated with the staining solution for 3 days at 37 ˚C without CO_2 and imaged with CKX53 Cell Culture Microscope (Olympus) using 20x magnification.

5.9 Immunocytochemistry and cell staining

For 10-day incubation, 320 A375 cells/well were plated on Corning® CellBIND® 96-well Flat Clear Bottom Black Polystyrene microplates (Corning, 3340) in the complete culture medium. On the following day, the medium was changed and a new culture medium containing 0.2 % DMSO or 30 nM dabrafenib alone or in combination with 1 nM trametinib was added to the cells. After 3, 7, and 10 days of treatment, one plate was fixed at each time point. The culture medium with compounds was changed every 3–4 days.

To compare A375, A375-D, and A375-DT cell lines, 6 000 A375 cells/well in the complete culture medium, 4 000 A375-D cells/well in the complete culture medium with 30 nM dabrafenib, and 4 000 A375-DT cells/well in the complete culture medium with 30 nM dabrafenib and 1 nM trametinib were plated on Corning® CellBIND® 96-well Flat Clear Bottom Black Polystyrene microplate (Corning, 3340). The cells were incubated overnight and fixed.

Finally, to study how TEAD inhibitor treatment affected A375- DT cells, 320 A375-DT cells/well were plated on Corning® CellBIND® 96-well Flat Clear Bottom Black Polystyrene microplate

(Corning, 3340) in the complete culture medium with 30 nM dabrafenib and 1 nM trametinib. On the following day, 0.1 % DMSO, or 10 µM Compound A or VT-103, was added on top of 30 nM dabrafenib and 1 nM trametinib treatment. The cells were incubated with TEADi for 3 days and fixed.

The cells were fixed with 3.7 % formaldehyde (Sigma-Aldrich, 252549-1L) in 1x DPBS (Gibco™ ThermoFisher Scientific, 14200-067) for 15 minutes at room temperature. Next, the cells were washed three times with 1x DPBS and permeabilized with 0.1 % Triton™ X-100 (Sigma-Aldrich, X100) in 1x DPBS (PBST). The cells were blocked with 5 % bovine serum albumin (BSA) (Sigma-Aldrich, A2153) in 0.1 % PBST for 1 h at room temperature. The primary antibodies were diluted into 5 % BSA in 0.1 % PBST and incubated overnight at 4 ˚C. On the following day, the cells were washed twice with 5 % BSA in 1x DPBS, and the cells were incubated with secondary antibodies and DAPI or cell dyes and DAPI in 5 % BSA in 1x DPBS for 1 h at room temperature. The lists of primary antibodies, secondary antibodies, and cell stains are provided in Tables 3, 4, and 5, respectively. Finally, the cells were washed twice with 5 % BSA in 1x DPBS and once with 1x DPBS, and the cells were left in 1x DPBS. The cells were imaged with Operetta CLS High-Content Analysis System (PerkinElmer) with Harmony software (PerkinElmer, 4.9.2137.273) using 20x air objective or 63x water immersion objective. The images were analyzed with Columbus™ Image Data Storage and Analysis system version 2.9.1 (Perkin Elmer).

Table 3. Primary antibodies used in Immunocytochemistry (ICC).

Antibody	**Host species**	**Dilution for ICC**	**Mono-/polyclonal**	**Supplier (Cat. number)**
Recombinant Anti-YAP1 antibody [EP1674Y]	Rabbit	1:200	Polyclonal	Abcam (ab52771)
Anti-Ki67 antibody	Rabbit	0.9 ug/ml	Polyclonal	Abcam (ab15580)
Phospho-p44/42 MAPK (Erk1/2) (Thr202/Tyr204)	Rabbit	1:200	Polyclonal	Cell Signaling Technology (#9101s)
Recombinant Anti-Vimentin antibody [EPR3776]	Rabbit	1:600	Monoclonal	Abcam (ab92547)

Table 4. Secondary antibody used in ICC.

Antibody	Target	Conjugate	Host species	Dilution	Mono/polyclonal	Supplier (Cat. number)
Goat Anti-Rabbit IgG (H+L) Cross-Adsorbed Secondary Antibody	Rabbit IgG (H+L)	Alexa Fluor® 568	Goat	1:1 000	Polyclonal	Invitrogen™ ThermoFisher (A11011)

Table 5. Cell staining dyes.

Cell dye	Target	Conjugate/ λex/λem	Dilution	Supplier (Cat. number)
Alexa Fluor™ Phalloidin	F-actin	Alexa Fluor™ 568	1:40	Invitrogen™ ThermoFisher (A12380)
DAPI (4′,6-Diamidino-2-phenylindole dihydrochloride)	DNA	364/454 nm	1:1 000	Sigma-Aldrich Finland/YA-Kemia (D9542-10MG)
Hoechst 33342, Trihydrochloride, Trihydrate	DNA	350/461 nm	1:10 000	Invitrogen™ ThermoFisher (H3570)

5.10 Image analysis

The image analysis was performed with Columbus™ Image Data Storage and Analysis system version 2.9.1 (Perkin Elmer). First, the nuclei of the cells were segmented with DAPI or HOECHST 33342. The nuclear protein Ki67 was detected with a secondary antibody and nuclei with high Ki67 intensity values (>4 500) were considered positive. Next, the cells' cytoplasm was detected with secondary antibodies (pERK, YAP1, Vimentin) or phalloidin. Cells with high pERK cytoplasmic intensity values (>1 200) were considered positive. YAP1 N/C ratio >1.3 was used to define if YAP1 was located in the nucleus. For vimentin, a ring region surrounding the nucleus was determined, and the intensity of vimentin in this region was calculated. The size, shape, and texture properties of the cells were calculated based on the phalloidin staining. The texture properties were calculated with the SER features method in Columbus. Finally, the Linear classifier algorithm was trained to recognize three different cell populations with different morphologies (normal, large, and elongated).

5.11 Data analysis

For dose-response and combination analyses, raw data were normalized to nocodazole (0 %) and DMSO (100 %). Dose-response curves were generated using GraphPad Prism 9.1.0 software (GraphPad Software) for Windows, and the IC50 and IC90 values were determined with nonlinear regression analysis using the log(inhibitor) vs. response – Variable slope -equation.

$$Y = Bottom\ +\ (Top - Bottom)/(1 + 10\text{^}((LogIC50 - X) * HillSlope))$$

An unpaired t-test was used to calculate the difference between the growth of A375 and A375-DT cells upon the triple combination treatment with TEADi and DT. The data were calculated as means ±SEM.

To determine the gene expression, the $2^{-\Delta\Delta Ct}$ method was used. First, ΔCt values were calculated by subtracting the averages of technical replicates of the housekeeping gene GAPDH from the averages of technical replicates of the studied genes. To calculate ΔΔCt, the ΔCt value of one DMSO biological replicate on treatment day 3 (the 10-day experiment) or the average of ΔCt values of biological replicates treated with DMSO (A375 and A375-DT cells treated with TEADi or DMSO) were subtracted from the ΔCt values of the cells treated with the compounds of interest. Finally, the fold gene expression values were calculated with $2^{-\Delta\Delta Ct}$. The fold gene expression values were visualized and analyzed with GraphPad Prism 9.1.0 software for Windows. Two-way ANOVA with Tukey’s multiple comparisons test was used to calculate significant differences in gene expression between the 3 treatment groups. Two-way ANOVA with Šídák's multiple comparisons test was used to calculate differences in gene expression between A375 and A375-DT cell lines. P-values less than 0.05 were considered statistically significant (95 % confidence interval). The data were calculated as means ±SEM.

The immunofluorescence data were analyzed and visualized using GraphPad Prism 9.1.0 software for Windows. Ordinary one-way ANOVA with Tukey’s multiple comparisons test was used to compare differences between 3 treatment groups or cell lines. A two-tailed unpaired t-test was used to compare YAP1 nuclear localization between A375 and A37-DT cell lines. P-values less than 0.05 were considered statistically significant (95 % confidence interval). The data were calculated as means ±SEM.

6 ACKNOWLEDGEMENTS

I want to sincerely thank my supervisors Maria Georgiadou and Reetta Riikonen for all the help, guidance, and support they have given me during this master's thesis project. They have given me a lot of their time to answer all my questions and give me new directions. I also want to thank the Cancer Cell Signalling team and other colleagues in Orion Pharma for all the help I have gotten during this process. Especially, I want to thank Marianne Laine for the valuable help I have received with my experiments, cell culturing, and in the lab.

Finally, I want to thank my family and friends for supporting me through my studies and this thesis project. A special mention to Marko for always encouraging me to chase my dreams and goals no matter what.

7 ABBREVIATIONS

A375-D	A375 cells treated with 30 nM dabrafenib for 14 weeks
A375-DT	A375 cells treated with 30 nM dabrafenib and 1 nM trametinib for 14 weeks
AKT	AKT Serine/Threonine Kinase
AMOTL2	Angiomotin like 2
ANKRD1	Ankyrin repeat domain 1
AXL	AXL receptor tyrosine kinase
BCL2L1	B-cell lymphoma-2 like 1
BRAF	v-raf murine sarcoma viral oncogene homolog B1
CDKN2A	Cyclin-dependent kinase inhibitor 2A
cDNA	Complementary DNA
CTGF	Connective tissue growth factor
CYR61	Cysteine-rich angiogenic inducer 61
DPBS	Dulbecco’s phosphate buffered saline
DT	Combined treatment with 30 nM dabrafenib and 1 nM trametinib
DTP	Drug tolerant persister
EGFR	Epidermal growth factor receptor
EMICERI	EQTN MOB3B IFNK C9orf72 enhancer RNA I
EMT	Epithelial to mesenchymal transition
ERK	Extracellular signal-regulated protein kinase
FDA	U.S. Food and Drug Administration
ICC	Immunocytochemistry

KRAS	Kirsten rat sarcoma viral oncogene homolog
LATS1/2	Large tumor suppressor kinase 1 and 2
MAPKi	MAPK pathway inhibitor
MEK	Mitogen-activated protein kinase kinase
MITF	Microphthalmia-associated transcription factor
MOB	Mps one binder kinase activator
MST1/2	Mammalian sterile 20-like kinase 1 and 2
MYC	MYC proto-oncogene
N/C	Nuclear-cytoplasmic
NF2	Neurofibromin-2
NRAS	Neuroblastoma RAS viral oncogene homolog
NSCLC	Non-small cell lung cancer
OS	Overall survival
PBST	Phosphate-buffered saline/tween
pERK	Phosphorylated ERK
PFS	Progression-free survival
PI3K	Phosphoinositide-3-kinase
PTEN	Phosphatase and tensin homolog
RAF	Rapidly accelerated fibrosarcoma
Rho	Ras homolog
RTK	Receptor tyrosine kinase
RT-qPCR	Quantitative real-time polymerase chain reaction
SAV1	Salvador family WW domain containing protein 1

SOS1/2	Son of sevenless homolog 1 and 2
SOX10	SRY-box transcription factor 10
TAZ	WW-domain-containing transcription regulator 1
TEAD	Transcriptional enhanced associate domain
TEADi	TEAD inhibitors
WNT	Wingless-related integration site
YAP	Yes-associated protein

8 REFERENCES

American Cancer Society. 2022. Cancer Facts and Figures 2022. American Cancer Society, Atlanta. 24–26 pp.

Bae, S.J., L. Ni, A. Osinski, D.R. Tomchick, C.A. Brautigam, and X. Luo. 2017. SAV1 promotes Hippo kinase activation through antagonizing the PP2A phosphatase STRIPAK. *Elife*. 6:e30278. doi:10.7554/ELIFE.30278.

Bai, H., N. Zhang, Y. Xu, Q. Chen, M. Khan, J.J. Potter, S.K. Nayar, T. Cornish, G. Alpini, S. Bronk, D. Pan, and R.A. Anders. 2012. Yes-associated protein regulates the hepatic response after bile duct ligation. *Hepatology*. 56:1097–1107. doi:10.1002/HEP.25769.

Bao, Y., Y. Hata, M. Ikeda, and K. Withanage. 2011. Mammalian Hippo pathway: from development to cancer and beyond. *The Journal of Biochemistry*. 149:361–379. doi:10.1093/JB/MVR021.

Batus, M., S. Waheed, C. Ruby, L. Petersen, S.D. Bines, and H.L. Kaufman. 2013. Optimal Management of Metastatic Melanoma: Current Strategies and Future Directions. *Am J Clin Dermatol*. 14:194. doi:10.1007/S40257-013-0025-9.

Bell, C.C., K.A. Fennell, Y.C. Chan, F. Rambow, M.M. Yeung, D. Vassiliadis, L. Lara, P. Yeh, L.G. Martelotto, A. Rogiers, B.E. Kremer, O. Barbash, H.P. Mohammad, T.M. Johanson, M.L. Burr, A. Dhar, N. Karpinich, L. Tian, D.S. Tyler, L. MacPherson, J. Shi, N. Pinnawala, C. Yew Fong, A.T. Papenfuss, S.M. Grimmond, S.J. Dawson, R.S. Allan, R.G. Kruger, C.R. Vakoc, D.L. Goode, S.H. Naik, O. Gilan, E.Y.N. Lam, J.C. Marine, R.K. Prinjha, and M.A. Dawson. 2019. Targeting enhancer switching overcomes non-genetic drug resistance in acute myeloid leukaemia. *Nat Commun*. 10:1–15. doi:10.1038/s41467-019-10652-9.

Bum-Erdene, K., D. Zhou, G. Gonzalez-Gutierrez, M.K. Ghozayel, Y. Si, D. Xu, H.E. Shannon, B.J. Bailey, T.W. Corson, K.E. Pollok, C.D. Wells, and S.O. Meroueh. 2019. Small-Molecule Covalent Modification of Conserved Cysteine Leads to Allosteric Inhibition of the TEAD·Yap Protein-Protein Interaction. *Cell Chem Biol*. 26:378-389.e13. doi:10.1016/j.chembiol.2018.11.010.

Burotto, M., V.L. Chiou, J.-M. Lee, and E.C. Kohn. 2014. The MAPK pathway across different malignancies: A new perspective. *Cancer*. 120:3456. doi:10.1002/CNCR.28864.

Cai, J., N. Zhang, Y. Zheng, R.F. de Wilde, A. Maitra, and D. Pan. 2010. The Hippo signaling pathway restricts the oncogenic potential of an intestinal regeneration program. *Genes Dev*. 24:2388. doi:10.1101/GAD.1978810.

Camargo, F.D., S. Gokhale, J.B. Johnnidis, D. Fu, G.W. Bell, R. Jaenisch, and T.R. Brummelkamp. 2007. YAP1 Increases Organ Size and Expands Undifferentiated Progenitor Cells. *Current Biology*. 17:2054–2060. doi:10.1016/j.cub.2007.10.039.

Caunt, C.J., M.J. Sale, P.D. Smith, and S.J. Cook. 2015. MEK1 and MEK2 inhibitors and cancer therapy: the long and winding road. *Nat Rev Cancer*. 15:577–592. doi:10.1038/NRC4000.

Chan, E.H.Y., M. Nousiainen, R.B. Chalamalasetty, A. Schäfer, E.A. Nigg, and H.H.W. Sillje. 2005. The Ste20-like kinase Mst2 activates the human large tumor suppressor kinase Lats1. *Oncogene*. 24:2076–2086. doi:10.1038/SJ.ONC.1208445.

Chan, P., X. Han, B. Zheng, M. Deran, J. Yu, G.K. Jarugumilli, H. Deng, D. Pan, X. Luo, and X. Wu. 2016. Autopalmitoylation of TEAD Proteins Regulates Transcriptional Output of Hippo Pathway. *Nat Chem Biol*. 12:289. doi:10.1038/NCHEMBIO.2036.

Chan, S.W., J.L. Chun, K. Guo, P.N. Chee, I. Lee, W. Hunziker, Q. Zeng, and W. Hong. 2008. A Role for TAZ in Migration, Invasion, and Tumorigenesis of Breast Cancer Cells. *Cancer Res*. 68:2592–2598. doi:10.1158/0008-5472.CAN-07-2696.

Chen, Q., N. Zhang, R.S. Gray, H. Li, A.J. Ewald, C.A. Zahnow, and D. Pan. 2014. A temporal requirement for Hippo signaling in mammary gland differentiation, growth, and tumorigenesis. *Genes Dev*. 28:437. doi:10.1101/GAD.233676.113.

Cheng, L., A. Lopez-Beltran, F. Massari, G.T. MacLennan, and R. Montironi. 2017. Molecular testing for BRAF mutations to inform melanoma treatment decisions: a move toward precision medicine. *Modern Pathology*. 31:24–38. doi:10.1038/modpathol.2017.104.

Chin, L., G. Merlino, and R.A. DePinho. 1998. Malignant melanoma: modern black plague and genetic black box. *Genes Dev*. 12:3467–3481. doi:10.1101/GAD.12.22.3467.

Chong, C.R., and P.A. Jänne. 2013. The quest to overcome resistance to EGFR-targeted therapies in cancer. *Nat Med*. 19:1389–1400. doi:10.1038/nm.3388.

Christie, E.L., S. Fereday, K. Doig, S. Pattnaik, S.J. Dawson, and D.D.L. Bowtell. 2017. Reversion of BRCA1/2 germline mutations detected in circulating tumor DNA from patients with high-grade serous ovarian cancer. *Journal of Clinical Oncology*. 35:1274–1280. doi:10.1200/JCO.2016.70.4627.

de Conti, G., M.H. Dias, and R. Bernards. 2021. Fighting Drug Resistance through the Targeting of Drug-Tolerant Persister Cells. *Cancers (Basel)*. 13:1–15. doi:10.3390/CANCERS13051118.

Cordaro, F.G., A.L. de Presbiteris, R. Camerlingo, N. Mozzillo, G. Pirozzi, E. Cavalcanti, A. Manca, G. Palmieri, A. Cossu, G. Ciliberto, P.A. Ascierto, S. Travali, E.J. Patriarca, and E. Caputo. 2017. Phenotype characterization of human melanoma cells resistant to dabrafenib. *Oncol Rep*. 38:2751. doi:10.3892/OR.2017.5963.

Cordenonsi, M., F. Zanconato, L. Azzolin, M. Forcato, A. Rosato, C. Frasson, M. Inui, M. Montagner, A.R. Parenti, A. Poletti, M.G. Daidone, S. Dupont, G. Basso, S. Bicciato, and S. Piccolo. 2011. The hippo transducer TAZ confers cancer stem cell-related traits on breast cancer cells. *Cell*. 147:759–772. doi:10.1016/j.cell.2011.09.048.

Cristofani, R., M. Piccolella, M. Montagnani Marelli, B. Tedesco, A. Poletti, and R.M. Moretti. 2022. HSPB8 counteracts tumor activity of BRAF- and NRAS-mutant melanoma cells by modulation of RAS-prenylation and autophagy. *Cell Death Dis*. 13. doi:10.1038/S41419-022-05365-9.

Dai, B., J. Meng, M. Peyton, L. Girard, W.G. Bornmann, L. Ji, J.D. Minna, B. Fang, and J.A. Roth. 2011. STAT3 mediates resistance to MEK inhibitor through microRNA miR-17. *Cancer Res*. 71:3658–3668. doi:10.1158/0008-5472.CAN-10-3647/649679/AM/STAT3-MEDIATES-RESISTANCE-TO-MEK-INHIBITOR-THROUGH.

Davies, H., G.R. Bignell, C. Cox, P. Stephens, S. Edkins, S. Clegg, J. Teague, H. Woffendin, M.J. Garnett, W. Bottomley, N. Davis, E. Dicks, R. Ewing, Y. Floyd, K. Gray, S. Hall, R. Hawes, J. Hughes, V. Kosmidou, A. Menzies, C. Mould, A. Parker, C. Stevens, S. Watt, S. Hooper, H. Jayatilake, B.A. Gusterson, C. Cooper, J. Shipley, D. Hargrave, K. Pritchard-Jones, N. Maitland, G. Chenevix-Trench, G.J. Riggins, D.D. Bigner, G. Palmieri, A. Cossu, A. Flanagan, A. Nicholson, J.W.C. Ho, S.Y. Leung, S.T. Yuen, B.L. Weber, H.F. Seigler, T.L. Darrow, H. Paterson, R. Wooster, M.R. Stratton, and P.A. Futreal. 2002. Mutations of the BRAF gene in human cancer. *Nature*. 417:949–954. doi:10.1038/NATURE00766.

Dhillon, A.S., S. Hagan, O. Rath, and W. Kolch. 2007. MAP kinase signalling pathways in cancer. *Oncogene*. 26:3279–3290. doi:10.1038/SJ.ONC.1210421.

Diaz, L.A., R. Williams, J. Wu, I. Kinde, J.R. Hecht, J. Berlin, B. Allen, I. Bozic, J.G. Reiter, M.A. Nowak, K.W. Kinzler, K.S. Oliner, and B. Vogelstein. 2012. The molecular evolution of acquired resistance to targeted EGFR blockade in colorectal cancers. *Nature*. 486:537–540. doi:10.1038/nature11219.

Dickson, P. v., and J.E. Gershenwald. 2011. Staging and Prognosis of Cutaneous Melanoma. *Surg Oncol Clin N Am*. 20:17. doi:10.1016/J.SOC.2010.09.007.

Dimri, G.P., X. Lee, G. Basile, M. Acosta, G. Scott, C. Roskelley, E.E. Medrano, M. Linskens, I. Rubelj, O. Pereira-Smith, M. Peacocke, and J. Campisi. 1995. A biomarker that identifies senescent human cells in culture and in aging skin in vivo. *Proc Natl Acad Sci U S A*. 92:9367. doi:10.1073/PNAS.92.20.9363.

Dobry, A.S., C.K. Zogg, F.S. Hodi, T.R. Smith, P.A. Ott, and J.B. Iorgulescu. 2018. Management of metastatic melanoma: improved survival in a national cohort following the approvals of checkpoint blockade immunotherapies and targeted therapies. *Cancer Immunology, Immunotherapy*. 67:1833–1844. doi:10.1007/s00262-018-2241-x.

Domingues, B., J.M. Lopes, P. Soares, and H. Pópulo. 2018. Melanoma treatment in review. *Immunotargets Ther*. 7:49. doi:10.2147/ITT.S134842.

Dong, J., G. Feldmann, J. Huang, S. Wu, N. Zhang, S.A. Comerford, M.F.F. Gayyed, R.A. Anders, A. Maitra, and D. Pan. 2007. Elucidation of a Universal Size-Control Mechanism in Drosophila and Mammals. *Cell*. 130:1120–1133. doi:10.1016/j.cell.2007.07.019.

Dupont, S., L. Morsut, M. Aragona, E. Enzo, S. Giulitti, M. Cordenonsi, F. Zanconato, J. le Digabel, M. Forcato, S. Bicciato, N. Elvassore, and S. Piccolo. 2011. Role of YAP/TAZ in mechanotransduction. *Nature*. 474:179–183. doi:10.1038/NATURE10137.

Fan, M., W. Lu, J. Che, N.P. Kwiatkowski, Y. Gao, H.-S. Seo, S.B. Ficarro, P.C. Gokhale, Y. Liu, E.A. Geffken, J. Lakhani, K. Song, M. Kuljanin, W. Ji, J. Jiang, Z. He, J. Tse, A.S. Boghossian, M.G. Rees, M.M. Ronan, J.A. Roth, J.D. Mancias, J.A. Marto, S. Dhe-Paganon, T. Zhang, and N.S. Gray. 2022. Covalent disruptor of YAP-TEAD association suppresses defective Hippo signaling. *Elife*. 11:e78810. doi:10.7554/ELIFE.78810.

Fisher, M.L., D. Grun, G. Adhikary, W. Xu, and R.L. Eckert. 2017. Inhibition of YAP function overcomes BRAF inhibitor resistance in melanoma cancer stem cells. *Oncotarget*. 8:110272. doi:10.18632/ONCOTARGET.22628.

Flaherty, K.T., J.R. Infante, A. Daud, R. Gonzalez, R.F. Kefford, J. Sosman, O. Hamid, L. Schuchter, J. Cebon, N. Ibrahim, R. Kudchadkar, H.A. Burris, G. Falchook, A. Algazi, K. Lewis, G. v. Long, I. Puzanov, P. Lebowitz, A. Singh, S. Little, P. Sun, A. Allred, D. Ouellet, K.B. Kim, K. Patel, and J. Weber. 2012. Combined BRAF and MEK Inhibition in Melanoma with BRAF V600 Mutations. *New England Journal of Medicine*. 367:1694–1703. doi:10.1056/nejmoa1210093.

Fratangelo, F., R. Camerlingo, M.V. Carriero, G. Pirozzi, G. Palmieri, G. Gentilcore, C. Ragone, M. Minopoli, P.A. Ascierto, and M.L. Motti. 2018. Effect of ABT-888 on the apoptosis, motility and invasiveness of BRAFi-resistant melanoma cells. *Int J Oncol*. 53:1149–1159. doi:10.3892/IJO.2018.4457.

Ghiso, E., C. Migliore, V. Ciciriello, E. Morando, A. Petrelli, S. Corso, E. de Luca, G. Gatti, M. Volante, and S. Giordano. 2017. YAP-Dependent AXL Overexpression Mediates Resistance to EGFR Inhibitors in NSCLC. *Neoplasia*. 19:1021. doi:10.1016/J.NEO.2017.10.003.

Gorgoulis, V., P.D. Adams, A. Alimonti, D.C. Bennett, O. Bischof, C. Bishop, J. Campisi, M. Collado, K. Evangelou, G. Ferbeyre, J. Gil, E. Hara, V. Krizhanovsky, D. Jurk, A.B. Maier, M. Narita, L. Niedernhofer, J.F. Passos, P.D. Robbins, C.A. Schmitt, J. Sedivy, K. Vougas, T. von

Zglinicki, D. Zhou, M. Serrano, and M. Demaria. 2019. Cellular Senescence: Defining a Path Forward. *Cell*. 179:813–827. doi:10.1016/J.CELL.2019.10.005/ATTACHMENT/84B2BABE-BEB1-4FB7-838C-E264EDC7473E/MMC3.PDF.

Gridnev, A., S. Maity, and J.R. Misra. 2022. Structure-based discovery of a novel small-molecule inhibitor of TEAD palmitoylation with anticancer activity. *bioRxiv*. 495565. doi:10.1101/2022.06.09.495565.

Halder, G., S. Dupont, and S. Piccolo. 2012. Transduction of mechanical and cytoskeletal cues by YAP and TAZ. *Nat Rev Mol Cell Biol*. 13:591–600. doi:10.1038/NRM3416.

Halilovic, E., Q.-B. She, Q. Ye, R. Pagliarini, W.R. Sellers, D.B. Solit, and N. Rosen. 2010. PIK3CA mutation uncouples tumor growth and cyclin D1 regulation from MEK/ERK and mutant KRAS signaling. *Cancer Res*. 70:6804–6814. doi:10.1158/0008-5472.CAN-10-0409/656220/P/PIK3CA-MUTATION-UNCOUPLES-TUMOR-GROWTH-AND-CYCLIN.

Hall, C.A., R. Wang, J. Miao, E. Oliva, X. Shen, T. Wheeler, S.G. Hilsenbeck, S. Orsulic, and S. Goode. 2010. Hippo Pathway Effector Yap is an Ovarian Cancer Oncogene. *Cancer Res*. 70:8525. doi:10.1158/0008-5472.CAN-10-1242.

Hata, A.N., M.J. Niederst, H.L. Archibald, M. Gomez-Caraballo, F.M. Siddiqui, H.E. Mulvey, Y.E. Maruvka, F. Ji, H.E.C. Bhang, V.K. Radhakrishna, G. Siravegna, H. Hu, S. Raoof, E. Lockerman, A. Kalsy, D. Lee, C.L. Keating, D.A. Ruddy, L.J. Damon, A.S. Crystal, C. Costa, Z. Piotrowska, A. Bardelli, A.J. Iafrate, R.I. Sadreyev, F. Stegmeier, G. Getz, L. v. Sequist, A.C. Faber, and J.A. Engelman. 2016. Tumor cells can follow distinct evolutionary paths to become resistant to epidermal growth factor receptor inhibition. *Nat Med*. 22:269. doi:10.1038/NM.4040.

Hauschild, A., J.J. Grob, L. v. Demidov, T. Jouary, R. Gutzmer, M. Millward, P. Rutkowski, C.U. Blank, W.H. Miller, E. Kaempgen, S. Martín-Algarra, B. Karaszewska, C. Mauch, V. Chiarion-Sileni, A.M. Martin, S. Swann, P. Haney, B. Mirakhur, M.E. Guckert, V. Goodman, and P.B. Chapman. 2012. Dabrafenib in BRAF-mutated metastatic melanoma: A multicentre, open-label, phase 3 randomised controlled trial. *The Lancet*. 380:358–365. doi:10.1016/S0140-6736(12)60868-X.

Hill, V.K., T. Dunwell, D. Catchpoole, D. Krex, A.T. Brini, M. Griffiths, C. Craddock, E.R. Maher, and F. Latif. 2011. Frequent epigenetic inactivation of KIBRA, an upstream member of the Salvador/Warts/Hippo (SWH) tumor suppressor network, is associated with specific genetic event in B-cell acute lymphocytic leukemia. *Epigenetics*. 6:332. doi:10.4161/EPI.6.3.14404.

Hirata, E., M.R. Girotti, A. Viros, S. Hooper, B. Spencer-Dene, M. Matsuda, J. Larkin, R. Marais, and E. Sahai. 2015. Intravital imaging reveals how BRAF inhibition generates drug-tolerant microenvironments with high integrin β1/FAK Signaling. *Cancer Cell*. 27:574–588. doi:10.1016/j.ccell.2015.03.008.

Hodis, E., I.R. Watson, G. v. Kryukov, S.T. Arold, M. Imielinski, J.-P. Theurillat, E. Nickerson, D. Auclair, L. Li, C. Place, D. Dicara, A.H. Ramos, M.S. Lawrence, K. Cibulskis, A. Sivachenko, D. Voet, G. Saksena, N. Stransky, R.C. Onofrio, W. Winckler, K. Ardlie, N. Wagle, J. Wargo, K. Chong, D.L. Morton, K. Stemke-Hale, G. Chen, M. Noble, M. Meyerson, J.E. Ladbury, M.A. Davies, J.E. Gershenwald, S.N. Wagner, D.S.B. Hoon, D. Schadendorf, E.S. Lander, S.B. Gabriel, G. Getz, L.A. Garraway, and L. Chin. 2012. A Landscape of Driver Mutations in Melanoma. *Cell*. 150:263. doi:10.1016/J.CELL.2012.06.024.

Hoek, K.S., O.M. Eichhoff, N.C. Schlegel, U. Döbbeling, N. Kobert, L. Schaerer, S. Hemmi, and R. Dummer. 2008. In vivo Switching of Human Melanoma Cells between Proliferative and Invasive States. *Cancer Res*. 68:650–656. doi:10.1158/0008-5472.CAN-07-2491.

Holden, J.K., J.J. Crawford, C.L. Noland, S. Schmidt, J.R. Zbieg, J.A. Lacap, R. Zang, G.M. Miller, Y. Zhang, P. Beroza, R. Reja, W. Lee, J.Y.K. Tom, R. Fong, M. Steffek, S. Clausen, T.J. Hagenbeek, T. Hu, Z. Zhou, H.C. Shen, and C.N. Cunningham. 2020. Small Molecule Dysregulation of TEAD Lipidation Induces a Dominant-Negative Inhibition of Hippo Pathway Signaling. *Cell Rep*. 31:107809. doi:10.1016/j.celrep.2020.107809.

Holohan, C., S. van Schaeybroeck, D.B. Longley, and P.G. Johnston. 2013. Cancer drug resistance: an evolving paradigm. *Nat Rev Cancer*. 13:714–726. doi:10.1038/nrc3599.

Hu, L., Y. Sun, S. Liu, H. Erb, A. Singh, J. Mao, X. Luo, and X. Wu. 2022. Discovery of a new class of reversible TEA domain transcription factor inhibitors with a novel binding mode. *Elife*. 11. doi:10.7554/ELIFE.80210.

Hugo, W., H. Shi, L. Sun, M. Piva, C. Song, X. Kong, G. Moriceau, A. Hong, K.B. Dahlman, D.B. Johnson, J.A. Sosman, A. Ribas, and R.S. Lo. 2015. Non-genomic and Immune Evolution of Melanoma Acquiring MAPKi Resistance. *Cell*. 162:1285. doi:10.1016/J.CELL.2015.07.061.

Huh, H.D., D.H. Kim, H.-S. Jeong, and H.W. Park. 2019. Regulation of TEAD Transcription Factors in Cancer Biology. *Cells*. 8:600. doi:10.3390/CELLS8060600.

Hwang, J., and D.C. Pallas. 2014. STRIPAK complexes: Structure, biological function, and involvement in human diseases. *Int J Biochem Cell Biol*. 47:118–148. doi:10.1016/J.BIOCEL.2013.11.021.

Ianevski, A., A.K. Giri, and T. Aittokallio. 2022. SynergyFinder 3.0: an interactive analysis and consensus interpretation of multi-drug synergies across multiple samples. *Nucleic Acids Res*. 50:W739–W743. doi:10.1093/NAR/GKAC382.

Isola, A.L., K. Eddy, S. Chen, and S. Lehman. 2016. Biology, Therapy and Implications of Tumor Exosomes in the Progression of Melanoma. *Cancers (Basel)*. 8:110. doi:10.3390/cancers8120110.

Jiao, S., H. Wang, Z. Shi, A. Dong, W. Zhang, X. Song, F. He, Y. Wang, Z. Zhang, W. Wang, X. Wang, T. Guo, P. Li, Y. Zhao, H. Ji, L. Zhang, and Z. Zhou. 2014. A Peptide Mimicking VGLL4 Function Acts as a YAP Antagonist Therapy against Gastric Cancer. *Cancer Cell*. 25:166–180. doi:10.1016/j.ccr.2014.01.010.

Johannessen, C.M., J.S. Boehm, S.Y. Kim, S.R. Thomas, L. Wardwell, L.A. Johnson, C.M. Emery, N. Stransky, A.P. Cogdill, J. Barretina, G. Caponigro, H. Hieronymus, R.R. Murray, K. Salehi-Ashtiani, D.E. Hill, M. Vidal, J.J. Zhao, X. Yang, O. Alkan, S. Kim, J.L. Harris, C.J. Wilson, V.E. Myer, P.M. Finan, D.E. Root, T.M. Roberts, T. Golub, K.T. Flaherty, R. Dummer, B.L. Weber, W.R. Sellers, R. Schlegel, J.A. Wargo, W.C. Hahn, and L.A. Garraway. 2010. COT drives resistance to RAF inhibition through MAP kinase pathway reactivation. *Nature*. 468:968–972. doi:10.1038/NATURE09627.

Joshi, M., S.J. Rice, X. Liu, B. Miller, and C.P. Belani. 2015. Trametinib with or without Vemurafenib in BRAF Mutated Non-Small Cell Lung Cancer. *PLoS One*. 10:e0118210. doi:10.1371/journal.pone.0118210.

Joung, J., J.M. Engreitz, S. Konermann, O.O. Abudayyeh, V.K. Verdine, F. Aguet, J.S. Gootenberg, N.E. Sanjana, J.B. Wright, C.P. Fulco, Y.Y. Tseng, C.H. Yoon, J.S. Boehm, E.S. Lander, and F. Zhang. 2017. Genome-scale activation screen identifies a lncRNA locus regulating a gene neighbourhood. *Nature*. 548:343–346. doi:10.1038/NATURE23451.

Kalluri, R., and R.A. Weinberg. 2009. The basics of epithelial-mesenchymal transition. *J Clin Invest*. 119:1428. doi:10.1172/JCI39104.

Kaneda, A., T. Seike, T. Danjo, T. Nakajima, N. Otsubo, D. Yamaguchi, Y. Tsuji, K. Hamaguchi, M. Yasunaga, Y. Nishiya, M. Suzuki, J. Saito, R. Yatsunami, S. Nakamura, Y. Sekido, and K. Mori. 2020. The novel potent TEAD inhibitor, K-975, inhibits YAP1/TAZ-TEAD protein-protein interactions and exerts an anti-tumor effect on malignant pleural mesothelioma. *Am J Cancer Res*. 10:4399–4415.

Kang, W., J.H.M. Tong, A.W.H. Chan, T.-L. Lee, R.W.M. Lung, P.P.S. Leung, K.K.Y. So, K. Wu, D. Fan, J. Yu, J.J.Y. Sung, and K.-F. To. 2011. Yes-associated protein 1 exhibits oncogenic property in gastric cancer and its nuclear accumulation associates with poor prognosis. *Clinical Cancer Research*. 17:2130–2139. doi:10.1158/1078-0432.CCR-10-2467/84023/AM/YES-ASSOCIATED-PROTEIN-1-EXHIBITS-ONCOGENIC.

Kapoor, A., W. Yao, H. Ying, S. Hua, A. Liewen, Q. Wang, Y. Zhong, C.J. Wu, A. Sadanandam, B. Hu, Q. Chang, G.C. Chu, R. Al-Khalil, S. Jiang, H. Xia, E. Fletcher-Sananikone, C. Lim, G.I. Horwitz, A. Viale, P. Pettazzoni, N. Sanchez, H. Wang, A. Protopopov, J. Zhang, T. Heffernan, R.L. Johnson, L. Chin, Y.A. Wang, G. Draetta, and R.A. DePinho. 2014. Yap1 activation enables bypass of oncogenic Kras addiction in pancreatic cancer. *Cell*. 158:197. doi:10.1016/J.CELL.2014.06.003.

Kemper, K., P.L. de Goeje, D.S. Peeper, and R. van Amerongen. 2014. Phenotype switching: Tumor cell plasticity as a resistance mechanism and target for therapy. *Cancer Res*. 74:5937–5941. doi:10.1158/0008-5472.CAN-14-1174/659572/P/PHENOTYPE-SWITCHING-TUMOR-CELL-PLASTICITY-AS-A.

Kim, M.H., J. Kim, H. Hong, S. Lee, J. Lee, E. Jung, and J. Kim. 2016. Actin remodeling confers BRAF inhibitor resistance to melanoma cells through YAP/TAZ activation. *EMBO J*. 35:478. doi:10.15252/EMBJ.201592081.

Knoechel, B., J.E. Roderick, K.E. Williamson, J. Zhu, J.G. Lohr, M.J. Cotton, S.M. Gillespie, D. Fernandez, M. Ku, H. Wang, F. Piccioni, S.J. Silver, M. Jain, D. Pearson, M.J. Kluk, C.J. Ott, L.D. Shultz, M.A. Brehm, D.L. Greiner, A. Gutierrez, K. Stegmaier, A.L. Kung, D.E. Root, J.E. Bradner, J.C. Aster, M.A. Kelliher, and B.E. Bernstein. 2014. An epigenetic mechanism of resistance to targeted therapy in T-cell acute lymphoblastic leukemia. *Nat Genet*. 46:370. doi:10.1038/NG.2913.

Konieczkowski, D.J., C.M. Johannessen, O. Abudayyeh, J.W. Kim, Z.A. Cooper, A. Piris, D.T. Frederick, M. Barzily-Rokni, R. Straussman, R. Haq, D.E. Fisher, J.P. Mesirov, W.C. Hahn, K.T. Flaherty, J.A. Wargo, P. Tamayo, and L.A. Garraway. 2014. A melanoma cell state distinction influences sensitivity to MAPK pathway inhibitors. *Cancer Discov*. 4:827. doi:10.1158/2159-8290.CD-13-0424.

Kozar, I., C. Margue, S. Rothengatter, C. Haan, and S. Kreis. 2019. Many ways to resistance: How melanoma cells evade targeted therapies. *Biochimica et Biophysica Acta (BBA) - Reviews on Cancer*. 1871:313–322. doi:10.1016/J.BBCAN.2019.02.002.

Kumari, A., S. Kesarwani, M.G. Javoor, K.R. Vinothkumar, and M. Sirajuddin. 2020. Structural insights into actin filament recognition by commonly used cellular actin markers. *EMBO J*. 39:e104006. doi:10.15252/EMBJ.2019104006.

Kun, E., Y.T.M. Tsang, C.W. Ng, D.M. Gershenson, and K.K. Wong. 2021. MEK inhibitor resistance mechanisms and recent developments in combination trials. *Cancer Treat Rev*. 92:102137. doi:10.1016/J.CTRV.2020.102137.

Kurppa, K.J., Y. Liu, C. To, T. Zhang, M. Fan, A. Vajdi, E.H. Knelson, Y. Xie, K. Lim, P. Cejas, A. Portell, P.H. Lizotte, S.B. Ficarro, S. Li, T. Chen, H.M. Haikala, H. Wang, M. Bahcall, Y. Gao, S. Shalhout, S. Boettcher, B.H. Shin, T. Thai, M.K. Wilkens, M.L. Tillgren, M. Mushajiang, M. Xu, J. Choi, A.A. Bertram, B.L. Ebert, R. Beroukhim, P. Bandopadhayay, M.M. Awad, P.C. Gokhale, P.T. Kirschmeier, J.A. Marto, F.D. Camargo, R. Haq, C.P. Paweletz, K.K. Wong, D.A. Barbie, H.W. Long, N.S. Gray, and P.A. Jänne. 2020. Treatment-Induced Tumor Dormancy through YAP-Mediated Transcriptional Reprogramming of the Apoptotic Pathway. *Cancer Cell*. 37:104-122.e12. doi:10.1016/j.ccell.2019.12.006.

Lamar, J.M., P. Stern, H. Liu, J.W. Schindler, Z.-G. Jiang, and R.O. Hynes. 2012. The Hippo pathway target, YAP, promotes metastasis through its TEAD-interaction domain. *Proc Natl Acad Sci U S A*. 109:E2450. doi:10.1073/PNAS.1212021109/-/DCSUPPLEMENTAL.

Larkin, J., V. Chiarion-Sileni, R. Gonzalez, J.-J. Grob, P. Rutkowski, C.D. Lao, C.L. Cowey, D. Schadendorf, J. Wagstaff, R. Dummer, P.F. Ferrucci, M. Smylie, D. Hogg, A. Hill, I. Márquez-Rodas, J. Haanen, M. Guidoboni, M. Maio, P. Schöffski, M.S. Carlino, C. Lebbé, G. McArthur, P.A. Ascierto, G.A. Daniels, G. v. Long, L. Bastholt, J.I. Rizzo, A. Balogh, A. Moshyk, F.S. Hodi, and J.D. Wolchok. 2019. Five-Year Survival with Combined Nivolumab and Ipilimumab in Advanced Melanoma. *N Engl J Med*. 381:1535–1546. doi:10.1056/NEJMOA1910836/SUPPL_FILE/NEJMOA1910836_DATA-SHARING.PDF.

Lasithiotakis, K., U. Leiter, F. Meier, T. Eigentler, G. Metzler, M. Moehrle, H. Breuninger, and C. Garbe. 2008. Age and Gender Are Significant Independent Predictors of Survival in Primary Cutaneous Melanoma. *Cancer*. 112:1795–1804. doi:10.1002/cncr.23359.

Lee, J.E., H.S. Park, D. Lee, G. Yoo, T. Kim, H. Jeon, M.K. Yeo, C.S. Lee, J.Y. Moon, S.S. Jung, J.O. Kim, S.Y. Kim, D. il Park, Y.H. Park, J.C. Lee, I.J. Oh, D.S. Lim, and C. Chung. 2016. Hippo pathway effector YAP inhibition restores the sensitivity of EGFR-TKI in lung adenocarcinoma having primary or acquired EGFR-TKI resistance. *Biochem Biophys Res Commun*. 474:154–160. doi:10.1016/J.BBRC.2016.04.089.

Lee, M.-J., M.R. Byun, M. Furutani-Seiki, J.-H. Hong, and H.-S. Jung. 2014. YAP and TAZ regulate skin wound healing. *Journal of Investigative Dermatology*. 134:518–525. doi:10.1038/jid.2013.339.

Lehmann, W., D. Mossmann, J. Kleemann, K. Mock, C. Meisinger, T. Brummer, R. Herr, S. Brabletz, M.P. Stemmler, and T. Brabletz. 2016. ZEB1 turns into a transcriptional activator by interacting with YAP1 in aggressive cancer types. *Nat Commun*. 7. doi:10.1038/NCOMMS10498.

Li, F.Z., A.S. Dhillon, R.L. Anderson, G. McArthur, and P.T. Ferrao. 2015a. Phenotype Switching in Melanoma: Implications for Progression and Therapy. *Front Oncol*. 5. doi:10.3389/FONC.2015.00031.

Li, L.T., G. Jiang, Q. Chen, and J.N. Zheng. 2015b. Ki67 is a promising molecular target in the diagnosis of cancer (Review). *Mol Med Rep*. 11:1566–1572. doi:10.3892/MMR.2014.2914/HTML.

Li, M., B. Zhang, B. Sun, X. Wang, X. Ban, T. Sun, Z. Liu, and X. Zhao. 2010. A novel function for vimentin: the potential biomarker for predicting melanoma hematogenous metastasis. *Journal of Experimental & Clinical Cancer Research*. 29.

Li, Q., Y. Sun, G.K. Jarugumilli, S. Liu, K. Dang, J.L. Cotton, J. Xiol, P.Y. Chan, M. DeRan, L. Ma, R. Li, L.J. Zhu, J.H. Li, A.B. Leiter, Y.T. Ip, F.D. Camargo, X. Luo, R.L. Johnson, X. Wu, and J. Mao. 2020. Lats1/2 Sustain Intestinal Stem Cells and Wnt Activation through TEAD-Dependent and Independent Transcription. *Cell Stem Cell*. 26:675-692.e8. doi:10.1016/j.stem.2020.03.002.

Li, S., Y. Song, C. Quach, H. Guo, G.B. Jang, H. Maazi, S. Zhao, N.A. Sands, Q. Liu, G.K. In, D. Peng, W. Yuan, K. Machida, M. Yu, O. Akbari, A. Hagiya, Y. Yang, V. Punj, L. Tang, and C. Liang. 2019. Transcriptional regulation of autophagy-lysosomal function in BRAF-driven melanoma progression and chemoresistance. *Nat Commun*. 10:1–18. doi:10.1038/s41467-019-09634-8.

Lim, S., N. Hermance, T. Mudianto, H.M. Mustaly, I.P.M. Mauricio, M.A. Vittoria, R.J. Quinton, B.W. Howell, H. Cornils, A.L. Manning, and N.J. Ganem. 2019. Identification of the kinase STK25 as an upstream activator of LATS signaling. *Nat Commun*. 10:1–17. doi:10.1038/s41467-019-09597-w.

Lin, L., A.J. Sabnis, E. Chan, V. Olivas, L. Cade, E. Pazarentzos, S. Asthana, D. Neel, J.J. Yan, X. Lu, L. Pham, M.M. Wang, N. Karachaliou, M.G. Cao, J.L. Manzano, J.L. Ramirez, J.M.S. Torres, F. Buttitta, C.M. Rudin, E.A. Collisson, A. Algazi, E. Robinson, I. Osman, E. Muñoz-Couselo, J. Cortes, D.T. Frederick, Z.A. Cooper, M. Mcmahon, A. Marchetti, R. Rosell, K.T. Flaherty, J.A. Wargo, and T.G. Bivona. 2015. The Hippo effector YAP promotes resistance to RAF- and MEK-targeted cancer therapies. *Nat Genet*. 47:250–256. doi:10.1038/NG.3218.

Lito, P., C.A. Pratilas, E.W. Joseph, M. Tadi, E. Halilovic, M. Zubrowski, A. Huang, W.L. Wong, M.K. Callahan, T. Merghoub, J.D. Wolchok, E. de Stanchina, S. Chandarlapaty, P.I. Poulikakos, J.A. Fagin, and N. Rosen. 2012. Relief of Profound Feedback Inhibition of Mitogenic Signaling by RAF Inhibitors Attenuates Their Activity in BRAFV600E Melanomas. *Cancer Cell*. 22:668–682. doi:10.1016/j.ccr.2012.10.009.

Liu, Y., and M.S. Sheikh. 2014. Melanoma: Molecular Pathogenesis and Therapeutic Management. *Mol Cell Pharmacol*. 6:228. doi:10.4255/mcpharmacol.14.03.

Liu-Chittenden, Y., B. Huang, J.S. Shim, Q. Chen, S.-J. Lee, R.A. Anders, J.O. Liu, and D. Pan. 2012. Genetic and pharmacological disruption of the TEAD–YAP complex suppresses the oncogenic activity of YAP. *Genes Dev*. 26:1305. doi:10.1101/GAD.192856.112.

Long, G. v., K.T. Flaherty, D. Stroyakovskiy, H. Gogas, E. Levchenko, F. de Braud, J. Larkin, C. Garbe, T. Jouary, A. Hauschild, V. Chiarion-Sileni, C. Lebbe, M. Mandalà, M. Millward, A. Arance, I. Bondarenko, J.B.A.G. Haanen, J. Hansson, J. Utikal, V. Ferraresi, P. Mohr, V. Probachai, D. Schadendorf, P. Nathan, C. Robert, A. Ribas, M.A. Davies, S.R. Lane, J.J. Legos, B. Mookerjee, and J.J. Grob. 2017. Dabrafenib plus trametinib versus dabrafenib monotherapy in patients with metastatic BRAF V600E/ K-mutant melanoma: Long-term survival and safety analysis of a phase 3 study. *Annals of Oncology*. 28:1631–1639. doi:10.1093/annonc/mdx176.

Long, G. v., C. Fung, A.M. Menzies, G.M. Pupo, M.S. Carlino, J. Hyman, H. Shahheydari, V. Tembe, J.F. Thompson, R.P. Saw, J. Howle, N.K. Hayward, P. Johansson, R.A. Scolyer, R.F. Kefford, and H. Rizos. 2014a. Increased MAPK reactivation in early resistance to dabrafenib/trametinib combination therapy of BRAF-mutant metastatic melanoma. *Nat Commun*. 5:1–9. doi:10.1038/ncomms6694.

Long, G. v, A.M. Menzies, A.M. Nagrial, L.E. Haydu, A.L. Hamilton, G.J. Mann, T.M. Hughes, J.F. Thompson, R.A. Scolyer, and R.F. Kefford. 2011. Prognostic and clinicopathologic associations of oncogenic BRAF in metastatic melanoma. *Journal of Clinical Oncology*. 29:1246. doi:10.1200/JCO.2010.32.4327.

Long, G. v., D. Stroyakovskiy, H. Gogas, E. Levchenko, F. de Braud, J. Larkin, C. Garbe, T. Jouary, A. Hauschild, J.J. Grob, V. Chiarion Sileni, C. Lebbe, M. Mandalà, M. Millward, A. Arance, I. Bondarenko, J.B.A.G. Haanen, J. Hansson, J. Utikal, V. Ferraresi, N. Kovalenko, P. Mohr, V. Probachai, D. Schadendorf, P. Nathan, C. Robert, A. Ribas, D.J. DeMarini, J.G. Irani, M. Casey, D. Ouellet, A.-M. Martin, N. Le, K. Patel, and K. Flaherty. 2014b. Combined BRAF and MEK Inhibition versus BRAF Inhibition Alone in Melanoma. *N Engl J Med*. 371:1877–1888. doi:10.1056/NEJMOA1406037/SUPPL_FILE/NEJMOA1406037_DISCLOSURES.PDF.

Long, G. v., D. Stroyakovskiy, H. Gogas, E. Levchenko, F. de Braud, J. Larkin, C. Garbe, T. Jouary, A. Hauschild, J.J. Grob, V. Chiarion-Sileni, C. Lebbe, M. Mandalà, M. Millward, A. Arance, I. Bondarenko, J.B.A.G. Haanen, J. Hansson, J. Utikal, V. Ferraresi, N. Kovalenko, P. Mohr, V. Probachai, D. Schadendorf, P. Nathan, C. Robert, A. Ribas, D.J. Demarini, J.G.

Irani, S. Swann, J.J. Legos, F. Jin, B. Mookerjee, and K. Flaherty. 2015. Dabrafenib and trametinib versus dabrafenib and placebo for Val600 BRAF-mutant melanoma: A multicentre, double-blind, phase 3 randomised controlled trial. *The Lancet*. 386:444–451. doi:10.1016/S0140-6736(15)60898-4.

Ma, X.H., S.F. Piao, S. Dey, Q. McAfee, G. Karakousis, J. Villanueva, L.S. Hart, S. Levi, J. Hu, G. Zhang, R. Lazova, V. Klump, J.M. Pawelek, X. Xu, W. Xu, L.M. Schuchter, M.A. Davies, M. Herlyn, J. Winkler, C. Koumenis, and R.K. Amaravadi. 2014. Targeting ER stress–induced autophagy overcomes BRAF inhibitor resistance in melanoma. *J Clin Invest*. 124:1417. doi:10.1172/JCI70454.

Marin-Bejar, O., A. Rogiers, M. Dewaele, J. Femel, P. Karras, J. Pozniak, G. Bervoets, N. van Raemdonck, D. Pedri, T. Swings, J. Demeulemeester, S. vander Borght, S. Lehnert, F. Bosisio, J.J. van den Oord, I. vanden Bempt, D. Lambrechts, T. Voet, O. Bechter, H. Rizos, M.P. Levesque, E. Leucci, A.W. Lund, F. Rambow, and J.C. Marine. 2021. Evolutionary predictability of genetic versus nongenetic resistance to anticancer drugs in melanoma. *Cancer Cell*. 39:1135-1149.e8. doi:10.1016/j.ccell.2021.05.015.

Marine, J.C., S.J. Dawson, and M.A. Dawson. 2020. Non-genetic mechanisms of therapeutic resistance in cancer. *Nat Rev Cancer*. 20:743–756. doi:10.1038/S41568-020-00302-4.

McCain, J. 2013. The MAPK (ERK) Pathway: Investigational Combinations for the Treatment Of BRAF-Mutated Metastatic Melanoma. *Pharmacy and Therapeutics*. 38:96 (105)-98 (108).

Meng, Z., T. Moroishi, V. Mottier-Pavie, S.W. Plouffe, C.G. Hansen, A.W. Hong, H.W. Park, J.-S. Mo, W. Lu, S. Lu, F. Flores, F.-X. Yu, G. Halder, and K.-L. Guan. 2015. MAP4K family kinases act in parallel to MST1/2 to activate LATS1/2 in the Hippo pathway. *Nat Commun*. 6:1–13. doi:10.1038/ncomms9357.

Miller, T.W., J.M. Balko, and C.L. Arteaga. 2011. Phosphatidylinositol 3-Kinase and Antiestrogen Resistance in Breast Cancer. *Journal of Clinical Oncology*. 29:4461. doi:10.1200/JCO.2010.34.4879.

Millet, A., A.R. Martin, C. Ronco, S. Rocchi, and R. Benhida. 2017. Metastatic Melanoma: Insights Into the Evolution of the Treatments and Future Challenges. *Med Res Rev*. 37:98–148. doi:10.1002/MED.21404.

Moriceau, G., W. Hugo, A. Hong, H. Shi, X. Kong, C.C. Yu, R.C. Koya, A.A. Samatar, N. Khanlou, J. Braun, K. Ruchalski, H. Seifert, J. Larkin, K.B. Dahlman, D.B. Johnson, A. Algazi, J.A. Sosman, A. Ribas, and R.S. Lo. 2015. Tunable-combinatorial Mechanisms of Acquired Resistance Limit the Efficacy of BRAF/MEK Co-targeting but Result in Melanoma Drug Addiction. *Cancer Cell*. 27:256. doi:10.1016/J.CCELL.2014.11.018.

Mudianto, T., K.M. Campbell, J. Webb, P. Zolkind, Z.L. Skidmore, R. Riley, E.K. Barnell, I. Ozgenc, T. Giri, G.P. Dunn, D.R. Adkins, M. Griffith, A.M. Egloff, O.L. Griffith, and R. Uppaluri. 2021. Yap1 Mediates Trametinib Resistance in Head and Neck Squamous Cell Carcinomas. *Clin Cancer Res*. 27:2326–2339. doi:10.1158/1078-0432.CCR-19-4179.

Müller, J., O. Krijgsman, J. Tsoi, L. Robert, W. Hugo, C. Song, X. Kong, P.A. Possik, P.D.M. Cornelissen-Steijger, M.H.G. Foppen, K. Kemper, C.R. Goding, U. McDermott, C. Blank, J. Haanen, T.G. Graeber, A. Ribas, R.S. Lo, and D.S. Peeper. 2014. Low MITF/AXL ratio predicts early resistance to multiple targeted drugs in melanoma. *Nat Commun*. 5:1–15. doi:10.1038/ncomms6712.

Muramatsu, T., I. Imoto, T. Matsui, K.I. Kozaki, S. Haruki, M. Sudol, Y. Shimada, H. Tsuda, T. Kawano, and J. Inazawa. 2011. YAP is a candidate oncogene for esophageal squamous cell carcinoma. *Carcinogenesis*. 32:389–398. doi:10.1093/CARCIN/BGQ254.

Nallet-Staub, F., V. Marsaud, L. Li, C. Gilbert, S. Dodier, V. Bataille, M. Sudol, M. Herlyn, and A. Mauviel. 2014. Pro-Invasive Activity of the Hippo Pathway Effectors YAP and TAZ in Cutaneous Melanoma. *J Invest Dermatol*. 134:132. doi:10.1038/JID.2013.319.

Nazarian, R., H. Shi, Q. Wang, X. Kong, R.C. Koya, H. Lee, Z. Chen, M.-K. Lee, N. Attar, H. Sazegar, T. Chodon, S.F. Nelson, G. McArthur, J.A. Sosman, A. Ribas, and R.S. Lo. 2010. Melanomas acquire resistance to B-RAF(V600E) inhibition by RTK or N-RAS upregulation. *Nature*. 468:973–977. doi:10.1038/NATURE09626.

Nguyen, C.D.K., and C. Yi. 2019. YAP/TAZ Signaling and Resistance to Cancer Therapy. *Trends Cancer*. 5:283–296. doi:10.1016/j.trecan.2019.02.010.

Noland, C.L., S. Gierke, P.D. Schnier, J. Murray, W.N. Sandoval, M. Sagolla, A. Dey, R.N. Hannoush, W.J. Fairbrother, and C.N. Cunningham. 2016. Palmitoylation of TEAD Transcription Factors Is Required for Their Stability and Function in Hippo Pathway Signaling. *Structure*. 24:179–186. doi:10.1016/j.str.2015.11.005.

Nouri, K., T. Azad, M. Ling, H.J.J. van Rensburg, A. Pipchuk, H. Shen, Y. Hao, J. Zhang, and X. Yang. 2019. Identification of Celastrol as a Novel YAP-TEAD Inhibitor for Cancer Therapy by High Throughput Screening with Ultrasensitive YAP/TAZ–TEAD Biosensors. *Cancers (Basel)*. 11:1596. doi:10.3390/CANCERS11101596.

Omholt, K., A. Platz, L. Kanter, U. Ringborg, and J. Hansson. 2003. NRAS and BRAF Mutations Arise Early during Melanoma Pathogenesis and Are Preserved throughout Tumor Progression. *Clinical Cancer Research*. 9:6483–6488.

Palmer, J.S., D.L. Duffy, N.F. Box, J.F. Aitken, L.E. O'Gorman, A.C. Green, N.K. Hayward, N.G. Martin, and R.A. Sturm. 2000. Melanocortin-1 Receptor Polymorphisms and Risk of

Melanoma: Is the Association Explained Solely by Pigmentation Phenotype? *Am J Hum Genet*. 66:186. doi:10.1086/302711.

Pan, D. 2010. The Hippo Signaling Pathway in Development and Cancer. *Dev Cell*. 19:505. doi:10.1016/J.DEVCEL.2010.09.011.

Patel, H., N. Yacoub, R. Mishra, A. White, L. Yuan, S. Alanazi, and J.T. Garrett. 2020. Current Advances in the Treatment of BRAF-Mutant Melanoma. *Cancers (Basel)*. 12:482. doi:10.3390/CANCERS12020482.

Patel, P.L., A. Suram, N. Mirani, O. Bischof, and U. Herbig. 2016. Derepression of hTERT gene expression promotes escape from oncogene-induced cellular senescence. *Proc Natl Acad Sci U S A*. 113:E5024–E5033. doi:10.1073/PNAS.1602379113/-/DCSUPPLEMENTAL.

Pedri, D., P. Karras, E. Landeloos, J.-C. Marine, and F. Rambow. 2022. Epithelial-to-mesenchymal-like transition events in melanoma. *FEBS J*. 289:1352–1368. doi:10.1111/FEBS.16021.

Pham, T.H., T.J. Hagenbeek, H.J. Lee, J. Li, C.M. Rose, E. Lin, M. Yu, S.E. Martin, R. Piskol, J.A. Lacap, D. Sampath, V.C. Pham, Z. Modrusan, J.R. Lill, C. Klijn, S. Malek, M.T. Chang, and A. Dey. 2021. Machine-learning and chemicogenomics approach defines and predicts cross-talk of hippo and MAPK pathways. *Cancer Discov*. 11:778–793. doi:10.1158/2159-8290.CD-20-0706/333567/AM/MACHINE-LEARNING-AND-CHEMICO-GENOMICS-APPROACH.

Piccolo, S., S. Dupont, and M. Cordenonsi. 2014. The biology of YAP/TAZ: Hippo signaling and beyond. *Physiol Rev*. 94:1287–1312. doi:10.1152/PHYSREV.00005.2014/ASSET/IMAGES/LARGE/Z9J0041427080004.JPEG.

Plouffe, S.W., Z. Meng, K.C. Lin, B. Lin, A.W. Hong, J. v. Chun, and K.-L. Guan. 2016. Characterization of Hippo Pathway Components by Gene Inactivation. *Mol Cell*. 64:993–1008. doi:10.1016/j.molcel.2016.10.034.

Pollock, P.M., U.L. Harper, K.S. Hansen, L.M. Yudt, M. Stark, C.M. Robbins, T.Y. Moses, G. Hostetter, U. Wagner, J. Kakareka, G. Salem, T. Pohida, P. Heenan, P. Duray, O. Kallioniemi, N.K. Hayward, J.M. Trent, and P.S. Meltzer. 2002. High frequency of BRAF mutations in nevi. *Nat Genet*. 33:19–20. doi:10.1038/NG1054.

Poulikakos, P.I., Y. Persaud, M. Janakiraman, X. Kong, C. Ng, G. Moriceau, H. Shi, M. Atefi, B. Titz, M.T. Gabay, M. Salton, K.B. Dahlman, M. Tadi, J.A. Wargo, K.T. Flaherty, M.C. Kelley, T. Misteli, P.B. Chapman, J.A. Sosman, T.G. Graeber, A. Ribas, R.S. Lo, N. Rosen, and D.B. Solit. 2011. RAF inhibitor resistance is mediated by dimerization of aberrantly spliced BRAF(V600E). *Nature*. 480:387–390. doi:10.1038/NATURE10662.

Rad, E.B., H. Hammerlindl, C. Wels, U. Popper, D.R. Menon, H. Breiteneder, M. Kitzwoegerer, C. Hafner, M. Herlyn, H. Bergler, and H. Schaider. 2016. Notch4 signaling induces a mesenchymal- Epithelial-like transition in melanoma cells to suppress malignant behaviors. *Cancer Res*. 76:1690–1697. doi:10.1158/0008-5472.CAN-15-1722/652055/AM/NOTCH4-SIGNALING-INDUCES-A-MESENCHYMAL-EPITHELIAL.

Rambow, F., A. Rogiers, O. Marin-Bejar, S. Aibar, J. Femel, M. Dewaele, P. Karras, D. Brown, Y.H. Chang, M. Debiec-Rychter, C. Adriaens, E. Radaelli, P. Wolter, O. Bechter, R. Dummer, M. Levesque, A. Piris, D.T. Frederick, G. Boland, K.T. Flaherty, J. van den Oord, T. Voet, S. Aerts, A.W. Lund, and J.C. Marine. 2018. Toward Minimal Residual Disease-Directed Therapy in Melanoma. *Cell*. 174:843-855.e19. doi:10.1016/j.cell.2018.06.025.

Robert, C., B. Karaszewska, J. Schachter, P. Rutkowski, A. Mackiewicz, D. Stroiakovski, M. Lichinitser, R. Dummer, F. Grange, L. Mortier, V. Chiarion-Sileni, K. Drucis, I. Krajsova, A. Hauschild, P. Lorigan, P. Wolter, G. v. Long, K. Flaherty, P. Nathan, A. Ribas, A.-M. Martin, P. Sun, W. Crist, J. Legos, S.D. Rubin, S.M. Little, and D. Schadendorf. 2015. Improved Overall Survival in Melanoma with Combined Dabrafenib and Trametinib. *New England Journal of Medicine*. 372:30–39. doi:10.1056/NEJMOA1412690/SUPPL_FILE/NEJMOA1412690_DISCLOSURES.PDF.

Robert, C., A. Ribas, J. Schachter, A. Arance, J.-J. Grob, L. Mortier, A. Daud, M.S. Carlino, C.M. McNeil, M. Lotem, J.M.G. Larkin, P. Lorigan, B. Neyns, C.U. Blank, T.M. Petrella, O. Hamid, S.-C. Su, C. Krepler, N. Ibrahim, and G. v. Long. 2019. Pembrolizumab versus ipilimumab in advanced melanoma (KEYNOTE-006): post-hoc 5-year results from an open-label, multicentre, randomised, controlled, phase 3 study. *Lancet Oncol*. 20:1239–1251. doi:10.1016/S1470-2045(19)30388-2.

Saleh, T., L. Tyutyunyk-Massey, and D.A. Gewirtz. 2019. Tumor cell escape from therapy-induced senescence as a model of disease recurrence after dormancy. *Cancer Res*. 79:1044–1046. doi:10.1158/0008-5472.CAN-18-3437/661365/P/TUMOR-CELL-ESCAPE-FROM-THERAPY-INDUCED-SENESCENCE.

Sanchez-Vega, F., M. Mina, J. Armenia, W.K. Chatila, A. Luna, K.C. La, S. Dimitriadoy, D.L. Liu, H.S. Kantheti, S. Saghafinia, D. Chakravarty, F. Daian, Q. Gao, M.H. Bailey, W.W. Liang, S.M. Foltz, I. Shmulevich, L. Ding, Z. Heins, A. Ochoa, B. Gross, J. Gao, H. Zhang, R. Kundra, C. Kandoth, I. Bahceci, L. Dervishi, U. Dogrusoz, W. Zhou, H. Shen, P.W. Laird, G.P. Way, C.S. Greene, H. Liang, Y. Xiao, C. Wang, A. Iavarone, A.H. Berger, T.G. Bivona, A.J. Lazar, G.D. Hammer, T. Giordano, L.N. Kwong, G. McArthur, C. Huang, A.D. Tward, M.J. Frederick, F. McCormick, M. Meyerson, S.J. Caesar-Johnson, J.A. Demchok, I. Felau, M. Kasapi, M.L. Ferguson, C.M. Hutter, H.J. Sofia, R. Tarnuzzer, Z. Wang, L. Yang, J.C. Zenklusen, J. (Julia) Zhang, S. Chudamani, J. Liu, L. Lolla, R. Naresh, T. Pihl, Q. Sun, Y.

Wan, Y. Wu, J. Cho, T. DeFreitas, S. Frazer, N. Gehlenborg, G. Getz, D.I. Heiman, J. Kim, M.S. Lawrence, P. Lin, S. Meier, M.S. Noble, G. Saksena, D. Voet, H. Zhang, B. Bernard, N. Chambwe, V. Dhankani, T. Knijnenburg, R. Kramer, K. Leinonen, Y. Liu, M. Miller, S. Reynolds, I. Shmulevich, V. Thorsson, W. Zhang, R. Akbani, B.M. Broom, A.M. Hegde, *et al*. 2018. Oncogenic Signaling Pathways in The Cancer Genome Atlas. *Cell*. 173:321-337.e10. doi:10.1016/j.cell.2018.03.035.

Santucci, M., T. Vignudelli, S. Ferrari, M. Mor, L. Scalvini, M.L. Bolognesi, E. Uliassi, and M.P. Costi. 2015. The Hippo Pathway and YAP/TAZ-TEAD Protein-Protein Interaction as Targets for Regenerative Medicine and Cancer Treatment. *J Med Chem*. 58:4857–4873. doi:10.1021/JM501615V/ASSET/IMAGES/MEDIUM/JM-2014-01615V_0009.GIF.

Savoia, P., P. Fava, F. Casoni, and O. Cremona. 2019. Targeting the ERK Signaling Pathway in Melanoma. *Int J Mol Sci*. 20:1483. doi:10.3390/IJMS20061483.

Schulz, A., J. Raetz, P.C. Karitzky, L. Dinter, J.K. Tietze, I. Kolbe, T. Käubler, B. Renner, S. Beissert, F. Meier, and D. Westphal. 2022. Head-to-Head Comparison of BRAF/MEK Inhibitor Combinations Proposes Superiority of Encorafenib Plus Trametinib in Melanoma. *Cancers (Basel)*. 14:4930. doi:10.3390/cancers14194930.

Shaffer, S.M., M.C. Dunagin, S.R. Torborg, E.A. Torre, B. Emert, C. Krepler, M. Beqiri, K. Sproesser, P.A. Brafford, M. Xiao, E. Eggan, I.N. Anastopoulos, C.A. Vargas-Garcia, A. Singh, K.L. Nathanson, M. Herlyn, and A. Raj. 2017. Rare cell variability and drug-induced reprogramming as a mode of cancer drug resistance. *Nature*. 546:431–435. doi:10.1038/NATURE22794.

Shalem, O., N.E. Sanjana, E. Hartenian, X. Shi, D.A. Scott, T.S. Mikkelsen, D. Heckl, B.L. Ebert, D.E. Root, J.G. Doench, and F. Zhang. 2013. Genome-scale CRISPR-Cas9 knockout screening in human cells. *Science (1979)*. 343:84–87. doi:10.1126/SCIENCE.1247005/SUPPL_FILE/SHALEM.SM.PDF.

Shao, D.D., W. Xue, E.B. Krall, A. Bhutkar, F. Piccioni, X. Wang, A.C. Schinzel, S. Sood, J. Rosenbluh, J.W. Kim, Y. Zwang, T.M. Roberts, D.E. Root, T. Jacks, and W.C. Hahn. 2014. KRAS and YAP1 converge to regulate EMT and tumor survival. *Cell*. 158:184. doi:10.1016/J.CELL.2014.06.004.

Sharma, S. v., D.Y. Lee, B. Li, M.P. Quinlan, F. Takahashi, S. Maheswaran, U. McDermott, N. Azizian, L. Zou, M.A. Fischbach, K.K. Wong, K. Brandstetter, B. Wittner, S. Ramaswamy, M. Classon, and J. Settleman. 2010. A Chromatin-Mediated Reversible Drug-Tolerant State in Cancer Cell Subpopulations. *Cell*. 141:69–80. doi:10.1016/j.cell.2010.02.027.

Shi, H., W. Hugo, X. Kong, A. Hong, R.C. Koya, G. Moriceau, T. Chodon, R. Guo, D.B. Johnson, K.B. Dahlman, M.C. Kelley, R.F. Kefford, B. Chmielowski, J.A. Glaspy, J.A. Sosman, N. van Baren, G. v. Long, A. Ribas, and R.S. Lo. 2014. Acquired resistance and clonal evolution in melanoma during BRAF inhibitor therapy. *Cancer Discov*. 4:80–93. doi:10.1158/2159-8290.CD-13-0642/43066/P/ACQUIRED-RESISTANCE-AND-CLONAL-EVOLUTION-IN.

Shi, H., G. Moriceau, X. Kong, M.K. Lee, H. Lee, R.C. Koya, C. Ng, T. Chodon, R.A. Scolyer, K.B. Dahlman, J.A. Sosman, R.F. Kefford, G. v. Long, S.F. Nelson, A. Ribas, and R.S. Lo. 2012. Melanoma whole-exome sequencing identifies V600EB-RAF amplification-mediated acquired B-RAF inhibitor resistance. *Nat Commun*. 3:1–8. doi:10.1038/ncomms1727.

Siegel, R.L., K.D. Miller, H.E. Fuchs, and A. Jemal. 2022. Cancer statistics, 2022. *CA Cancer J Clin*. 72:7–33. doi:10.3322/CAAC.21708.

Silva, I.P., and G. v. Long. 2017. Systemic therapy in advanced melanoma: Integrating targeted therapy and immunotherapy into clinical practice. *Curr Opin Oncol*. 29:484–492. doi:10.1097/CCO.0000000000000405.

Siravegna, G., B. Mussolin, M. Buscarino, G. Corti, A. Cassingena, G. Crisafulli, A. Ponzetti, C. Cremolini, A. Amatu, C. Lauricella, S. Lamba, S. Hobor, A. Avallone, E. Valtorta, G. Rospo, E. Medico, V. Motta, C. Antoniotti, F. Tatangelo, B. Bellosillo, S. Veronese, A. Budillon, C. Montagut, P. Racca, S. Marsoni, A. Falcone, R.B. Corcoran, F. di Nicolantonio, F. Loupakis, S. Siena, A. Sartore-Bianchi, and A. Bardelli. 2015. Monitoring clonal evolution and resistance to EGFR blockade in the blood of metastatic colorectal cancer patients. *Nat Med*. 21:801. doi:10.1038/NM.3870.

Straussman, R., T. Morikawa, K. Shee, M. Barzily-Rokni, Z.R. Qian, J. Du, A. Davis, M.M. Mongare, J. Gould, D.T. Frederick, Z.A. Cooper, P.B. Chapman, D.B. Solit, A. Ribas, R.S. Lo, K.T. Flaherty, S. Ogino, J.A. Wargo, and T.R. Golub. 2012. Tumour micro-environment elicits innate resistance to RAF inhibitors through HGF secretion. *Nature*. 487:500–504. doi:10.1038/nature11183.

Su, T., T. Bondar, X. Zhou, C. Zhang, H. He, and R. Medzhitov. 2015. Two-signal requirement for growth-promoting function of yap in hepatocytes. *Elife*. 4. doi:10.7554/ELIFE.02948.

Sullivan, R.J., and K. Flaherty. 2013. MAP kinase signaling and inhibition in melanoma. *Oncogene*. 32:2373–2379. doi:10.1038/ONC.2012.345.

Sun, Y., L. Hu, Z. Tao, G.K. Jarugumilli, H. Erb, A. Singh, Q. Li, J.L. Cotton, P. Greninger, R.K. Egan, Y. Tony Ip, C.H. Benes, J. Che, J. Mao, and X. Wu. 2022. Pharmacological blockade of TEAD–YAP reveals its therapeutic limitation in cancer cells. *Nat Commun*. 13:1–18. doi:10.1038/s41467-022-34559-0.

Sun, Z., R. Xu, X. Li, W. Ren, C. Ou, Q. Wang, H. Zhang, X. Zhang, J. Ma, H. Wang, and G. Li. 2015. Prognostic Value of Yes-Associated Protein 1 (YAP1) in Various Cancers: A Meta-Analysis. *PLoS One*. 10:e0135119. doi:10.1371/JOURNAL.PONE.0135119.

Tang, T.T., A.W. Konradi, Y. Feng, X. Peng, M. Ma, J. Li, F.X. Yu, K.L. Guan, and L. Post. 2021. Small molecule inhibitors of TEAD auto-palmitoylation selectively inhibit proliferation and tumor growth of NF2-deficient mesothelioma. *Mol Cancer Ther*. 20:986–998. doi:10.1158/1535-7163.MCT-20-0717.

Tang, Y., T. Feinberg, E.T. Keller, X.Y. Li, and S.J. Weiss. 2016. Snail/Slug binding interactions with YAP/TAZ control skeletal stem cell self-renewal and differentiation. *Nat Cell Biol*. 18:917–929. doi:10.1038/NCB3394.

Usman, S., N.H. Waseem, T.K.N. Nguyen, S. Mohsin, A. Jamal, M.-T. Teh, and A. Waseem. 2021. Vimentin Is at the Heart of Epithelial Mesenchymal Transition (EMT) Mediated Metastasis. *Cancers (Basel)*. 13:4985. doi:10.3390/CANCERS13194985.

Varelas, X., P. Samavarchi-Tehrani, M. Narimatsu, A. Weiss, K. Cockburn, B.G. Larsen, J. Rossant, and J.L. Wrana. 2010. The Crumbs Complex Couples Cell Density Sensing to Hippo-Dependent Control of the TGF-β-SMAD Pathway. *Dev Cell*. 19:831–844. doi:10.1016/j.devcel.2010.11.012.

Verfaillie, A., H. Imrichova, Z.K. Atak, M. Dewaele, F. Rambow, G. Hulselmans, V. Christiaens, D. Svetlichnyy, F. Luciani, L. van den Mooter, S. Claerhout, M. Fiers, F. Journe, G.E. Ghanem, C. Herrmann, G. Halder, J.C. Marine, and S. Aerts. 2015. Decoding the regulatory landscape of melanoma reveals TEADS as regulators of the invasive cell state. *Nat Commun*. 6:1–16. doi:10.1038/ncomms7683.

Viale, A., P. Pettazzoni, C.A. Lyssiotis, H. Ying, N. Sánchez, M. Marchesini, A. Carugo, T. Green, S. Seth, V. Giuliani, M. Kost-Alimova, F. Muller, S. Colla, L. Nezi, G. Genovese, A.K. Deem, A. Kapoor, W. Yao, E. Brunetto, Y. Kang, M. Yuan, J.M. Asara, Y.A. Wang, T.P. Heffernan, A.C. Kimmelman, H. Wang, J.B. Fleming, L.C. Cantley, R.A. DePinho, and G.F. Draetta. 2014. Oncogene ablation-resistant pancreatic cancer cells depend on mitochondrial function. *Nature*. 514:632. doi:10.1038/NATURE13611.

Villanueva, J., J.R. Infante, C. Krepler, P. Reyes-Uribe, M. Samanta, H.Y. Chen, B. Li, R.K. Swoboda, M. Wilson, A. Vultur, M. Fukunaba-Kalabis, B. Wubbenhorst, T.Y. Chen, Q. Liu, K. Sproesser, D.J. DeMarini, T.M. Gilmer, A.-M. Martin, R. Marmorstein, D.C. Schultz, D.W. Speicher, G.C. Karakousis, W. Xu, R.K. Amaravadi, X. Xu, L.M. Schuchter, M. Herlyn, and K.L. Nathanson. 2013. Concurrent MEK2 mutation and BRAF amplification confer resistance to BRAF and MEK inhibitors in melanoma. *Cell Rep*. 4:1099. doi:10.1016/J.CELREP.2013.08.023.

Wang, B., W. Zhang, G. Zhang, L. Kwong, H. Lu, J. Tan, N. Sadek, M. Xiao, J. Zhang, M. Labrie, S. Randell, A. Beroard, E. Sugarman, V.W. Rebecca, Z. Wei, Y. Lu, G.B. Mills, J. Field, J. Villanueva, X. Xu, M. Herlyn, and W. Guo. 2021. Targeting mTOR signaling overcomes acquired resistance to combined BRAF and MEK inhibition in BRAF-mutant melanoma. *Oncogene*. 40:5590–5599. doi:10.1038/s41388-021-01911-5.

Wang, J., S.K. Huang, D.M. Marzese, S.C. Hsu, N.P. Kawas, K.K. Chong, G. v. Long, A.M. Menzies, R.A. Scolyer, S. Izraely, O. Sagi-Assif, I.P. Witz, and D.S.B. Hoon. 2015. Epigenetic changes of EGFR have an important role in BRAF inhibitor-resistant cutaneous melanomas. *Journal of Investigative Dermatology*. 135:532–541. doi:10.1038/JID.2014.418.

Wang, L., R. Leite de Oliveira, S. Huijberts, E. Bosdriesz, N. Pencheva, D. Brunen, A. Bosma, J.-Y. Song, J. Zevenhoven, G.T. Los-de Vries, H. Horlings, B. Nuijen, J.H. Beijnen, J.H.M. Schellens, and R. Bernards. 2018a. An Acquired Vulnerability of Drug-Resistant Melanoma with Therapeutic Potential. *Cell*. 173:1413-1425.e14. doi:10.1016/j.cell.2018.04.012.

Wang, Y., Q. Dong, Q. Zhang, Z. Li, E. Wang, and X. Qiu. 2010. Overexpression of yes-associated protein contributes to progression and poor prognosis of non-small-cell lung cancer. *Cancer Sci*. 101:1279–1285. doi:10.1111/J.1349-7006.2010.01511.X.

Wang, Y., X. Xu, D. Maglic, M.T. Dill, K. Mojumdar, P.K.-S. Ng, K.J. Jeong, Y.H. Tsang, D. Moreno, V.H. Bhavana, X. Peng, Z. Ge, H. Chen, J. Li, Z. Chen, H. Zhang, L. Han, D. Du, C.J. Creighton, G.B. Mills, S.J. Caesar-Johnson, J.A. Demchok, I. Felau, M. Kasapi, M.L. Ferguson, C.M. Hutter, H.J. Sofia, R. Tarnuzzer, Z. Wang, L. Yang, J.C. Zenklusen, J. (Julia) Zhang, S. Chudamani, J. Liu, L. Lolla, R. Naresh, T. Pihl, Q. Sun, Y. Wan, Y. Wu, J. Cho, T. DeFreitas, S. Frazer, N. Gehlenborg, G. Getz, D.I. Heiman, J. Kim, M.S. Lawrence, P. Lin, S. Meier, M.S. Noble, G. Saksena, D. Voet, H. Zhang, B. Bernard, N. Chambwe, V. Dhankani, T. Knijnenburg, R. Kramer, K. Leinonen, Y. Liu, M. Miller, S. Reynolds, I. Shmulevich, V. Thorsson, W. Zhang, R. Akbani, B.M. Broom, A.M. Hegde, Z. Ju, R.S. Kanchi, A. Korkut, J. Li, H. Liang, S. Ling, W. Liu, Y. Lu, K.S. Ng, A. Rao, M. Ryan, J. Wang, J.N. Weinstein, J. Zhang, A. Abeshouse, J. Armenia, D. Chakravarty, W.K. Chatila, I. de Bruijn, J. Gao, B.E. Gross, Z.J. Heins, R. Kundra, K. La, M. Ladanyi, A. Luna, M.G. Nissan, A. Ochoa, S.M. Phillips, *et al*. 2018b. Comprehensive Molecular Characterization of the Hippo Signaling Pathway in Cancer. *Cell Rep*. 25:1317.e5. doi:10.1016/J.CELREP.2018.10.001.

Welsh, S.J., H. Rizos, R.A. Scolyer, and G. v. Long. 2016. Resistance to combination BRAF and MEK inhibition in metastatic melanoma: Where to next? *Eur J Cancer*. 62:76–85. doi:10.1016/J.EJCA.2016.04.005.

Wolf Horrell, E.M., M.C. Boulanger, and J.A. D'Orazio. 2016. Melanocortin 1 receptor: Structure, function, and regulation. *Front Genet*. 7:95. doi:10.3389/FGENE.2016.00095/BIBTEX.

Xie, C., X. Chen, M. Zheng, X. Liu, H. Wang, and L. Lou. 2017. Pharmacologic characterization of SHR8443, a novel dual inhibitor of phosphatidylinositol 3-kinase and mammalian target of rapamycin. *Oncotarget*. 8:107990. doi:10.18632/ONCOTARGET.22439.

Xu, M.Z., T.-J. Yao, N.P.Y. Lee, I.O.L. Ng, Y.T. Chan, L. Zender, S.W. Lowe, R.T.P. Poon, and J.M. Luk. 2009. Yes-Associated Protein Is an Independent Prognostic Marker in Hepatocellular Carcinoma. *Cancer*. 115:4585. doi:10.1002/CNCR.24495.

Xu, W., Y. Wei, S. Wu, Y. Wang, Z. Wang, Y. Sun, S.Y. Cheng, and J. Wu. 2015. Up-regulation of the Hippo pathway effector TAZ renders lung adenocarcinoma cells harboring EGFR-T790M mutation resistant to gefitinib. *Cell Biosci*. 5:1–9. doi:10.1186/2045-3701-5-7.

Yamaguchi, H., and G.M. Taouk. 2020. A Potential Role of YAP/TAZ in the Interplay Between Metastasis and Metabolic Alterations. *Front Oncol*. 10. doi:10.3389/fonc.2020.00928.

Yang, C., C. Tian, T.E. Hoffman, N.K. Jacobsen, and S.L. Spencer. 2021. Melanoma subpopulations that rapidly escape MAPK pathway inhibition incur DNA damage and rely on stress signalling. *Nat Commun*. 12:1–14. doi:10.1038/s41467-021-21549-x.

Yin, F., J. Yu, Y. Zheng, Q. Chen, N. Zhang, and D. Pan. 2013. Spatial organization of hippo signaling at the plasma membrane mediated by the tumor suppressor merlin/NF2. *Cell*. 154:1355. doi:10.1016/j.cell.2013.08.025.

Yu, F.-X., B. Zhao, N. Panupinthu, J.L. Jewell, I. Lian, L.H. Wang, J. Zhao, H. Yuan, K. Tumaneng, H. Li, X.D. Fu, G.B. Mills, and K.L. Guan. 2012. Regulation of the Hippo-YAP pathway by G-protein-coupled receptor signaling. *Cell*. 150:780–791. doi:10.1016/j.cell.2012.06.037.

Zanconato, F., G. Battilana, M. Cordenonsi, and S. Piccolo. 2016a. YAP/TAZ as therapeutic targets in cancer. *Curr Opin Pharmacol*. 29:26–33. doi:10.1016/J.COPH.2016.05.002.

Zanconato, F., M. Cordenonsi, and S. Piccolo. 2016b. YAP/TAZ at the Roots of Cancer. *Cancer Cell*. 29:783–803. doi:10.1016/j.ccell.2016.05.005.

Zhang, N., H. Bai, K.K. David, J. Dong, Y. Zheng, J. Cai, M. Giovannini, P. Liu, R.A. Anders, and D. Pan. 2010. The Merlin/NF2 Tumor Suppressor Functions through the YAP Oncoprotein to Regulate Tissue Homeostasis in Mammals. *Dev Cell*. 19:27–38. doi:10.1016/J.DEVCEL.2010.06.015.

Zhang, X., J. George, S. Deb, J.L. Degoutin, E.A. Takano, S.B. Fox, AOCS Study group, D.D.L. Bowtell, and K.F. Harvey. 2011. The Hippo pathway transcriptional co-activator, YAP, is an ovarian cancer oncogene. *Oncogene 2011*. 30:2810–2822. doi:10.1038/ONC.2011.8.

Zhang, X., L. Yang, P. Szeto, G.K. Abali, Y. Zhang, A. Kulkarni, K. Amarasinghe, J. Li, I.A. Vergara, R. Molania, A.T. Papenfuss, C. McLean, M. Shackleton, and K.F. Harvey. 2020. The Hippo pathway oncoprotein YAP promotes melanoma cell invasion and spontaneous metastasis. *Oncogene*. 39:5267–5281. doi:10.1038/S41388-020-1362-9.

Zhao, B., L. Li, K. Tumaneng, C.-Y. Wang, and K.-L. Guan. 2010. A coordinated phosphorylation by Lats and CK1 regulates YAP stability through SCFβ-TRCP. *Genes Dev*. 24:85. doi:10.1101/GAD.1843810.

Zhao, B., X. Wei, W. Li, R.S. Udan, Q. Yang, J. Kim, J. Xie, T. Ikenoue, J. Yu, L. Li, P. Zheng, K. Ye, A. Chinnaiyan, G. Halder, Z.-C. Lai, and K.-L. Guan. 2007. Inactivation of YAP oncoprotein by the Hippo pathway is involved in cell contact inhibition and tissue growth control. *Genes Dev*. 21:2761. doi:10.1101/GAD.1602907.

Zhao, B., X. Ye, J. Yu, L. Li, W. Li, S. Li, J. Yu, J.D. Lin, C.-Y. Wang, A.M. Chinnaiyan, Z.-C. Lai, and K.-L. Guan. 2008. TEAD mediates YAP-dependent gene induction and growth control. *Genes Dev*. 22:1971. doi:10.1101/GAD.1664408.

Zhao, X., X. Wang, L. Fang, C. Lan, X. Zheng, Y. Wang, Y. Zhang, X. Han, S. Liu, K. Cheng, Y. Zhao, J. Shi, J. Guo, J. Hao, H. Ren, and G. Nie. 2017. A combinatorial strategy using YAP and pan-RAF inhibitors for treating KRAS-mutant pancreatic cancer. *Cancer Lett*. 402:61–70. doi:10.1016/J.CANLET.2017.05.015.

Zheng, Y., W. Wang, B. Liu, H. Deng, E. Uster, and D. Pan. 2015. Identification of Happyhour/MAP4K as Alternative Hpo/Mst-like Kinases in the Hippo Kinase Cascade. *Dev Cell*. 34:642–655. doi:10.1016/j.devcel.2015.08.014.

Zhou, Z., T. Hu, Z. Xu, Z. Lin, Z. Zhang, T. Feng, L. Zhu, Y. Rong, H. Shen, J.M. Luk, X. Zhang, and N. Qin. 2014. Targeting Hippo pathway by specific interruption of YAP-TEAD interaction using cyclic YAP-like peptides. *The FASEB Journal*. 29:724–732. doi:10.1096/FJ.14-262980.

Zuo, Q., J. Liu, L. Huang, Y. Qin, T. Hawley, C. Seo, G. Merlino, and Y. Yu. 2018. AXL/AKT axis mediated-resistance to BRAF inhibitor depends on PTEN status in melanoma. *Oncogene*. 37:3289. doi:10.1038/S41388-018-0205-4.